Principes et techniques de calorimétrie

R. Wigmans

PRINCIPES ET TECHNIQUES DE CALORIMETRIE

R. Wigmans

CERN, Genève, Suisse

CONTENTS

1. INTRODUCTION

Experimental particle physicists study the fundamental structure of matter by making fast particles collide with each other, and by analyzing the reaction products. Ideally, one would like to know the 4-vectors of all the particles produced in these processes as accurately as possible. For many years the bubble chamber, still unsurpassed in accuracy, was the major experimental tool. The overwhelming majority of the known particles and resonances have been discovered in bubble chamber experiments.

In order to be able to study more rare processes one started using other techniques, based on a digitized recording of experimental data, in order to speed up the analysis, but yet trying to approach as much as possible the accuracy of bubble chambers. In particular, charm and beauty studies have taken advantage of this approach. The experimental setup consisted of (usually many) detector planes recording the passage of charged particles, for which a wide variety of techniques were employed. In addition, converters for γ's, an absorber allowing muon identification, and a magnetic field for momentum analysis were standard items.

In the last decade, a different class of detectors have gradually become more and more important. We call them calorimeters, or total absorption detectors. Basically, a calorimeter is a block of matter, in which the particle that is to be measured interacts, and deposits all its energy in the form of a *shower* of decreasingly lower-energy particles. The block is made such that a certain (usually small and hopefully constant) fraction of the initial particle energy is transformed into a measurable signal (light, electrical charge).

Multiton calorimeters play a key role in almost any big experiment currently running or being prepared at high-energy colliding beam machines, in fixed-target neutrino or heavy-ion scattering, and in nucleon decay experiments. This will a *fortiori* be true for experiments at a future supercollider, which will be rather useless without powerful calorimetry.

The reasons for this development can be divided into two classes. Firstly, there are reasons related to the *calorimeter properties*:

a) Calorimeters are sensitive to both charged and neutral particles.

b) Owing to differences in the characteristic shower patterns some crucial particle identification is possible (hadron/electron/muon/neutrino separation).

c) Since calorimetry is based on statistical processes, the measurement accuracy *improves* with increasing energy. For magnetic spectrometers, the accuracy of the momentum measurement $\Delta p/p$ can only be kept *the same* at the expense of enlarging the detector proportional to $\sqrt{p}$.

d) The calorimeter dimensions needed to contain showers increase only slightly with the energy (log E), which means that even at the highest energies envisaged one can work with a rather compact instrument (cost!).

e) Calorimeters are fast; response times better than 100 ns are very well feasible, which is important if the detector has to operate in a high rate environment.

f) They don't require a magnetic field for energy measurements.

g) They can be segmented to a very high degree, which allows a precise measurement of the direction of the incoming particles.

Secondly, there are reasons related to the *physics* that one wants to study. In the bubble chamber era the interest was focused on *hadron* physics. The 4-vectors of all individual final state particles were important in order to see whether a combination of these were decay products of a new type of hadron (fig. 1). Nowadays, experimental physics has penetrated deeply inside the *quark* level. Imagine a heavy particle, e.g a W-boson, that decays into a quark and an antiquark, e.g. $u\bar{d}$ (fig. 2). Because of the large mass difference, the quark and antiquark are given an enormous kinetic energy. In a process called fragmentation they "dress" themselves into bunches of hadrons, which are called *jets*. Each jet may contain $\sim$ 10 particles. In order to measure the properties of the new particle we first of all have to recognize these jets as such. If we want for example to determine the particle's mass, the total energy carried by the particles in

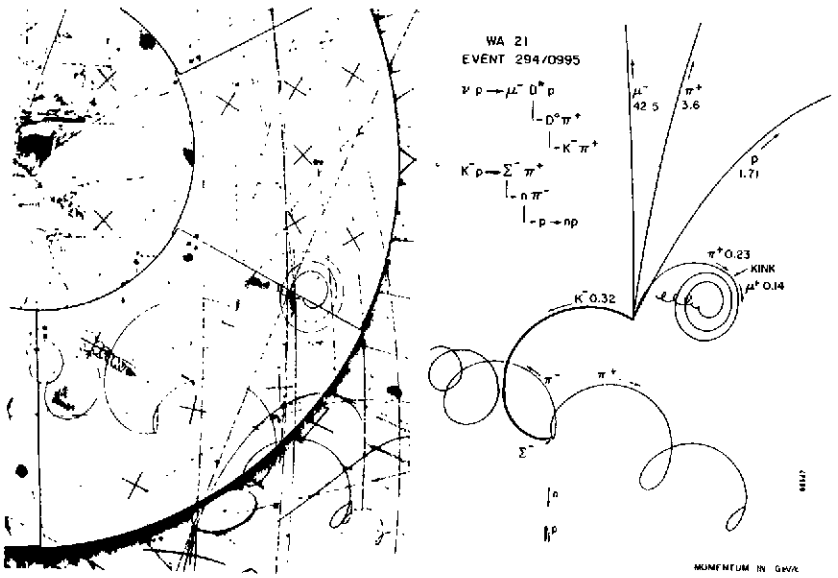

1. Example of an event recorded in a bubble chamber, revealing the production of a charmed meson.

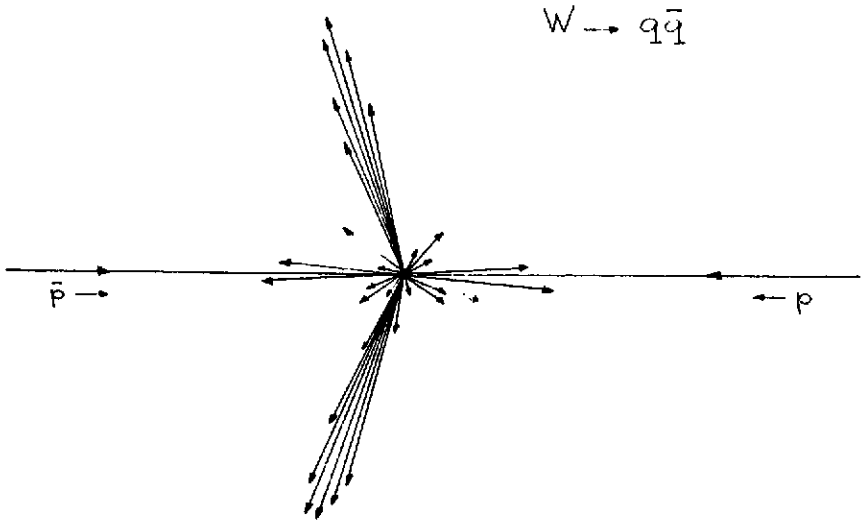

2. Production of a W-boson decaying in a quark-antiquark pair, at the CERN $p\overline{p}$ collider.

the jet, and the jet direction have to be measured. To first order, the properties of the individual particles that constitute the jet are not important.

The new particle may also decay leptonically. If it is charged, this implies the production of a very energetic neutrino, which will *not* contribute to the calorimeter signal. However, because of the disturbed transverse energy balance the ν can be easily recognized, and its properties determined. In this way the W vector bosons were discovered in $p\overline{p}$ collisions at CERN (fig. 3).

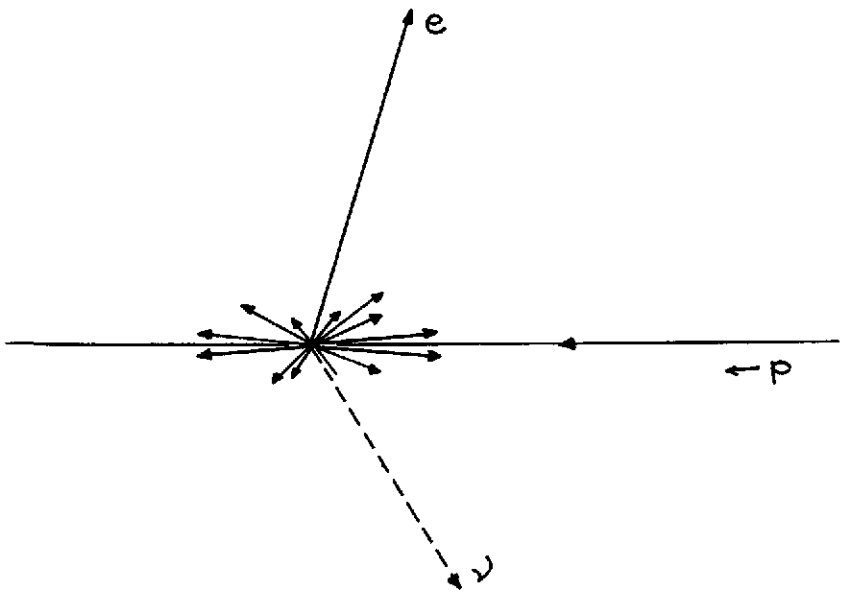

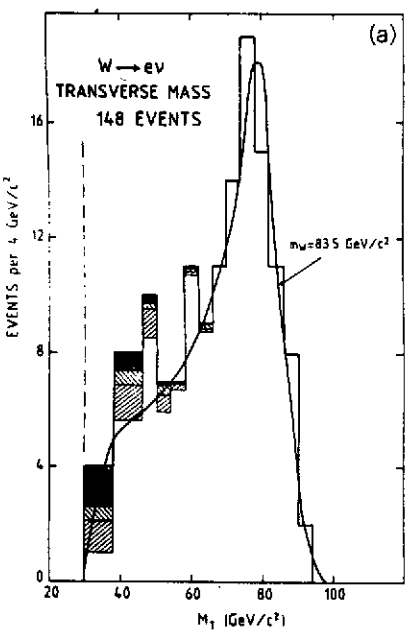

3. The discovery of the W-boson, through the missing E_T characteristic for the $W \to e\nu$ decay mode, at the CERN $p\bar{p}$ collider.

These examples illustrate that the emphasis has clearly shifted from a precise measurement of the 4-vectors of all *individual* reaction products to more *global* event characteristics like missing (transverse) energy, total transverse energy, jet production, *etc.* Calorimeters are extremely well suited for this purpose. They can make sense out of the very discouraging forest of tracks that (electronic) bubble chambers would yield in the TeV era (fig. 4). Moreover, they can make this sense within 100 ns. This is perhaps the most crucial advantage offered by calorimeters.

The cross sections at e.g a multi-TeV *pp* supercollider are such that new physics may be expected in at maximum 10^{-8} of all collisions, probably even several orders of magnitude less (fig. 5). That is why the design luminosity of these machines is so high. Calorimeters are unique in their capability of reducing the primary event rate of 100 MHz down to a level that can be handled by the readout and data recording electronics ($\sim$ 1 Hz), while retaining all those events that might contain signatures of new physics.

Being so crucial for their successes, it is clear that experiments will want to have the best possible calorimetry. In order to achieve this goal, a detailed understanding of the factors that limit the performance of calorimeters is required. These notes are intended as an introduction to this very exciting and challenging field, which rapidly develops. They are certainly *not* meant as a review of past and ongoing activities.

We will mainly concentrate on *sampling* calorimeters, because of their importance for future high-energy experiments. Nevertheless, we will also briefly treat fully sensitive devices, in section 2. In this section, calorimeters for detecting electromagnetic (em) showers are discussed. We examine the physics processes relevant to em shower development, and the factors that limit the performance of em calorimeters. Section 3 is devoted to readout techniques for sampling calorimeters. In sections 4 - 7 hadron calorimeters are discussed. We examine the physics processes relevant to hadron shower development, their consequences for the calorimeter signals, and the possibilities for optimizing the performance of hadron calorimeters. In section 8 an outlook on future developments is given.

For those who want to get more familiar with the subject, we can strongly recommend the excellent paper by Fabjan[1] , which contains a lot of complementary information, and also an extensive bibliography.

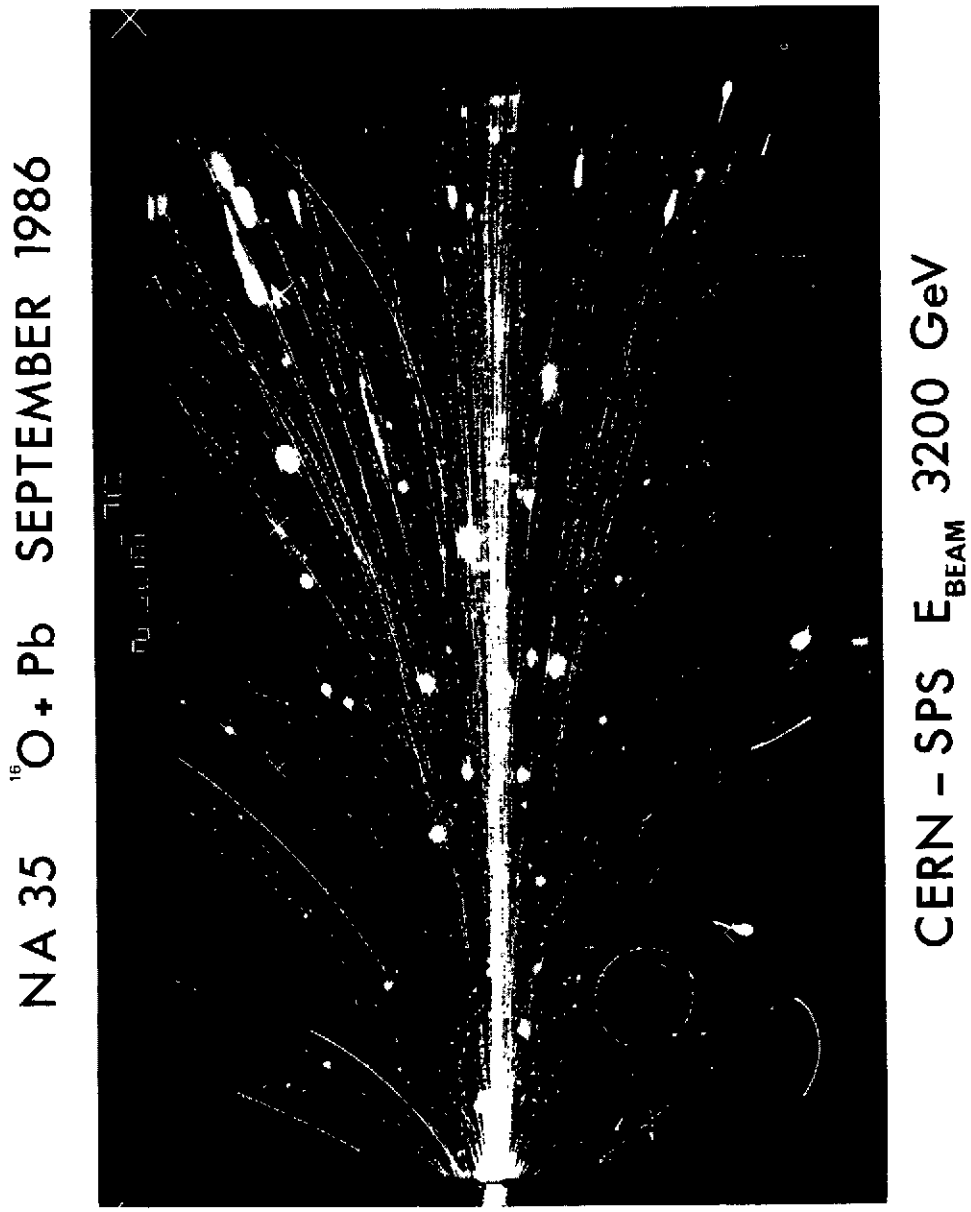

4. Streamer chamber picture of a collision between a 3.2 TeV ^{16}O ion and a tungsten nucleus at rest. The picture does *not* show the few hundred neutral particles also produced in this interaction.

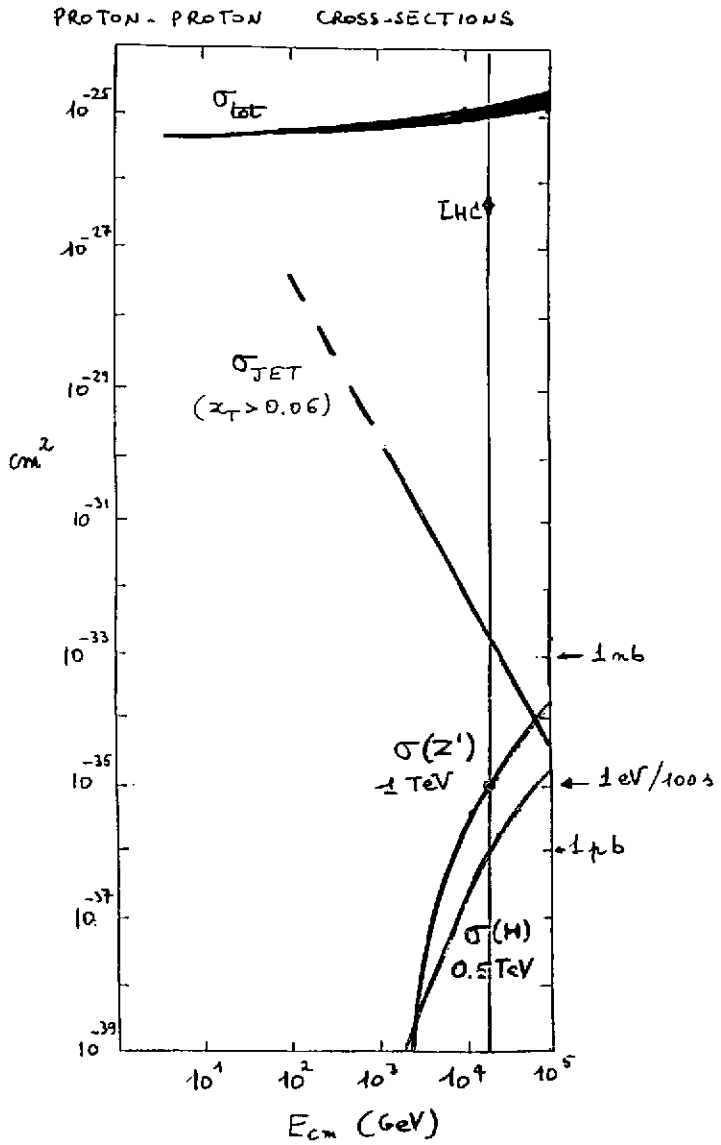

5. The total cross section and the jet-jet cross section as a function of the center-of-mass energy, in pp collisions.

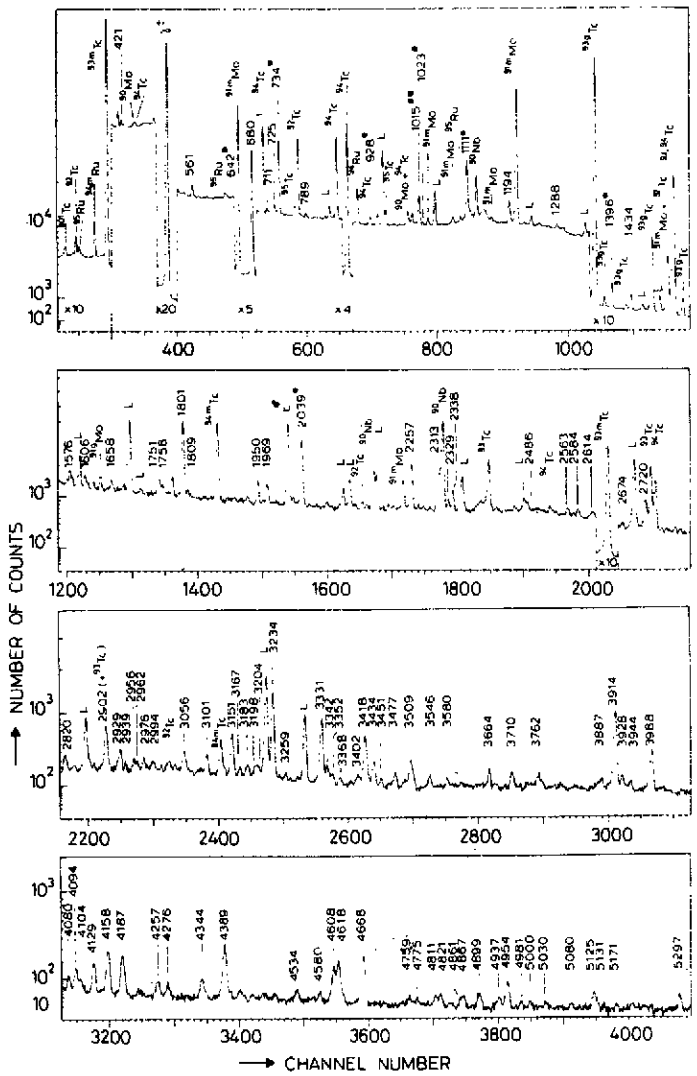

6. A complicated nuclear γ spectrum measured with a large Ge(Li) crystal.

2. CALORIMETERS FOR DETECTING ELECTROMAGNETIC SHOWERS

2.1 Calorimetry at very low energies

Calorimeters for detecting electromagnetically interacting particles have been used since more than half a century in *nuclear physics* experiments. The best results are obtained with semiconductor devices like high-purity Ge, Ge(Li) and Si(Li) crystals. In such detectors an electric field is set up across the semiconducting medium, that has a low conductivity. Usually this low conductivity region is the charge-depletion region in a semiconductor diode operating at reverse bias. When a charged particle passes through the semiconductor, electron-hole pairs are created in it. The charges are separated by the electric field, and the resulting electrical signal can be measured.

One advantage of these detectors is that it takes very little energy to create one electron-hole pair, only 2.9 eV in Ge. The signal of a 1 MeV particle fully absorbed in the crystal will, therefore, consists of some 350,000 electrons. The energy resolution is determined by the statistical fluctuations in this number, which gives $\sigma/E = 0.17\%$, at 1 MeV. Such good resolutions are indeed observed in practice. Since the number of electron-hole pairs is proportional to the energy of the incoming particle, the resolution σ/E varies with E as $c/\sqrt{E}$, *i.e.* it improves with increasing energy. This is clearly what one observes with this type of detector. The largest Ge crystals used in practice have a sensitive volume of $\sim 100\,\mathrm{cm}^3$. The are used as nuclear γ detectors. An example of their impressive resolving power is shown in fig. 6.

Although the energy of these γ's is only a few MeV, they will already develop simple showers in the crystal. The sequence of processes through which the γ's of a particular energy are absorbed and contribute to the corresponding peak, may be very different from event to event. An example of such a sequence is given in fig. 7. A γ of 3370 keV enters the detector and converts into an electron-positron pair. Both particles get a kinetic energy of 1174 keV (point A), the remaining energy is going into the mass of the e^+ and e^-. The electron loses its kinetic energy by creating electron-hole pairs in the semiconductor and stops inside the detector; and so does the positron. When the positron is stopped, it annihilates with an electron, thus releasing the energy $E = M_{e^+e^-}$ in the form of two γ's of 511 keV each (B). The γ's undergo Compton scattering (C,D), in which part of the energy is transferred to an electron and part into a new γ. The electrons lose their energy as described, the γ's may either undergo another Compton scattering (F), or give photo-electric effect in which the full γ-energy is transferred to an electron (E,G). This is only one example out of an infinite number of different possibilities.

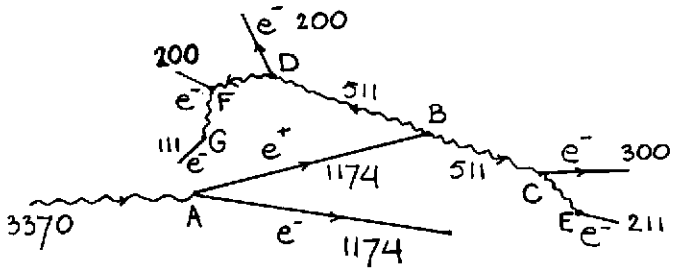

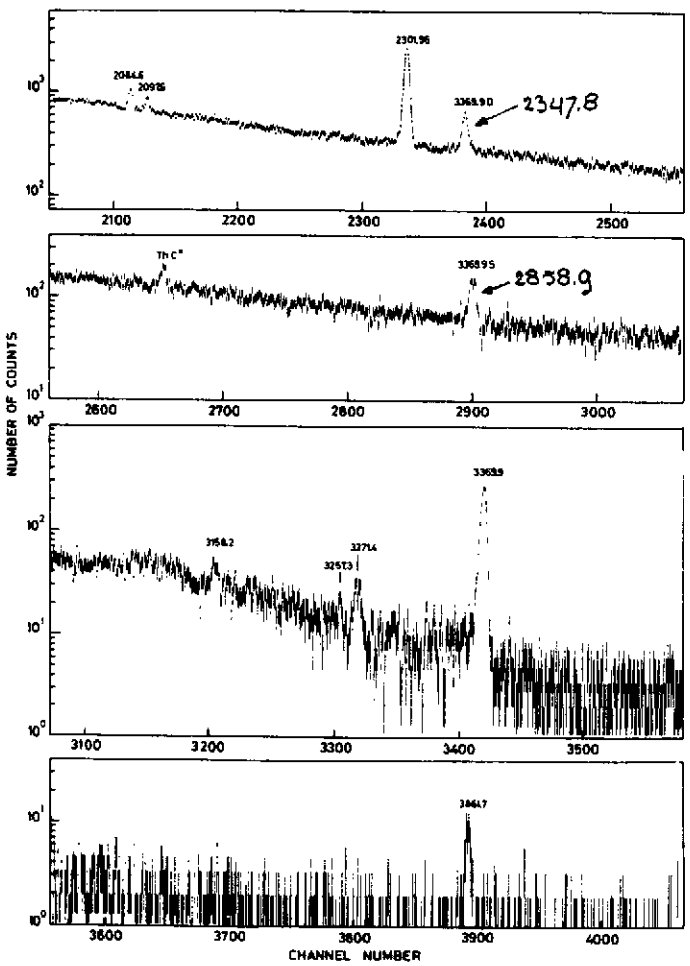

7. Shower development by few-MeV nuclear γ's. In small semiconductor crystals, leakage effects may occur (see text).

For events that contribute to the peaks, the whole sequence has taken place inside the sensitive detector volume. Especially in smaller crystals, leakage phenomena may occur. This is shown by the γ-spectrum in fig. 7. Either one or both 511 keV γ's from our example may escape the detector. This will lead to peaks at energies lower by 511 and 1022 keV. And if *they* don't escape, some of the tertiary or higher order γ's might, leading to a continuous background.

Although this example in itself has no importance for applications in high-energy physics experiments, it nicely illustrates some aspects of calorimetry that are also relevant for our purpose: Shower development, the effect of fluctuations on the signal distribution, leakage.

Other detectors used for nuclear γ detection are based on the creation of scintillation light, *e.g.* NaI(Tl) crystals. When the molecules are excited by a charged particle that traverses the crystal, they fall back in their ground state by emitting photons with a wavelength in or near the visible spectrum. The crystals are read out with a device that transforms the photons in an electrical signal, *e.g.* through the photo-electric effect as in photomultipliers.

It is already much more complicated to understand the signal from such detectors than for the semiconductors discussed before. The following complications arise:

i) The scintillation photons are not mono-energetic but cover a broad spectrum.

ii) The sensitivity of the photocathode is strongly wavelength dependent.

iii) Only a fraction of the photons reach the photocathode. The rest is either absorbed inside the crystal, or refracted out of it. These effects strongly depend on the detector geometry and on the position where the scintillation photons are produced.

As a consequence, the fluctuations in the signal (*i.e.* in the number of photo-electrons) will be much larger than the fluctuations in the number of photons released in the primary processes. And if the fluctuations in the signal are dominated by other factors than the statistical fluctuations in the primary processes, there is also *a priori* no reason to expect that the energy resolution σ/E will improve as $c/\sqrt{E}$ with increasing energy.

This is confirmed by experimental results. Measurements on 8 keV X-rays yielded $\sigma/E \approx 15\%$. If we assume that this result is dominated by fluctuations in the primary processes, this means that on average $\sim$ 40 photo-electrons are observed. In other words, it takes $\sim$ 200 eV of the primary particle to create one photo-electron. For 1 MeV γ's, one should therefore expect on average 5000 photo-electrons, which would yield $\sigma/E = 1.4\%$. Yet, the best resolutions obtained at this energy are at least three times worse than that.

2.2 Mechanisms of energy loss in high-energy em showers

We now change our energy units from eV, keV and MeV to GeV and TeV, still far away from the unit that has given its name to our detectors (1 cal $\approx 2.6 \times 10^7$ TeV).

In fact, most of the energy loss mechanisms relevant to high-energy em showers were already mentioned in the previous subsection: Ionization for electrons and positrons, pair production, Compton scattering and photo-electric effect for photons. There is only one more, be it crucial mechanism that comes in at higher energies: *Bremsstrahlung*.

When they pass through matter, electrons and positrons may radiate photons as a result of the Coulomb interaction with the nuclear electric field. These photons have an exponentially falling energy spectrum that in principle extends to the electron energy, but in general the emitted photon carries only a small fraction of this energy. In this process, the electron itself undergoes a (usually small) change in direction. The deviation depends on the angle and the energy of the emitted photon, which in turn depend on the strength of the Coulomb field, *i.e.* on the Z of the absorber medium. This is called multiple scattering.

Bremsstrahlung is by far the principle source of energy loss by electrons and positrons at high energies. As a consequence, high-energy em showers are very different from the ones discussed so far (fig. 7), since an important multiplication of shower particles occurs. A primary GeV-type electron may radiate on its way through the detector say a thousand photons. The ones faster than 5 - 10 MeV will create e^+e^- pairs. The fast electrons and positrons from this process will in turn lose their energy by radiation as well, *etc.*, *etc.* The result is a shower that may consist of thousands of different particles, electrons, positrons and photons (see fig. 8). The overwhelming majority of these particles are very soft. The *average* energy of the shower particles is obviously a function of the age of the shower, or the depth inside the detector: The farther the shower has developed, the softer the spectrum of its constituents becomes.

The energy loss mechanisms are governed by the laws of quantum electrodynamics[2] one of the best established theoretical frameworks in physics. They primarily depend on the electron density of the medium in which the shower develops. Since the number of atoms per unit volume is within a factor of ~ 2 the same for all materials in the solid state, this density is roughly proportional to the (average) Z of the medium.

Figures 9 and 10 show the results of calculations on the energy loss mechanisms for photons and electrons, as a function of energy, in three materials with very different Z-values: Carbon ($Z = 6$), iron ($Z = 26$) and uranium ($Z = 92$)[3,4] . At high energies, beyond $\sim$ 100 MeV, pair production by photons and energy loss by radiation

8. Impression of the development of (the early part of) an em shower, as recorded by the Big European Bubble Chamber filled with neon/hydrogen. The fast γ's produce e^+e^- pairs (the V-type tracks on the picture), the soft ones are Compton-scattered (the single tiny corkscrews).

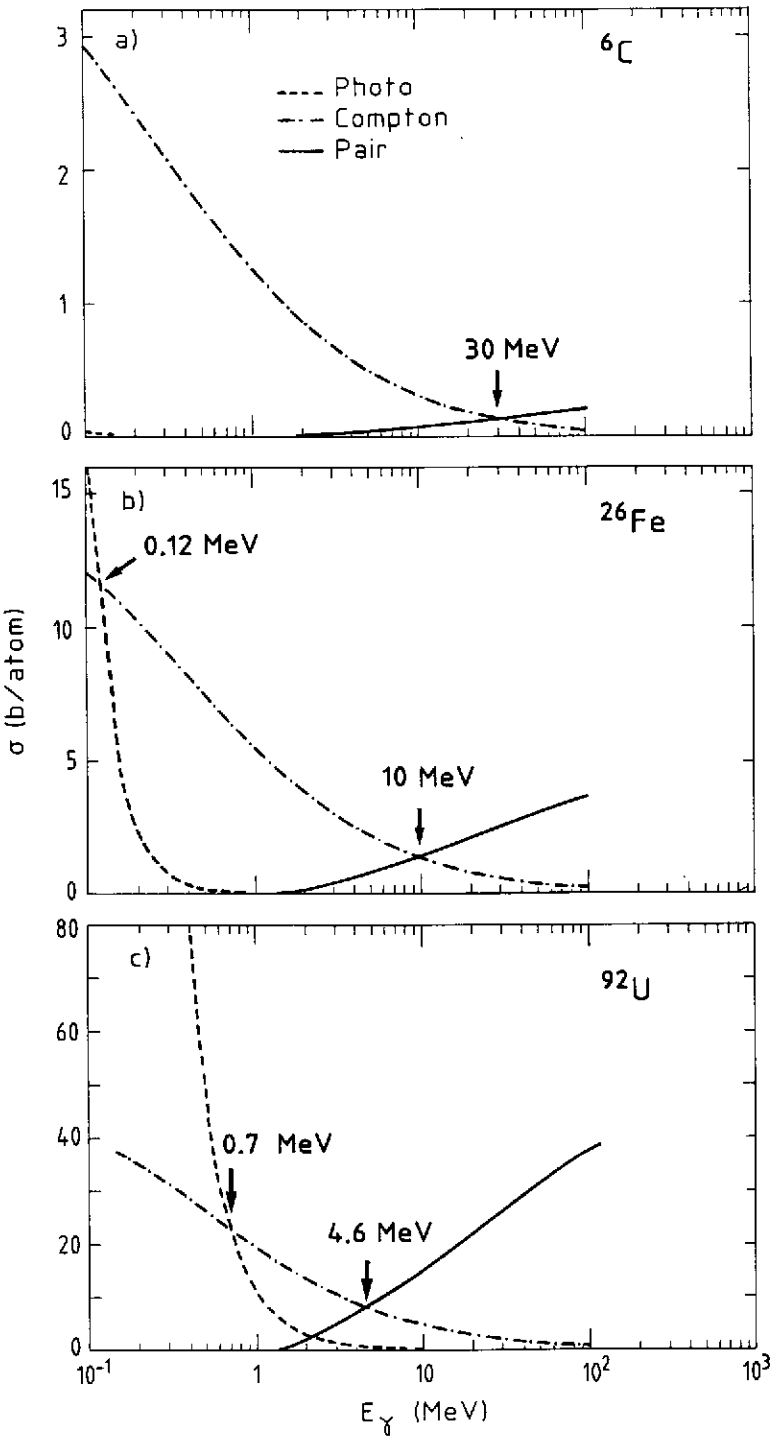

9. The cross sections for pair production, Compton scattering and photo-electric effect, as a function of the photon energy, in carbon, iron and uranium.

dominate in all cases, but at low energies the differences between the various materials are considerable. Both the energy at which Compton scattering starts dominating pair production by photons, and the energy at which ionization losses become more important than Bremsstrahlung, are strongly material dependent: They are roughly inversely proportional to Z.

These conditions determine the so-called *critical energy* (ϵ_c), *i.e.* the point where no further particle multiplication occurs in the shower. Above this energy, γ's produce on average more than one charged particle (pair production), and electrons lose their energy predominantly by creating *new* γ's. Below ϵ_c, γ's produce only *one* electron each, and these electrons do not produce new γ's themselves.

Figure 9 also shows that the contribution of photo-electric effect is extremely Z-dependent ($\sigma \sim Z^5$). In carbon, it does not play any role at all, while in uranium it is the dominating process below 0.7 MeV.

From the information in figs. 9 and 10 one can already imagine what the longitudinal shower profile will look like. If one would measure the number of e^+ and e^- as a function of depth in the detector, one would first find a rather steep rise, owing to the multiplication. This will continue up to the depth at which the average particle energy equals ϵ_c. Beyond that point no further multiplication will take place, and due to the fact that more and more electrons are stopped, the total number of remaining particles slowly decreases.

The positrons will predominantly be found in the early shower part, *i.e.* before the maximum is reached. Showers in high-Z materials will contain *more* positrons than in low-Z materials, because positron production continues until lower energies. The *average* energy of the shower particles will also be lower in high-Z materials, since radiation losses dominate until lower energies. These effects will turn out to have interesting consequences.

Owing to the fact that the underlying physics is well-understood and relatively simple, the em shower development can be simulated in great detail by Monte-Carlo techniques. One program, EGS4[6] has emerged as the world-wide standard for this purpose. It is extremely reliable, provided it is used in the right way, and in the following sections several results of it will be shown.

2.3 Em shower characteristics

Since the em shower development is primarily determined by the electron density in the absorber medium, it is to some extent possible and in any case convenient to describe

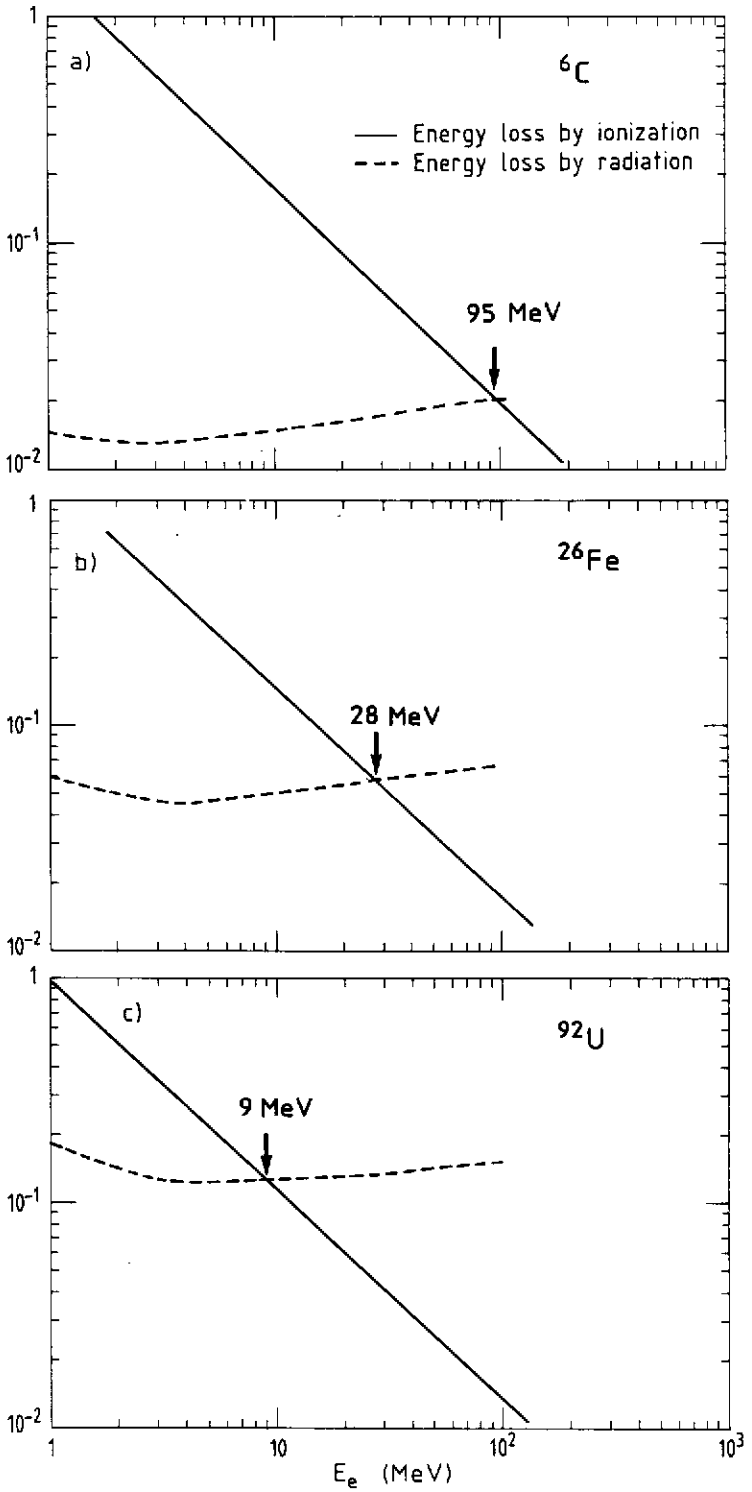

10. The fractional energy loss by radiation and ionization, as a function of the electron energy, in carbon, iron and uranium.

the shower characteristics in a material-independent way. The units that are frequently used to describe the characteristic shower dimensions are the *radiation length* (X_0, for the longitudinal development) and the *Molière radius* (ρ_M, transverse).

The radiation length is defined as the distance L over which a high-energy (> 1 GeV) electron loses on average 63.2% ($1-1/e$) of its energy to Bremsstrahlung. It almost equals (7/9) the average distance that very high-energy photons travel before converting into an e^+e^- pair. The Molière radius is defined through the ratio of X_0 and the critical energy, usually taken as the energy at which electrons lose equal amounts of energy through ionization and radiation (fig. 10). For rapid calculations, the following relations approximately hold:

$$X_0 \approx 180A/Z^2 \text{ (g/cm}^2\text{)} \text{ and } \rho_M \approx 7A/Z \text{ (g/cm}^2\text{)}$$

Expressed in these quantities, the shower development is approximately material-independent. Figure 11 shows the longitudinal development of a 10 GeV electron shower in Al, Fe and Pb, as obtained with EGS4 simulations. The profile is as expected from the discussion in sect 2.2. Globally, it scales indeed with X_0. The differences between the various materials can be understood too. The radiation length is defined for GeV-type particles and, therefore, does not take into account the peculiarities occurring in the MeV region. The shift of the shower maximum to greater depth for high-Z absorbers is a consequence of the fact that particle multiplication continues until lower energies. And the slower decay beyond this maximum is due to the fact that lower-energy electrons still radiate.

These data and EGS4 results at other energies can be reasonably fit by the formula

$$N = N_0 L^a \exp(-bL)$$

where a and b depend on Z, and a in addition on E. The shower maximum is defined by a/b and is proportional to log E.

Figure 11 shows that it takes $\sim 25X_0$ to absorb these showers for at least 99%. This corresponds to 14 cm Pb, 44 cm Fe, or 220 cm Al. If the energy is increased, only very little *extra* material is needed to achieve the same containment. A 20 GeV photon will travel on average 9/7 radiation length before converting into an e^+e^- pair of 10 GeV each. It therefore takes only an extra 1.3 X_0 to contain twice as much energy.

The radiation length is, strictly speaking, defined for infinite energy, it has no meaning in the MeV energy range. We just showed that $\sim$ 15 cm lead absorb 20 GeV photon showers for more than 99%, while everybody knows that it takes *more* than that to make a proper shielding for a strong ^{60}Co source, that emits 1.3 MeV γ's. The reason for this is clear from fig. 9 . The total cross section around the region where Compton scattering

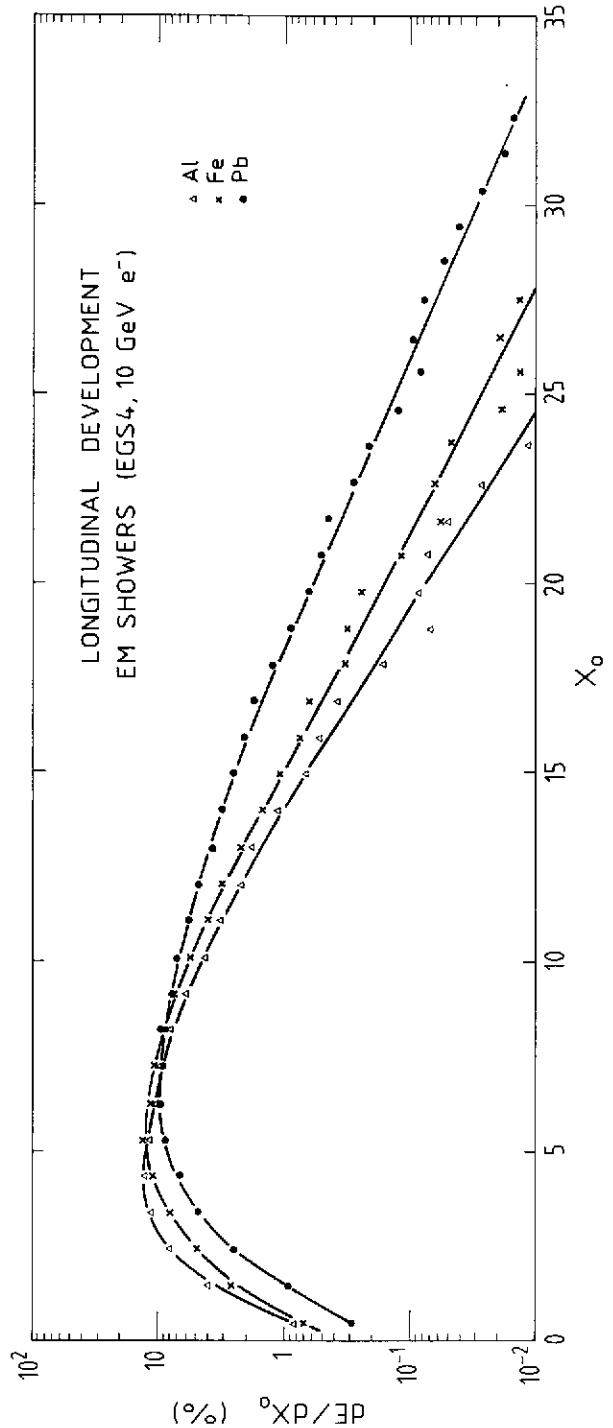

11. The longitudinal development of a 10 GeV electron shower in aluminium, iron and lead. Results of EGS4 calculations.

takes over from pair production is conssiderably lower than at very high energies, particularly in high-Z materials. As a consequence, the mean free path of few-MeV photons in lead is $\sim$ 3 cm, or $\sim 5X_0$!

The *lateral spread* of an em shower is caused by two effects:

a) Electrons move away from the axis by multiple scattering.

b) Bremsstrahlung photons in the energy region where the total cross section is minimal may travel quite far from the shower axis, in particular if they are emitted by electrons that themselves travel under a considerable angle with this axis.

The first process will dominate in the early stages of the shower development. The second process can be expected to become important beyond the shower maximum and, for reasons just given, particularly in high-Z media. This is confirmed by EGS4 calculations[7] . Figure 12 shows the lateral distribution of the energy deposited by an em shower in lead, at various oepths. The two components can be clearly distinguished (note the logarithmic vertical scale). The radial profile shows a pronounced central core surrouded by a "halo". The central core disappears beyond the shower maximum. Similar calculations in aluminium showed that the radial profile, expressed in ρ_M units, is indeed more narrow than in lead. Like the radiation length, also the Molière radius does not take into account the peculiarities occurring in the MeV region.

Figure 12 shows that em showers are very narrow, especially in the first few radiation lengths. The Molière radius of lead is $\sim$ 1.7 cm. With a sufficiently fine-grained calorimeter, the showering particle can therefore be localized with a precision of $\sim$ 1 mm.

2.4 Homogeneous em shower detectors

The fully sensitive calorimeters that have been used as em shower counters are all based on the detection of light. The NaI(Tl) crystals discussed in sect. 2.1 were also used for this purpose. For 1 GeV showers an energy resolution $\sigma/E = 0.9\%$ was measured, with a 24 X_0 (60 cm) long crystal. For shower detection this is an excellent result, but it confirms the tendency already noticed for nuclear γ's, that the energy resolution does *not* improve with increasing energy as $c/\sqrt{E}$, but more slowly. Based on the 5% resolution typical at 1 MeV one would have expected $\sigma/E \approx 0.2\%$ at 1 GeV in case of a $c/\sqrt{E}$ behaviour.

Another frequently used crystal detector based on scintillation light is bismuth germanate (BGO). It is popular because of its short radiation length (1.1 cm) and its good mechanical properties (unlike NaI(Tl), it is *not* hygroscopic). The energy resolution for a sufficiently large detector will, expectedly, be similar to NaI(Tl). Also here, the fluctu-

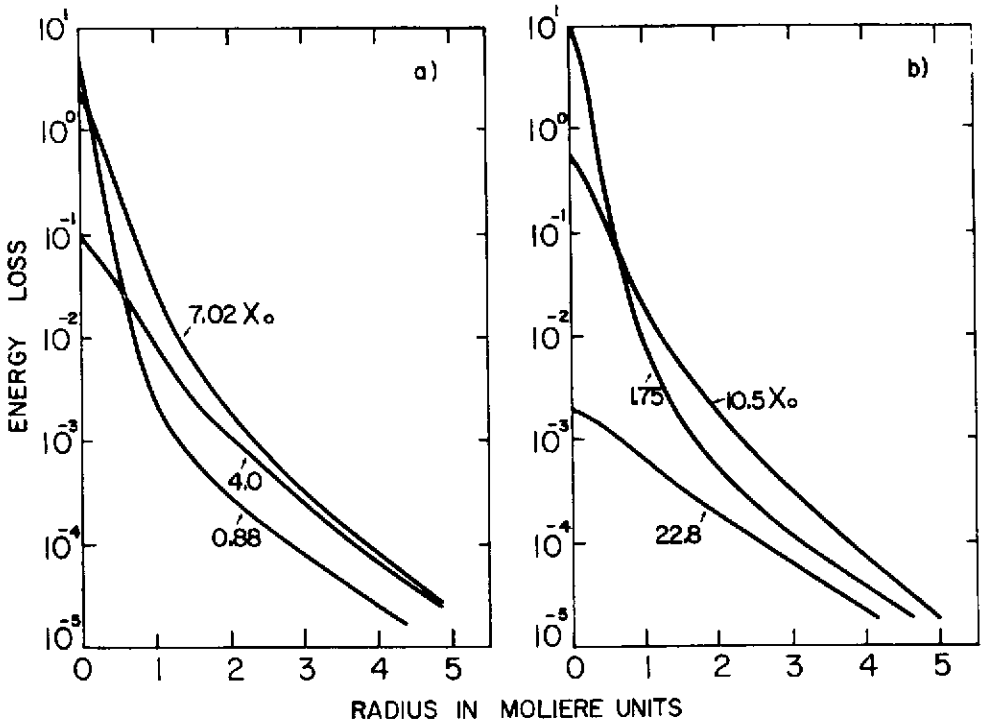

12. The lateral distribution of the energy deposited by a 1 GeV em shower in lead, at various depths. Results of EGS4 calculations.

ations in the primary processes by which the light is created, are by no means limiting the calorimeter performance.

This is different for *lead glass* counters (a mixture of PbO and SiO_2. They are based on the detection of *Čerenkov* light produced by the electrons and positrons from the shower. Particles travelling at a velocity lower than the velocity of light in the absorber will *not* emit this light, and therefore the lead glass detects only the shower electrons with a kinetic energy larger than $\sim$ 0.7 MeV. This means that at maximum only $1000/0.7 \sim 1400$ photons will be produced per GeV shower energy, and that the resolution σ/E can not become better than $\sim$ 3% at 1 GeV because of fluctuations in this number. If in addition losses in the *detection* of these photons occur, the resolution will further deteriorate.

Geometrical losses are in this case much less important than for scintillation light. The Čerenkov photons are emitted at a fixed angle with respect to the direction in which the electrons move, while scintillation light is isotropically emitted. Absorption of Čerenkov photons by the crystal itself will play a role, but in practice about half of them can be detected by the photocathode.

The energy resolution of em calorimeters based on the detection of Čerenkov light is clearly limited by fluctuations in the shower development, which determine the number of Čerenkov photons produced. This contribution to the energy resolution σ/E scales as $c/\sqrt{E}$. For detectors that are sufficiently large to contain the shower, it is the dominating contribution. For lead glass, one has found[8] $\sigma/E \approx 5\%/\sqrt{E}$ for em showers in the energy range 1 - 20 GeV. In this result, and in all the other ones written similarly in the following, E is expressed in GeV.

2.5 Sampling calorimeters

Sampling calorimeters are devices where the energy is measured in a number of sensitive layers interspersed by passive absorber. The usual configuration is a stack of many plates of a dense metallic absorber, interleaved with planes of active material. The signals are obtained from these planes, for which a variety of choices exist. These are subject of sect. 3. Sampling calorimeters are much cheaper than the homogeneous ones we discussed, and thus they can be sufficiently large to avoid shower leakage, and to cover the full solid angle in a collider experiment.

In these calorimeters, one measures the ionization loss of shower particles that traverse (part of) an active layer. This represents a small, but for em showers (on average) fixed fraction of the total energy of the particle that generated the shower. This *sampling fraction* is to first order roughly equal to the mass ratio of the active and passive materials in the calorimeter. For calorimeters with solid or liquid active media it is usually somewhere in the $1\% - 10\%$ range, for detectors with gaseous readout it is considerably lower, $\sim 10^{-4}$.

Of all the different active media used in sampling calorimeters, none is based on the detection of Čerenkov light. There is an obvious reason for this. In sect. 2.4 it was shown that per GeV shower energy at maximum only $\sim$ 1400 Čerenkov photons are produced. If we now have a calorimeter with a sampling fraction of 1%, on average only 14 photons would be produced in the active layers, leading to a ridiculously large contribution of photon statistics to the energy resolution.

This illustrates why active media in sampling calorimeters should be based on abundant primary processes. In practice they are all using either scintillation light or direct charge production, e.g. by ionization, as the source of signals. These processes occur at least 10^6 times per GeV deposited shower energy (see sect. 2.1). In spite of this large number, (photo-)electron statistics may well be a non-negligible factor contributing to the energy resolution, since large reduction factors apply. For a sampling calorimeter with scintillator readout, 1000 photo-electrons per GeV is already considered a very good

result, which would contribute $\sim 3\%/\sqrt{E}$ to the energy resolution σ/E. The reduction of a factor $10^3 - 10^4$ comes in this case from the combined effects of sampling fraction, and a very low efficiency of scintillation light reaching the photocathode (geometry, absorption).

An effect of the same type occurs in calorimeters with wire chamber readout. These detect the direct ionization charge via gas amplification. Because of the very small sampling fraction, only ~ 100 out of the primary $\sim 10^6$ ionization processes per GeV are taking place in the sensitive layers, yielding a $10\%/\sqrt{E}$ contribution to the energy resolution. In practice the contribution will even be larger than that, since the number of ionizations N in the active layers is very asymmetrically distributed (Landau tail), and hence the σ_{RMS} of the distribution is considerably larger than $\sqrt{N}$.

The major contribution to the energy resolution of calorimeters with *non-gaseous* readout has a different origin, *i.e.* the fluctuations in the *number* of charged shower particles that contribute to the signal. These are called *sampling fluctuations*. In order to evaluate their effect, we will distinguish two kinds of particles:

a) Those created in the absorber layers and crossing the boundary with the active layers.

b) Those created in the active layers themselves.

By far most particles through which the shower energy is deposited in the calorimeter are *electrons*. Simulations with EGS4 have shown that per GeV em energy on average only 65 positrons are created, via $\gamma \to e^+e^-$, in high-Z materials like Pb and U. In low-Z materials this number is even lower (see sect. 2.3). In the soft shower part, below the critical energy, considerable numbers of soft electrons are produced, through Compton scattering and photo-electric effect. Figure 13 is illustrative in this respect. It shows which fraction of the shower energy of a 10 GeV electron is deposited through ionization by particles below or above a certain threshold energy. Particles with a kinetic energy below 1 MeV account for a considerable fraction, ranging from $\sim 25\%$ in Al to $\sim 40\%$ in high-Z materials like Pb and U. If we assume that these particles carry on average 0.5 MeV, this leads to 500 - 800 particles per GeV shower energy, almost exclusively electrons. In practice there will be even *more* particles than that, since the electron energy spectrum is not flat but (exponentially) increasing at lower energy.

In a sampling calorimeter, most of the soft shower electrons will *not* contribute to the signal, because of their short range. For example, the range of a 1 MeV electron in uranium is only 0.4 mm, and for a 0.1 MeV electron it is only 0.02 mm. Therefore, in a sampling calorimeter with 3 mm uranium plates more than 80% of the 1 MeV electrons produced in the absorber layers will *not* manage to reach a sensitive plane, and even more than 99% of the 0.1 MeV electrons.

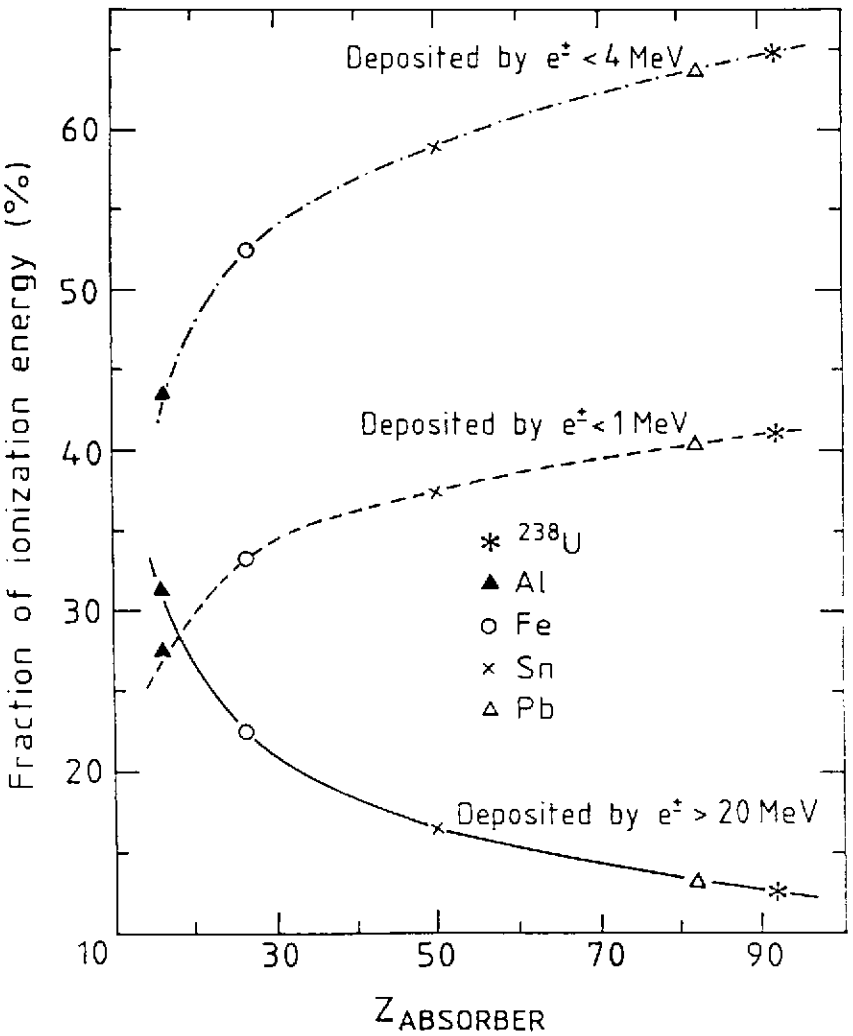

13. The fraction of the energy of a 10 GeV electron shower, that is deposited through ionization by electrons and positrons slower than 1 or 4 MeV, or faster than 20 MeV, as a function of the Z-value of the calorimeter absorber. Results from EGS4 Monte-Carlo simulations.

The fraction of the soft shower electrons produced in the *absorber layers*, which *do* reach the active planes is inversely proportional to the thickness of the absorber layers, to a very good approximation. Only for very thin (< 1 mm) absorber plates deviations will occur.

The soft shower electrons produced in the *active layers* will *all* contribute to the calorimeter signal. The fraction of the total number of soft shower electrons that they represent depends on the sampling fraction: If the absorber plates are made thicker, or the active plates thinner, the number of soft shower electrons generated in the active planes decreases proportionally.

The number of soft shower electrons contributing to the calorimeter signal is, therefore, in both cases inversely proportional to the thickness of the absorber plates (t_{abs}). The part *produced in the active planes* is in addition *proportional* to the thickness of these planes. The fluctuations in the number of soft shower electrons detected by the active planes give a contribution to the calorimeter energy resolution that thus can be written as

$$\sigma_{\mathrm{samp}}/E = c\sqrt{t_{\mathrm{abs}}/E}$$

for a particular combination of active and passive media, and a fixed thickness of the active planes. From the numbers given above it is clear that in practical calorimeters, the number of these electrons will not exceed a few hundred per GeV shower energy, and thus the fluctuations will be at least $5 - 10\%$ at 1 GeV.

The contribution of the *fast* shower particles to the sampling fluctuations will show somewhat different characteristics. These particles are predominantly produced in pairs ($\gamma \rightarrow e^+e^-$). This means that the fluctuations in their numbers are given by $\sqrt{N/2}$ rather than by $\sqrt{N}$. As indicated before, their number is small compared to the soft electrons. Their contribution to the signal may be somewhat enhanced by the fact that they may traverse *several* active planes, particularly if the absorber layers are thin ($< 1X_0$). The contribution of fluctuations in their number to the energy resolution will only scale with $\sqrt{t_{\mathrm{abs}}}$ if $t_{\mathrm{abs}} > 1X_0$, and is independent on the thickness of the active layers.

Summarizing, we have three classes of shower particles, which contribute very differently to the sampling fluctuations:

1) The fast particles, whose range is longer than the sampling distance. The contributions of fluctuations in their number to the energy resolution is affected by the e^+e^- correlation (Z-dependent, see fig. 9), and is much weaker dependent on the thickness of the passive layers than for the other components.

2) Soft (incompletely sampled) shower electrons generated in the passive layers. Their contribution to the energy resolution scales with $\sqrt{t_{\mathrm{abs}}}$ and is independent on the thickness of the active layers.

3) Soft shower electrons generated in the active layers. Their contribution to the energy resolution scales with $\sqrt{t_{abs}}$ for a fixed thickness of the active planes t_{act}, and with $\sqrt{1/t_{act}}$ for a fixed t_{abs}.

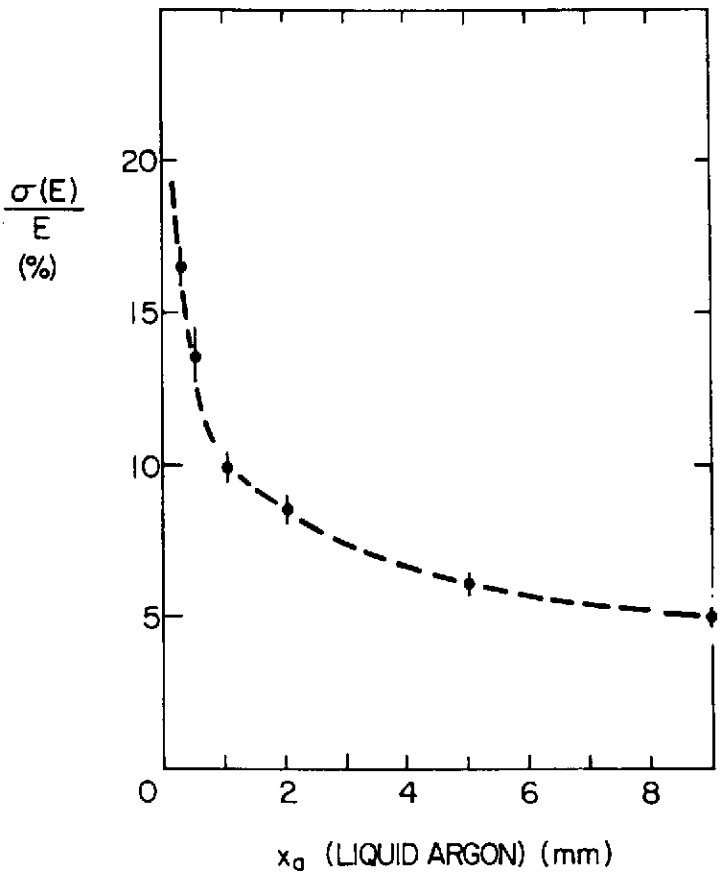

14. Energy resolution vs thickness of the active layers for 1 GeV electron showers in a Fe/LAr sampling calorimeter.

The number of particles in 1) is limited by default. The number of particles in 2) is limited because the electron range cuts off the contribution of the very soft component. The number of particles in 3) is *potentially* much larger than in the other categories, since the low-energy cut-off value is much lower than for 2). A cut-off occurs here only if the γ's that *generate* the electrons can no longer escape from the absorber.

The sampling fluctuations, *i.e* the fluctuations in the *total number* of shower particles observed in the active planes, depend on the relative contribution of these three categories to the signal of a given calorimeter. This is very calorimeter-dependent. Let us illustrate this with a few examples.

i) In iron/liquid-argon (LAr) calorimeters, shower electrons produced in the LAr are the dominating contribution to the signal. This can be concluded from fig. 14 . The energy resolution is to a good approximation proportional to $\sqrt{1/t_{\mathrm{act}}}$, which is characteristic for this component.

ii) This is completely different in calorimeters with gaseous active layers. Owing to the very small sampling fraction, very few γ's will undergo interactions in the gas. Only particles produced in the absorber contribute to the signal. As a consequence, the *number* of detected shower particles per GeV is much smaller than in the previous example, and the fluctuations correspondingly larger. This is confirmed experimentally, since the energy resolution of calorimeters with gaseous readout is always found to be considerably worse than when dense active layers interleave the *same* absorber plates (fig. 15), although part of this effect is due to other phenomena, *e.g.* Landau fluctuations.

iii) A similar effect occurs when the calorimeter consists of high-Z absorber plates and low-Z active planes. The production of soft shower electrons in the active planes is then strongly reduced by the photo-electric effect, for which the cross section is proportional to Z^5. The soft shower photons will, therefore, almost exclusively interact in the absorber layers. As a consequence, the energy resolution for em showers in lead and uranium calorimeters is worse than for iron calorimeters, at the same sampling fraction, which is indeed observed in practice (fig. 15).

These examples illustrate that the energy resolution of sampling calorimeters is a complicated matter, for which no simple formulae can be given. They also illustrate that computer simulations with EGS4 will only give reliable results, if the energy deposition by the soft shower component is treated correctly, *i.e.* if cut-off values in the keV region are used.

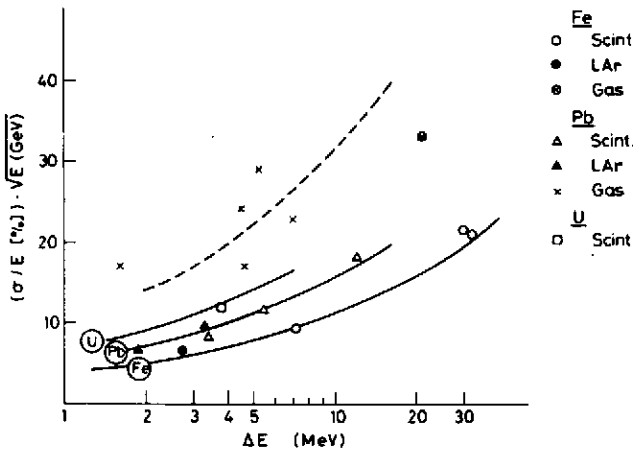

15. Measured values of the energy resolution for electrons with different sampling calorimeters; ΔE is the energy loss by a minimum ionizing particle in a single sampling layer.

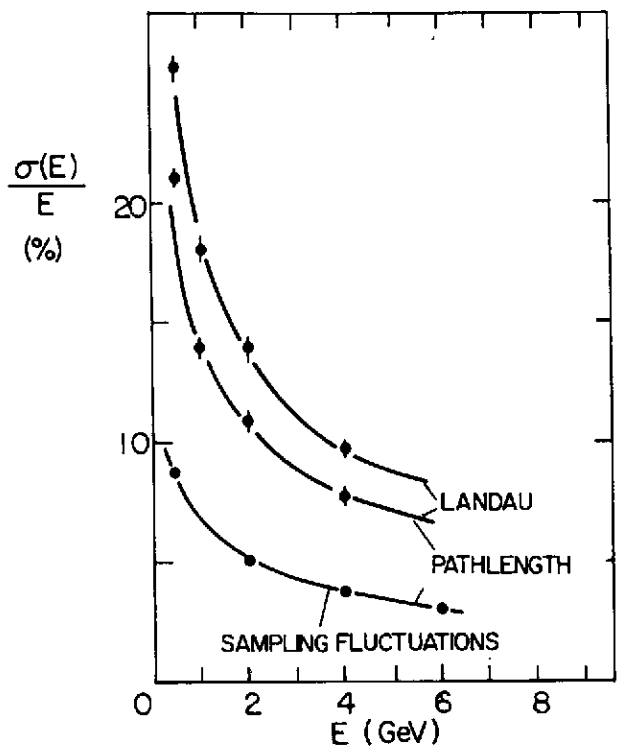

16. The contribution of sampling, Landau and path length fluctuations to the energy resolution for em showers in a gas sampling lead calorimeter. Results of calculations from ref. 9 .

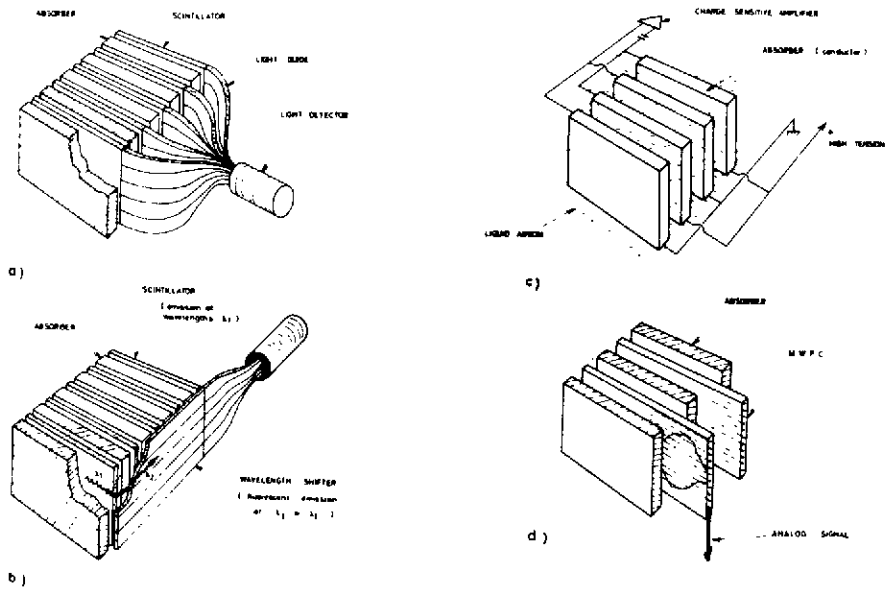

17. Schematic representation for frequently used calorimeter readout techniques: Scintillator plates individually coupled to a photomultiplier (a). Scintillator plates read out by WLS plates (b). Charge produced in an electron-transporting medium (e.g. LAr) collected at electrodes (c). Charge produced in a gas, amplified internally, and detected on suitable readout wires (d).

The fluctuations in the number of shower particles contributing to the signal give certainly a major contribution to the energy resolution of sampling calorimeters. In a more refined treatment, one should also consider the fluctuations in the *energy* that individual electrons deposit in the active layers. Such fluctuations will occur because of the *angular distribution* of the electrons travelling through the gaps. In calorimeters with dense active layers, the effect of these *path length fluctuations* is generally small, because the range of the electrons that dominate the signal is compatible to the thickness of a typical active layer, so that the angle at which the electron traverses the plane makes little difference to the signal.

This is different for calorimeters with gaseous active media, where electrons travelling *in* the active plane may give signals that are very much larger than particles crossing the plane perpendicularly. Figure 16 shows the results of calculations by Fisher[9] on the various contributions to the energy resolution of gas sampling em calorimeters. Also in calorimeters with very thin non-gaseous active layers like Si, the contribution of path length fluctuations to the energy resolution is probably not negligible. The typical thickness of 0.2 mm Si corresponds to the range of $\sim$ 0.2 MeV electrons, well below the effective cut-off value for electrons generated in the absorber and penetrating the active layers, so that the angular distribution of these electrons is important for the calorimeter signal.

3. READOUT TECHNIQUES FOR SAMPLING CALORIMETERS

For the active layers in sampling calorimeters, both for detecting em and hadronic showers, a variety of possibilities exist, which we briefly review in this section. The choice for using either one of these options in a particular calorimeter will be imposed by the requirements on the calorimeter performance. These requirements frequently concern:

a) The energy resolution.

b) The signal linearity, as a function of energy.

c) The signal uniformity: The signal should, ideally, *not* depend on the spatial position of the detected particle.

d) The position resolution, intimately linked to the readout *granularity*.

e) The hermeticity: The fraction of the solid angle which is occupied by support structures and other "dead" elements, rather than by the sensitive detector volume.

f) The rate capability, crucial at hadron colliders (see fig. 5).

g) The radiation resistivity of the active material.

h) The electronic stability, and possibilities for calibrating the detector.

i) The capability of operating in a magnetic field.

j) The compactness.

The relative importance of these requirements depends on the type of accelerator, and on the energy domain that is covered. Cost aspects are frequently a limiting boundary condition.

Energy resolution and signal linearity of hadron calorimeters are a major item in the next sections. We will keep the other mentioned requirements in mind when discussing the various readout options below.

All active media applied so far in sampling calorimeters are based on the detection of either scintillation light or electrical charge induced by the charged shower particles in the active detector planes.

3.1 Plastic scintillators

Scintillating plastic has become very popular as active medium in sampling calorime-

ters. The material is cheap and allows a simple and compact construction. In addition, the signal readout technology is easy and reliable. Most systems consist of a sandwich structure of absorber plates interleaved with scintillator sheets. The light is read out through wave length shifter (WLS) plates, which run perpendicular to the sampling layers and which are optically coupled to a device that transforms the light in an electrical signal, *e.g.* a photomultiplier (fig. 17 b). The scintillation light travels through internal reflection to the edge of the plate, crosses a thin air gap, is absorbed and reemitted at a longer wave length, better matched to the sensitivity of the photocathode, to which it continues its journey under 90^0 through internal reflection in the WLS plates.

This scheme replaces the cumbersome and expensive structures in which each individual scintillator plate is optically coupled to a photomultiplier (fig. 17 a), and minimizes the dead space. The prize to pay for this advantage concerns the number of detected photons. Photo-electron statistics is usually marginal in such devices (sect. 2.5).

Another important advantage of scintillator readout concerns the rate capability. The response time of plastic scintillators is extremely short, and time resolutions of a few ns can be achieved for shower detection. The main *disadvantages* compared to other systems concern the granularity, the signal uniformity and, at least for some types of scintillator, the radiation sensitivity.

A very interesting new development is the use of scintillating *fibres* instead of sheets. The fibres are embedded in a metal matrix, and are running parallel to each other, roughly in the direction of the particles that one wants to detect. This scheme offers major advantages concerning almost all the points mentioned in the list of requirements[10] and may well turn out to be the ultimate calorimeter configuration.

3.2 Charge collection

The charge produced by the passage of charged shower particles may be collected from solids, liquids or gases.

3.2.1 Silicon

The mechanism of charge creation in semiconductor devices was outlined in sect. 2.1. Silicon layers have been successfully used as active material in small em sampling calorimeters. The specific advantages of this technique concern the compactness, the granularity, the signal uniformity and stability, and the rate capability.

The Si layers are very thin (< 0.5 mm), permitting the construction of extremely

compact devices ($X_0 < 4$ mm). They can be segmented to a very high degree (*cf.* strip detectors), hence offering the ultimate localization of showers. Silicon is approximately as fast as scintillation counters, but it is more stable than these.

The disadvantages of the inherent small sampling fraction were already discussed in sect. 2.5. Other disadvantages concern the large cost of a full size Si sampling calorimeter, and the vulnerability of Si to neutrons which cause lattice dislocations.

Nevertheless, Si is being considered as one of the options for a hadron calorimeter at a supercollider experiment[11].

3.2.2 Liquid media

The other detectors discussed in this section detect *ionization* charge. Liquid media can only detect this charge in an ionization chamber mode, *i.e.* without any internal signal amplification (fig. 17 c). In order to be effective, one needs a liquid in which the electrons released by the ionised atoms or molecules may drift freely over sufficiently long distances (cm), given an electric field of adequate strength. Inert elements are suited for this purpose (that's why they are inert), provided that the level of electron-absorbing impurities (*e.g.* O_2) is sufficiently low. Liquid argon is the best known example, the oxygen concentrations should be kept at less than 1 ppm, which is no major problem in practice.

The specific advantages of LAr concern the long-term operating stability, owing to the absence of radiation damage. Like Si, it can be finely segmented, and the response is uniform to better than $\sim 1\%$. The weak points of this technique concern the hermeticity, a consequence of the fact that the detector has to be cryogenically operated, and the rate capability. The latter problem is common to all techniques based on electrons drifting over macroscopic distances. The charge collection time is larger than 100 ns, most frequently ~ 1 μs in such devices.

More recently, liquids have been developed which offer similar advantages as LAr, but can be operated at room temperature, thus avoiding the dead space taken by the cryogenics, and the related problems with hermeticity. They carry code names like TMS, 2.2,4,4 TMP, Neopentane, 2,2 DMB, *etc.* Their feasibility remains yet to be demonstrated in a large scale experiment. The tolerable impurity level is orders of magnitude lower than for LAr, requiring space-type technology for production (ultra-high vacuum, *etc.*). The signal-to-noise ratio, already a non-negligible problem for LAr, is worse by at least a factor of 5 in these liquids. In terms of energy resolution and signal linearity, they offer a *potential* advantage relative to LAr (sect. 6,7).

3.2.3 Wire chamber readout

Wire chambers serving as active elements in sampling calorimeters can be operated in a *proportional* or a *saturated* (Geiger, streamer, flash tube) mode (fig. 17 d). The ionization charge is internally amplified through avalanche development, and detected on sense wires. Like for liquid media and Si, a very good spatial resolution can be achieved. Another advantage of this technique is the low cost.

The disadvantages concern the energy resolution (see sect. 2.5), a consequence of the extremely small sampling fraction, and the rate capability. The devices operating in a saturated mode ("digital" calorimeters or quantameters) suffer in addition from quite severe signal alinearities. One charged particle causes an insensitive region along the struck wire, which prevents nearby particles from being detected.

Much more information about calorimeter readout technology is given in the paper by Fabjan[1] .

4. CHARACTERISTICS OF HADRON SHOWERS

4.1 General properties

Conceptually, the calorimetric energy measurement of hadron showers is the same as for em showers, but the large variety of possible interaction processes complicates the detailed understanding of the calorimeter response.

When a high-energy hadron penetrates a block of matter, it will at some point interact with one of the nuclei in this block. In this process, usually mesons are produced (π, K, *etc*). Some other fraction of the particle energy is transferred to the nucleus. The excited nucleus will release this energy by emitting a certain number of nucleons, and in a later stage γ's, and lose its kinetic (recoil) energy by ionization. The particles produced in this reaction (mesons, nucleons, γ's) may either lose their energy by ionization or induce new reactions in turn, and so a shower develops.

The calorimeter signal is the result of all the charged particles produced in this process, which ionise the active calorimeter layers. The much larger variety of interaction processes implies much larger fluctuations in the shower development compared to purely em showers, and therefore it is no surprise that the energy resolution for calorimetric hadron detection is worse.

Since the hadronic shower development is (for an important part) based on *nuclear* interactions, its dimensions are governed by the *nuclear interaction length* $\lambda_{\rm int}$. The interaction probability is determined by the fraction of a two-dimensional plane occupied by atomic nuclei; if we assume that the number of atoms per unit volume is material independent, $\lambda_{\rm int}$ will scale with the nuclear radius, *i.e.* as $A^{1/3}$. Figure 18 shows the results of measurements that give a good impression of the longitudinal and lateral development of 300 GeV π^- showers in uranium. The profiles look very similar to em showers (figs. 11,12), be it that the scale is very different. In this example it takes $\sim$ 80 cm to contain the pion shower at the 95 % level, while 10 cm would be sufficient for electrons at the same energy.

The leakage as a function of the detector depth is shown in fig. 19, for hadron energies ranging from 5 to 210 GeV. It turns out that the detector size needed to contain e.g. more than 99% of the shower energy increases only very slightly with the energy, from 6 $\lambda_{\rm int}$ at 5 GeV to 9 $\lambda_{\rm int}$ at 210 GeV.

One may use the differences in the characteristic energy deposit for *particle identification*. The separation between electromagnetically interacting particles (e, γ, π^0) and hadrons works best for high-Z materials. This is illustrated in fig. 20 where the ratio between $\lambda_{\rm int}$ and X_0 is given as a function of Z, showing an almost linear dependence. Figures 21 and 22 show examples of e/π separation based on the longitudinal and lateral shower information, respectively, obtained with a uranium/plastic-scintillator calorimeter[14] . The lateral cell-size was 20×20 cm^2. The lateral distinction between electrons and pions would of course become much more pronounced if this cell-size would be reduced to a few Molière radii, *e.g.* 5×5 cm^2.

4.2 Introduction to the optimization of hadron calorimetry

Calorimeters for the detection of electromagnetically interacting particles (e,γ) are well understood and can be reliably simulated in great detail by Monte-Carlo techniques (e.g. EGS4). This is by no means the case for hadron calorimeters. To date there exists no computer program that is capable of simulating the complete development of a hadronic cascade and predicting reliably the response of a given calorimeter to it. As a consequence, progress in this area of detector technology had to proceed on a trial-and-error basis for a long time. Many results obtained in this process were considered extremely confusing.

The crucial role of the so-called e/h signal ratio for the energy resolution was already recognized in the early days of hadron calorimetry[15] . The R807 group at CERN demonstrated that energy resolutions of $35\%/\sqrt{E}$ could be achieved for hadron detection

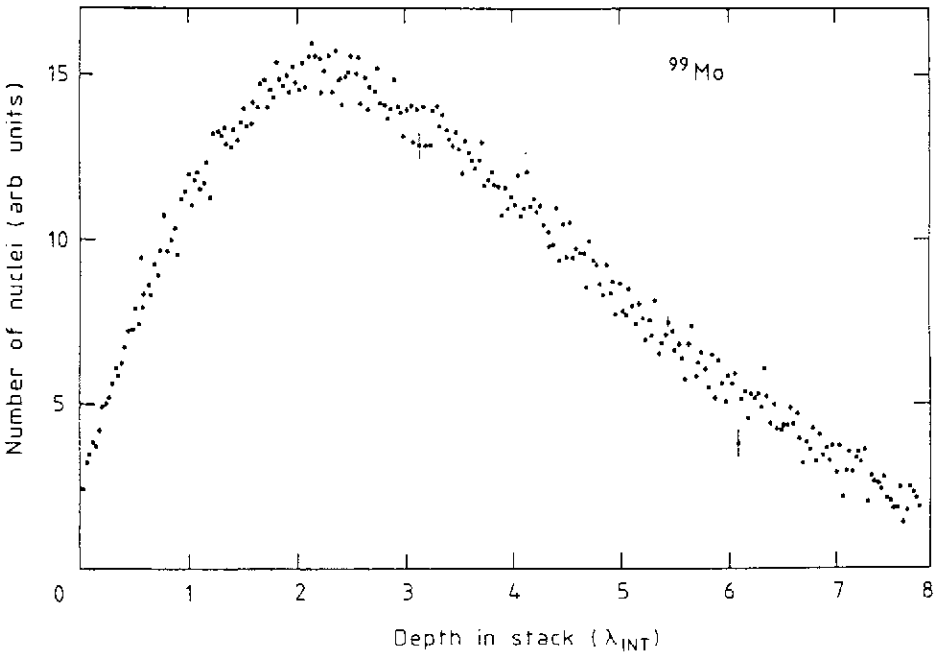

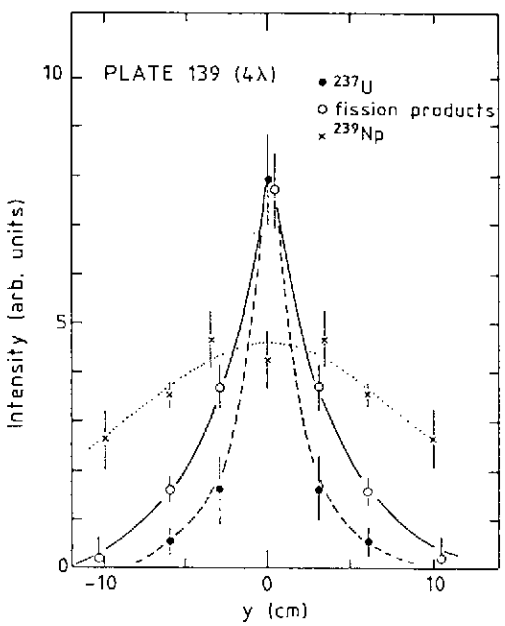

18. Longitudinal and lateral shower profiles for 300 GeV π^- interacting in a block of uranium, measured from the induced radioactivity. Data from ref. 12.

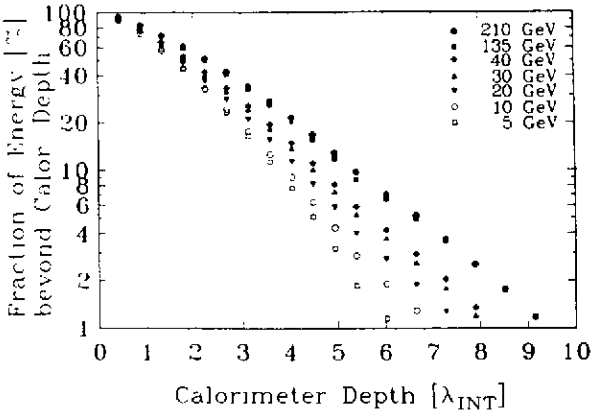

19. The leakage as a function of the detector depth, for pions from 5 - 210 GeV, measured in a uranium/plastic scintillator calorimeter. Data from ref. 13.

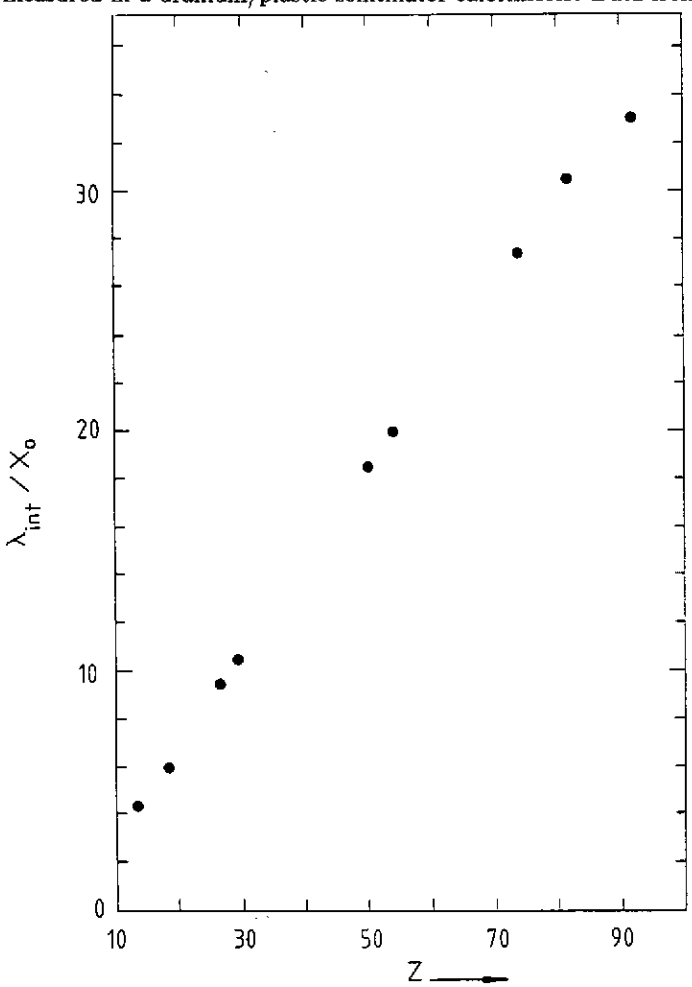

20. The ratio of the nuclear interaction length and the radiation length as a function of Z.

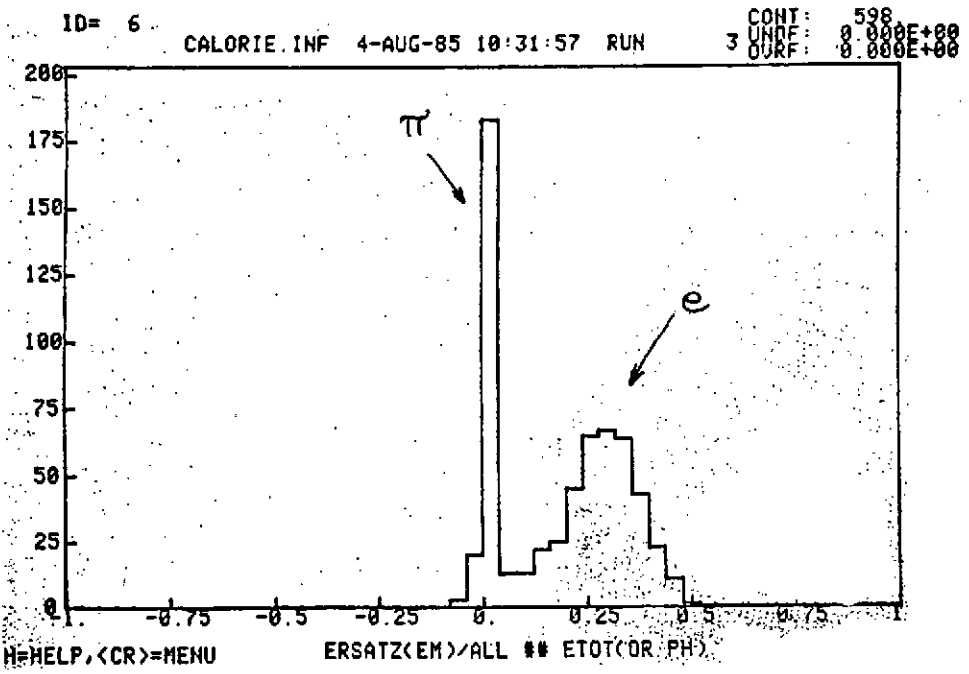

21. Electron /pion separation from longitudinal shower information. The distribution of the fraction of the signal recorded in the first 6 X_0 of a uranium/plastic-scintillator calorimeter, for a mixed e/π beam. Data from HELIOS[114] .

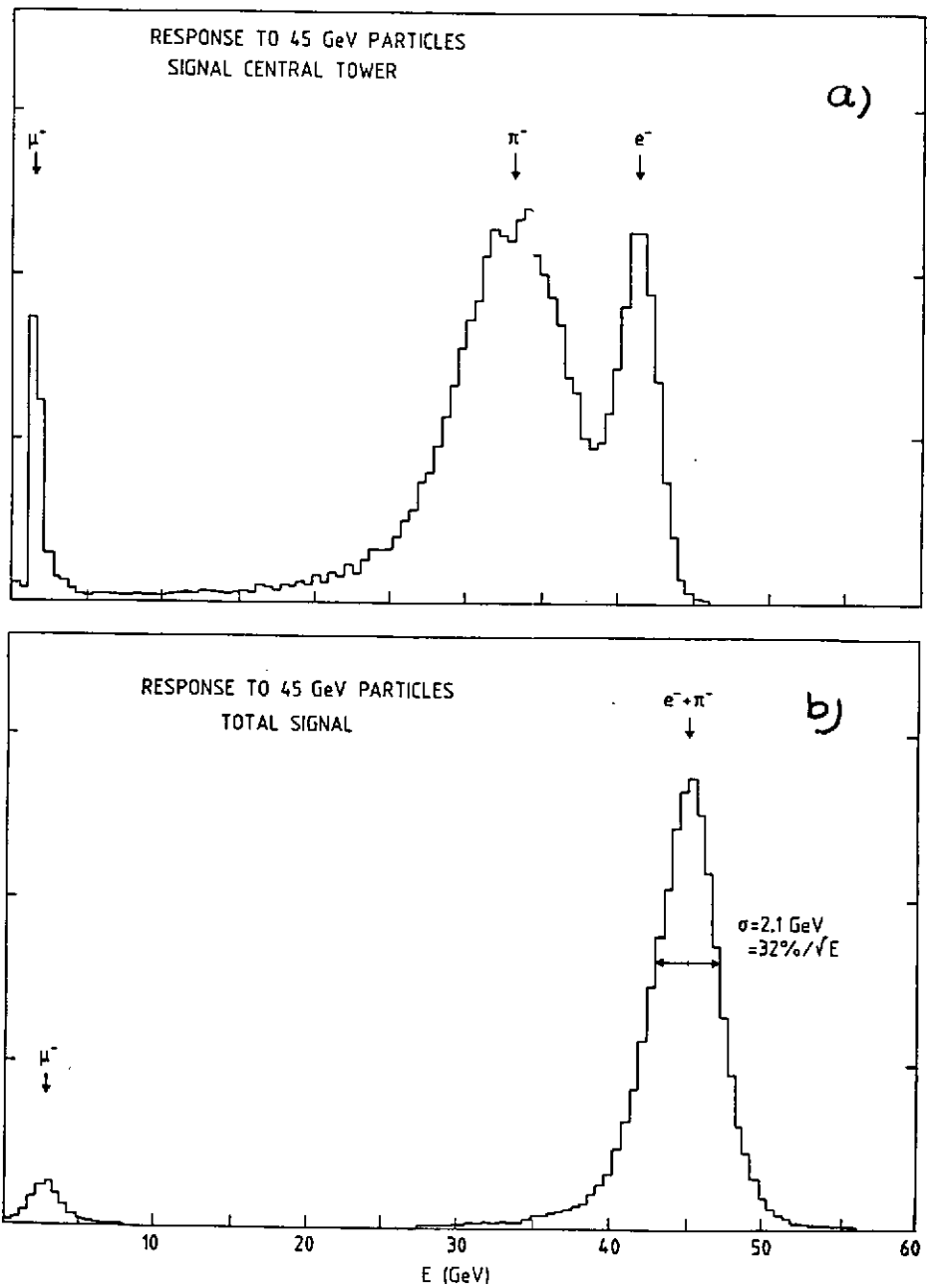

22. Electron/pion separation from lateral shower information. The signal recorded in the central 20×20 cm^2 tower (a) and the *total* signal (b) of a uranium/plastic-scintillator calorimeter, for a mixed e/π beam at 45 GeV. Data from HELIOS[14]

with their uranium/plastic-scintillator sandwich calorimeter, which had an e/h ratio close to the desired value 1.0[16] . Measurements performed by HELIOS recently showed that the energy resolution of this detector scales with $E^{-\frac{1}{2}}$ up to the TeV regime, and that deviations from signal linearity are negligible over 3 orders of magnitude in energy[14] .

Measurements performed with non-compensating ($e/h \neq 1$) devices, however, showed considerable deviations from linearity, and energy resolutions σ/E that do not improve as $E^{-\frac{1}{2}}$ with increasing energy[17] . The constant term that has to be introduced in order to describe the energy resolution is typically 5 % and, therefore, dominates the result at energies beyond 100 GeV, where the new physics has to be found.

However, the use of ^{238}U as absorber material is by no means a guarantee for superior performance. Prototype tests by SLD and D0, using liquid argon readout, gave disappointing results, to the extent that SLD even abandoned the idea of using uranium and switched to a lead absorber that gave results of similar quality. Also the combination uranium/plastic-scintillator turned out not to be magic: WA78 found overcompensation ($e/h \approx 0.8$) and rather poor energy resolutions[18] . On the other hand Brückmann *et al.* from the ZEUS Collaboration, who basically copied the HELIOS design for their prototype studies, found equally good performance[19] .

Recently, understanding of hadron calorimetry has considerably improved. We systematically investigated in detail the response of a sampling calorimeter to the various components of a hadron shower[20] . It turned out that the calorimeter performance in terms of energy resolution and signal linearity is crucially determined by its response to the abundantly present soft neutrons in the shower. The presence of a considerable fraction of hydrogen atoms in the readout medium is essential for the best possible performance. Firstly, this allows one to tune e/h to the desired value (1.0) by choosing the appropriate sampling fraction. And secondly, the efficient neutron detection via recoil protons in the readout medium itself reduces considerably the effect of fluctuations in binding energy losses at the nuclear level, which dominate the intrinsic energy resolution. The confusing experimental results mentioned before were quite nicely reproduced in this study.

In these notes, the theoretical framework that lead to this improved understanding is briefly described. In section 5, we will discuss how the e/h value affects the calorimeter performance. In section 6, we describe how the properties of the passive and active calorimeter materials determine its e/h value. In section 7, the factors that determine the energy resolution of practical calorimeters are examined.

5. EFFECTS OF e/h ON THE PERFORMANCE OF HADRON CALORIMETERS

Since calorimetry is based on statistical processes, the measurement accuracy increases with energy, contrary to tracking detectors based on momentum analysis in a magnetic field. This is a very attractive feature. When a particle develops a shower in a block of matter that we call a sampling calorimeter, some fraction of its energy is transformed into a measurable signal, usually a pulse of electrical charge. This pulse is the result of all the charged particles generated in the shower development, that traverse and ionise the active layers of the detector. The energy resolution for detecting the original particle is determined by the fluctuations occurring in this process, which affect the size of the resulting signal. Amongst these we mention

a) Sampling fluctuations, due to the fact that only a (small) fraction of the energy is deposited in the active layers and, therefore, contributes to the calorimeter signal. It has been shown[18] that if this fraction is larger than $\sim 1\%$, the effect is dominated by fluctuations in the total number of gap crossings by charged particles generated in the shower. Therefore, the contribution of this source of fluctuations is, to first order, for a given absorber material proportional to the square root of the thickness of the absorber plates, and insensitive to the type and thickness of the active layers. The latter part of this statement is not correct if the active layers are so thin (expressed in g/cm^2), that the statistical fluctuations in the number of ionization processes per gap crossing become important. This is for example the case for gaseous media, where Landau and path length fluctuations dominate those mentioned before. In *electromagnetic* sampling calorimeters, sampling fluctuations are the major contribution to the energy resolution.

b) Fluctuations in the fraction of the energy deposited in the form of ionizing particles. These effects usually dominate the energy resolution of *hadron* calorimeters. An obvious component comes from incomplete shower containment, *i.e.* from secondary particles like $\mu, \nu, \mathrm{n}, \mathrm{K}^0_\mathrm{L}$, etc. that (partly) escape detection. A somewhat less obvious, but usually far more important source of fluctuations comes from the energy losses at the nuclear level. The energy needed to release the nucleons and nucleon aggregates like α-particles that are bound in atomic nuclei, is lost for detection. The fraction of the initial hadron energy spent in this way is considerable, up to $\sim 40\%$ on average for the non-electromagnetic part of hadron showers in high-Z elements. Due to the enormous variety of possible nuclear interactions, the fluctuations about this number are a major contribution to the energy resolution of hadron calorimeters.

The latter class of effects has no equivalent in electromagnetic showers. This has consequences for calorimetric hadron detection. Firstly, the signal distribution for hadrons of energy E will be broader than for electromagnetic showers at the same energy, because of the larger fluctuations. Secondly, the average response (signal per unit of energy) will have a different value for electromagnetic and hadronic showers ($e/h \neq 1$). Because of the losses mentioned before, the latter will in general be smaller ($e/h > 1$).

In the development of a shower generated by a high-energy hadron some fraction (f_{em}) of the energy is usually spent on the production of π^0's and η's. A hadron shower, therefore, has in general an electromagnetic (em) and a non-electromagnetic component. Because of the reasons just given, the calorimeter response to these components will be different (see fig. 23). The fluctuations in f_{em} are large and non-Gaussian. Moreover, $< f_{em} >$ increases (logarithmically) with energy. If $e/h \neq 1$, this has the following consequences for the calorimeter performance:

i) The fluctuations in f_{em} give an additional contribution to the energy resolution.

ii) Because of the non-Gaussian nature of the fluctuations in f_{em} the energy resolution σ/E will not improve as $E^{-\frac{1}{2}}$ with increasing energy.

iii) The signal distribution for mono-energetic hadrons (the *line shape*) is not Gaussian.

iv) The calorimeter signal is not proportional to the hadron energy (alinearity).

v) The measured e/h signal ratio is energy dependent.

All these effects have been experimentally observed. This is illustrated by fig. 24 , which shows experimental data on calorimetric hadron detection with an iron/plastic-scintillator ($e/h \approx 1.4$) calorimeter[17] , and with uranium/plastic-scintillator[14] ($e/h = 1$). The energy resolution obtained with iron is much worse than for uranium and it does not scale as $E^{-\frac{1}{2}}$. The calorimeter response for iron rises with energy, and consequently the e/h signal ratio decreases as the energy is increased. Such effects are absent for uranium.

To avoid the confusion caused by the latter effect, we prefer to use the energy-independent quantity $e/h^{\rm intr}$, given by the ratio of the mean values of the two curves in fig. 23 . The relation between $e/h^{\rm intr}$ and e/h is given by

$$e/h(E) = \frac{e/h^{\rm intr}}{1 - < f_{em}(E) > [1 - e/h^{\rm intr}]}$$

where

$$< f_{em}(E) > = 0.1 \ln E(\mathrm{GeV})$$

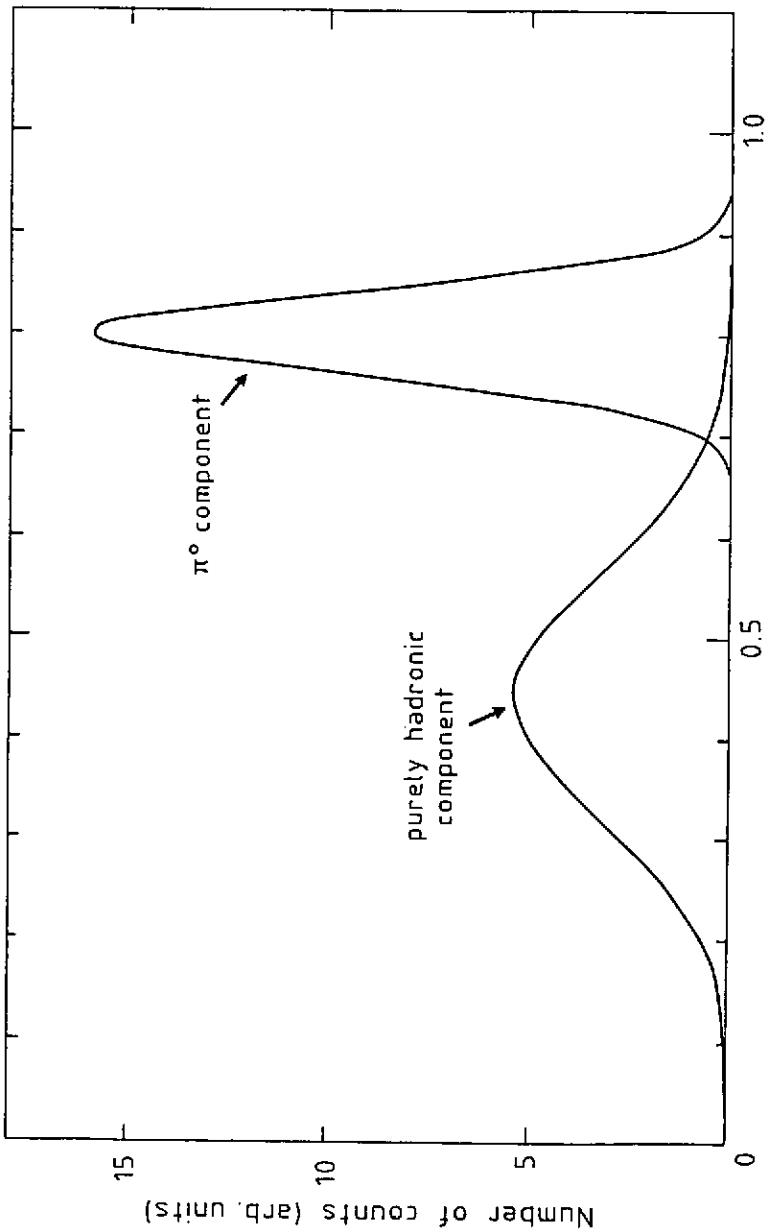

23. The calorimeter response to the em and non-em components of a hadron shower.

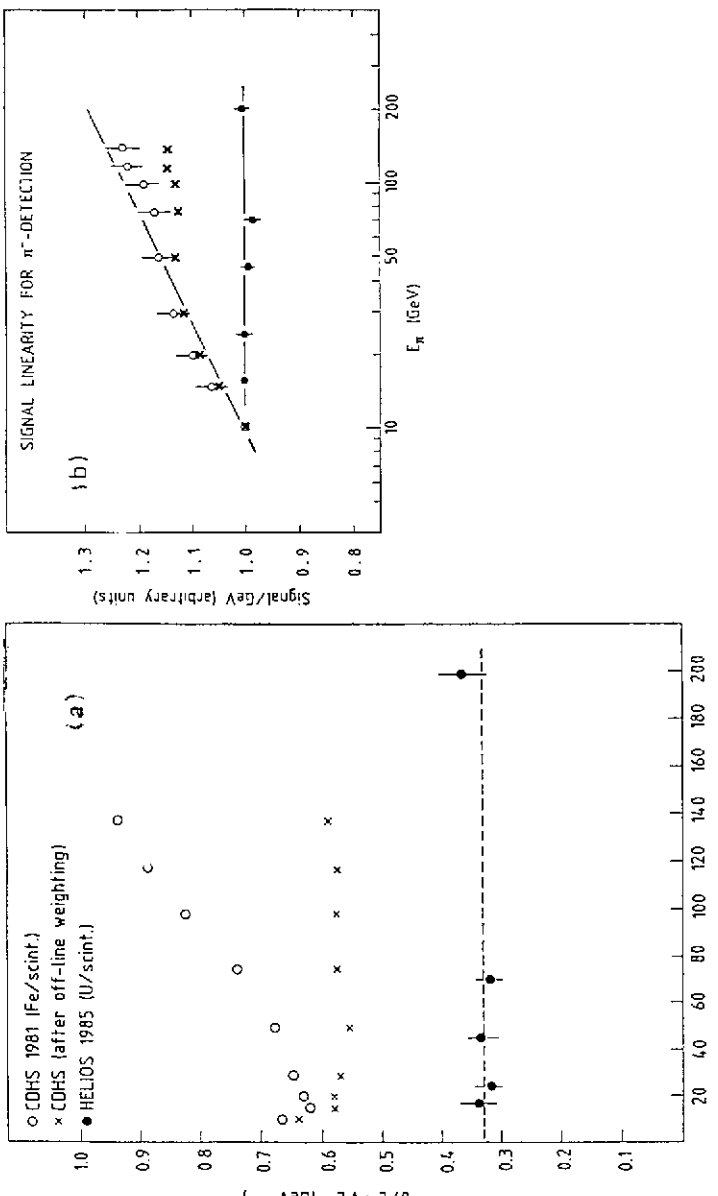

24. Experimental data obtained with an iron/plastic-scintillator calorimeter (the open circles), and with uranium/plastic-scintillator (full circles). The crosses represent the off-line weighted iron results. Data are given on energy resolution (a) and linearity (b) as a function of energy.

is a reasonable approximation in the energy range 10 - 100 GeV[21] . At 10 GeV, where e/h ratios are frequently given, the difference between the measured e/h value and $e/h^{\rm intr}$ is usually small, less than 10%.

We investigated the effects of $e/h \neq 1$ on the calorimeter performance with a very simple Monte Carlo simulation, making some reasonable assumptions on the widths of the distributions in fig. 23 , on $< f_{\rm em}(E) >$, and on the fluctuations in $f_{\rm em}(E)$. The results are given in fig. 25 , where curves for the energy resolution and the calorimeter response are plotted for various values of e/h(10 GeV). The data on the energy resolution are plotted using an abcissa linear in $E^{-\frac{1}{2}}$. This shows that the deviation from $E^{-\frac{1}{2}}$ scaling can be very reasonably described as a constant term, the value of which is determined by e/h. This figure makes it very clear that, in particular at high energies, the value of $e/h^{\rm intr}$ is crucial for the energy resolution that can be obtained. For the CDHS calorimeter ($e/h = 1.36$ at 10 GeV), the resolution σ/E does not become better than $\sim$ 7%, even at the highest energies. For calorimeters with $e/h^{\rm intr} = 1$, the energy resolution will continue to improve with increasing energy, until limitations due to instrumental effects become important. HELIOS have experimentally shown that energy resolutions close to 1% are feasible for such devices[14] .

If $e/h = 1$, the contribution of fluctuations in $f_{\rm em}$ to the energy resolution are eliminated. It has been advocated that there are other ways to (partly) achieve this goal. The em and non-em shower components have very different characteristic dimensions, particularly in high-Z absorber materials. If the calorimeter is sufficiently finely segmented one might, therefore, determine $f_{\rm em}$ on an event-by-event basis and hence eliminate, at least partly, the effects of fluctuations in this number. The CDHS Collaboration developed an algorithm for this purpose, with which they were able to restore $E^{-\frac{1}{2}}$ scaling for the energy resolution of single pion detection in their very fine-grained detector (read out every 7 radiation lengths in depth)[17] . Unfortunately, alinearities of $\sim$ 10% remained after this procedure, which involved energy-dependent weighting factors (see fig. 24). This means that the procedure will probably not work (as well) for the detection of jets, where the showers generated by individual hadrons overlap, and where the number of jet particles and their energy is not a priori known. In any case, these methods have never been experimentally demonstrated to improve the resolution under such conditions.

Apart from the signal alinearities and the degradation of the energy resolution, $e/h \neq 1$ has another, probably even more dramatic consequence for the calorimeter performance. The non-Gaussian line shape will cause severe problems if one wants for example to trigger on transverse energy[21] . It will be practically impossible to unfold the steeply falling $E_{\rm T}$ distribution (fig. 5) and the line shape. Moreover, severe *trigger biases* are likely to occur: If $e/h > 1$ (< 1), one will predominantly select events

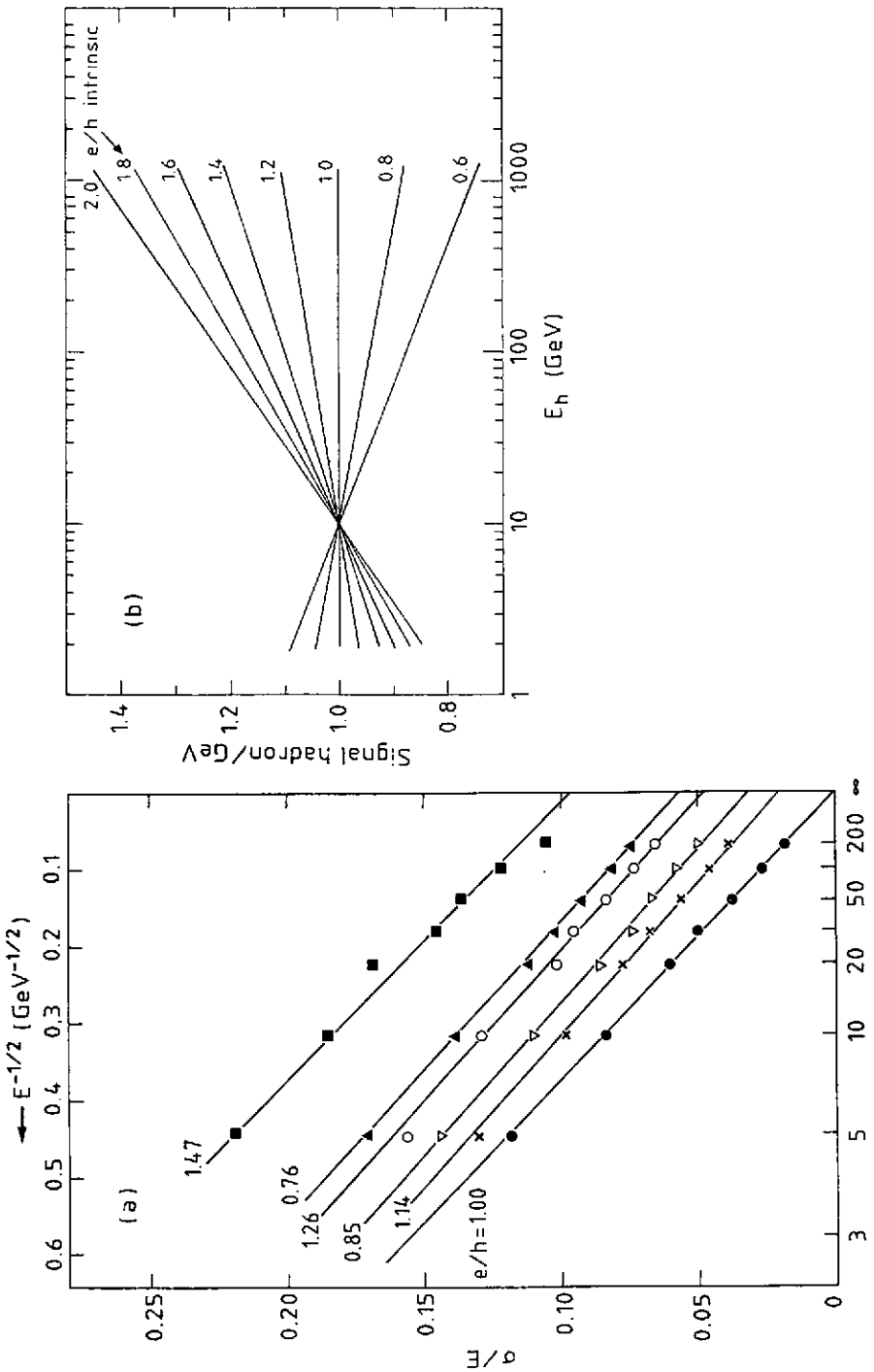

25. Monte Carlo simulation of the effects of $e/h \neq 1$ on the energy resolution and signal linearity of hadron calorimeters.

that contain little (a lot of) em energy from π^0's. This is illustrated by fig. 26, which shows pulse height distributions for hadrons and electrons, measured with the overcompensating WA78 calorimeter[13]. The curves represent Gaussian fits to the data. The hadron pulse height distribution clearly shows deviations of the Gaussian shape, which are typical for the fluctuating π^0 content of the shower.

Because of these reasons, we think that a calorimeter with $e/h^{\rm intr} = 1$ has essential advantages, which cannot be compensated for by a very fine-grained readout in case $e/h \neq 1$. We will now examine which factors determine the e/h signal ratio, and how this ratio is affected by the properties of the calorimeter materials.

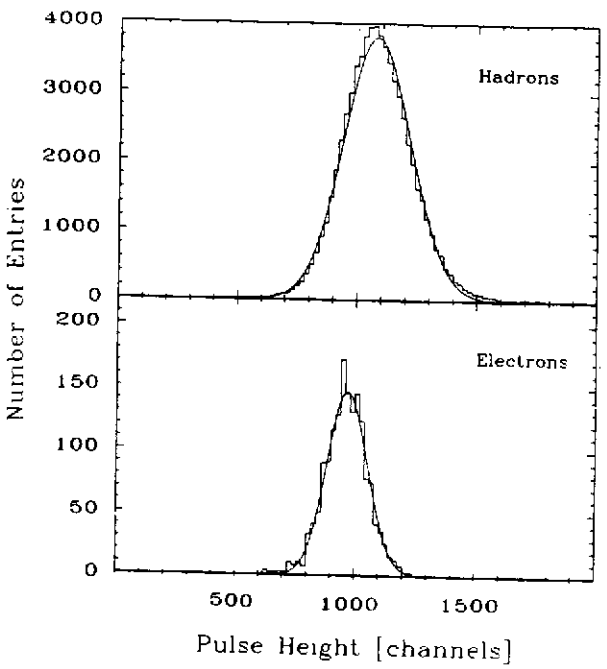

26. Pulse height distribution for 30 GeV pions and electrons in an overcompensating uranium/plastic-scintillator calorimeter ($e/h = 0.8$). The curves represent Gaussian fits. Data from ref. 13.

6. THE CALORIMETER RESPONSE TO THE SHOWER COMPONENTS

6.1 The procedure of calculating e/h

In this section we will investigate the calorimeter response to the various components of a hadron shower. For a particular type of secondary particles, the signal will be determined by two factors:

i) The fraction of the energy used to ionise the active layers.

ii) The ionization density in these layers. Saturation effects may reduce the signal from densely ionizing particles, *e.g.* soft protons, considerably.

We distinguish the following classes of secondary particles:

a) High-energy photons and electrons from π^0 and η decay, that form the em shower component.

b) Ionizing hadrons (charged pions, kaons, protons, etc.).

c) Soft neutrons.

d) Soft γ's from nuclear deexcitation.

As a scale for the calorimeter signal, the response to a minimum-ionizing particle (mip) will be used. The fraction of the energy deposited by such a particle in the active layers of a given sampling calorimeter is called the sampling fraction $f_{\rm samp}$, and can be calculated immediately from the mean dE/dx value's for mip's in the calorimeter materials:

$$f_{\rm samp} = \frac{dE/dx[\text{1 readout layer}]}{dE/dx[\text{1 readout} + \text{1 absorber layer}]}$$

In practical calorimeters $f_{\rm samp}$ amounts to about $5-10\%$ for plastic scintillator or liquid argon (LAr) readout, $\sim 1\%$ for Si and $\sim 10^{-4}$ for wire chambers.

Relating the responses of the 4 mentioned types of particles to mip's, one can schematically write the e/h signal ratio as follows

$$e/h^{\rm intr} = \frac{e/mip}{f_{\rm ion}\, ion/mip + f_{\rm n}\, n/mip + f_\gamma\, \gamma/mip}$$

where $f_{\rm ion}$, $f_{\rm n}$ and f_γ are the average fractions of the energy in the non-em component, that are deposited in the form of ionizing hadrons, neutrons and nuclear γ's. We will now discuss the various terms of this expression.

6.2 The response to high-energy electron and photon showers (e/mip)

The signal from an em shower is the result of the ionization of the active layers by all the electrons and positrons generated in the shower development, which traverse these layers. Naïvely, one might therefore expect that this signal is equal to the one from muons traversing the detector, which lose an amount of energy $\Delta E = E_{\rm em}$. This is in practice usually not the case. Experimentally, one observes that in calorimeters with

high-Z absorber material, the em signal is considerably suppressed with respect to mip's ($e/mip < 1$). If the Z-values of the active and passive media are about equal, like in Fe/LAr, e/mip is close to 1.

For historical reasons these phenomena are usually called transition effects, since it was assumed that they should be attributed to mechanisms affecting the shower composition at the boundary between layers of materials with different Z. This is not true.

The explanation of the transition effects is closely linked to the way in which soft γ's ($E_\gamma < 1\,\mathrm{MeV}$) that are generated in large numbers in an em shower, are absorbed in a mixture of materials. At these low energies, the photo-electric effect is an important mechanism. The cross section for this process is proportional to Z^5, while the ionization cross section for charged particles is to first order proportional to Z. In a calorimeter consisting of high-Z absorber material and low-Z active layers, the soft γ's will, therefore, almost exclusively interact with absorber atoms. Only if the interaction occurs sufficiently close to a boundary can the photo-electron produced in this process contribute to the measured signal. To illustrate this point, it can be mentioned that the mean range of a 1 (0.1) MeV electron in uranium is only 0.4 mm (20 microns). As a result, the calorimeter response to an em shower is suppressed with respect to mip's.

Analysis of shower simulation data from EGS4 clearly support this conclusion. Needless to say that for obtaining accurate results, the program should be run with cut-off values that are sufficiently low to correctly describe the peculiarities of the energy deposition by the soft shower component. Although we are dealing with very soft particles, the total amount of energy carried by them is considerable. The evolution of the computer time needed for the simulation when lowering the cut-off values for E_γ and E_e, is already an indication for this. Figure 13 shows that in lead or uranium calorimeters $\sim 40\%$ of the total energy of a 10 GeV em shower is deposited through ionization by particles softer than 1 MeV, in which energy region the photo-electric effect is the dominating process.

For what concerns the response of high-Z sampling calorimeters, em showers consist of two rather well-separable components: The hard part ($> 1\,\mathrm{MeV}$), that can be reasonably described as a bunch of mip's, and the soft part ($< 1\,\mathrm{MeV}$) for which the detector is less efficient. This has some quite interesting consequences for (hadron) calorimetry, all of which are confirmed by EGS4 calculations:

a) The e/mip ratio changes with the depth of the shower, since the relative contribution of both components is a function of depth: The shower gets softer as the depth increases. In a longitudinally segmented calorimeter, calibrated with muons, the energy deposited by an electromagnetic shower in individual segments will be wrongly measured if the shower exceeds a segment boundary, although the *total* energy may be correct.

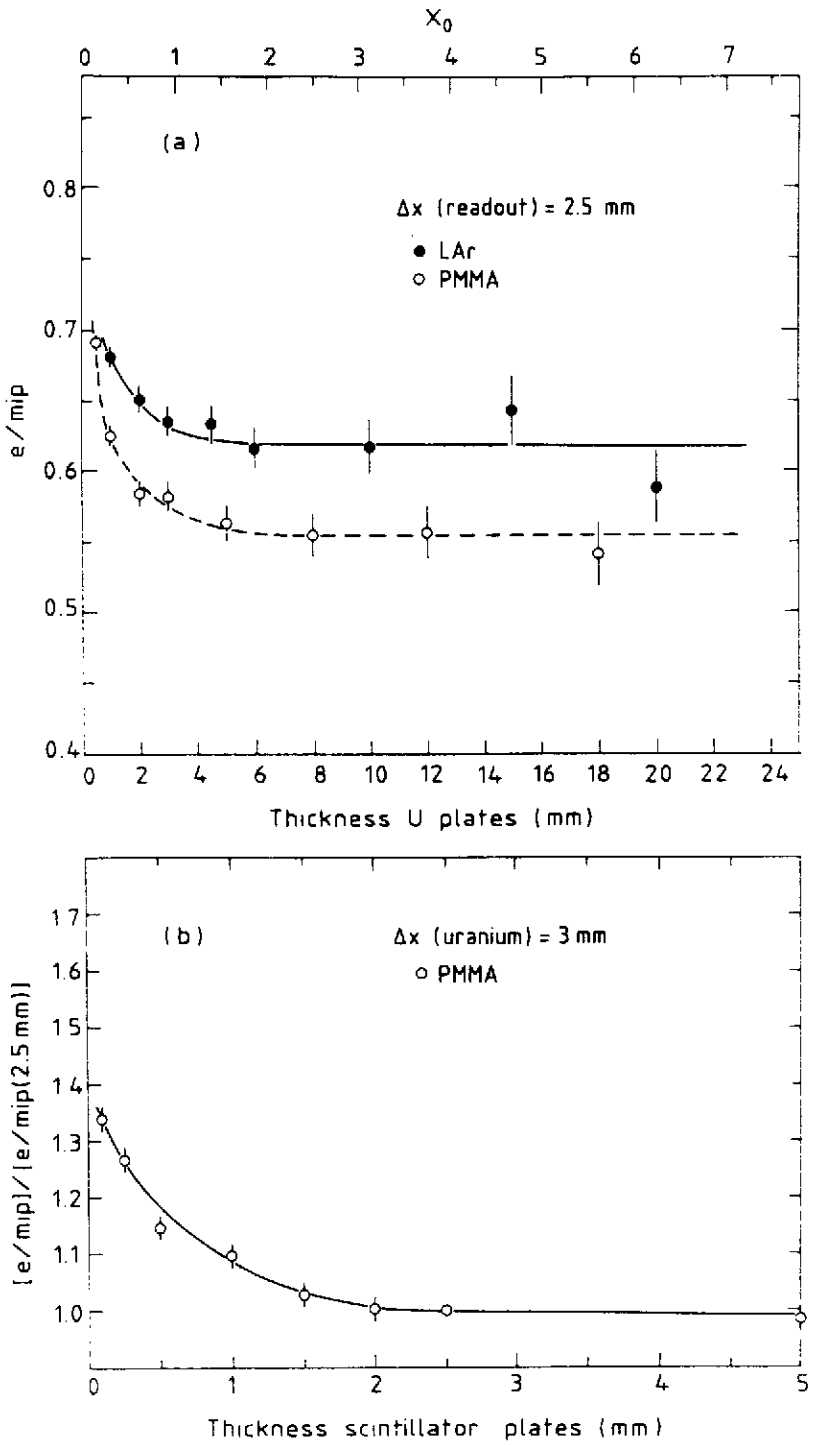

27. The *e/mip* signal ratio as a function of the thickness of the active (a) and passive (b) layers, for uranium calorimeters. Results from EGS4 calculations.

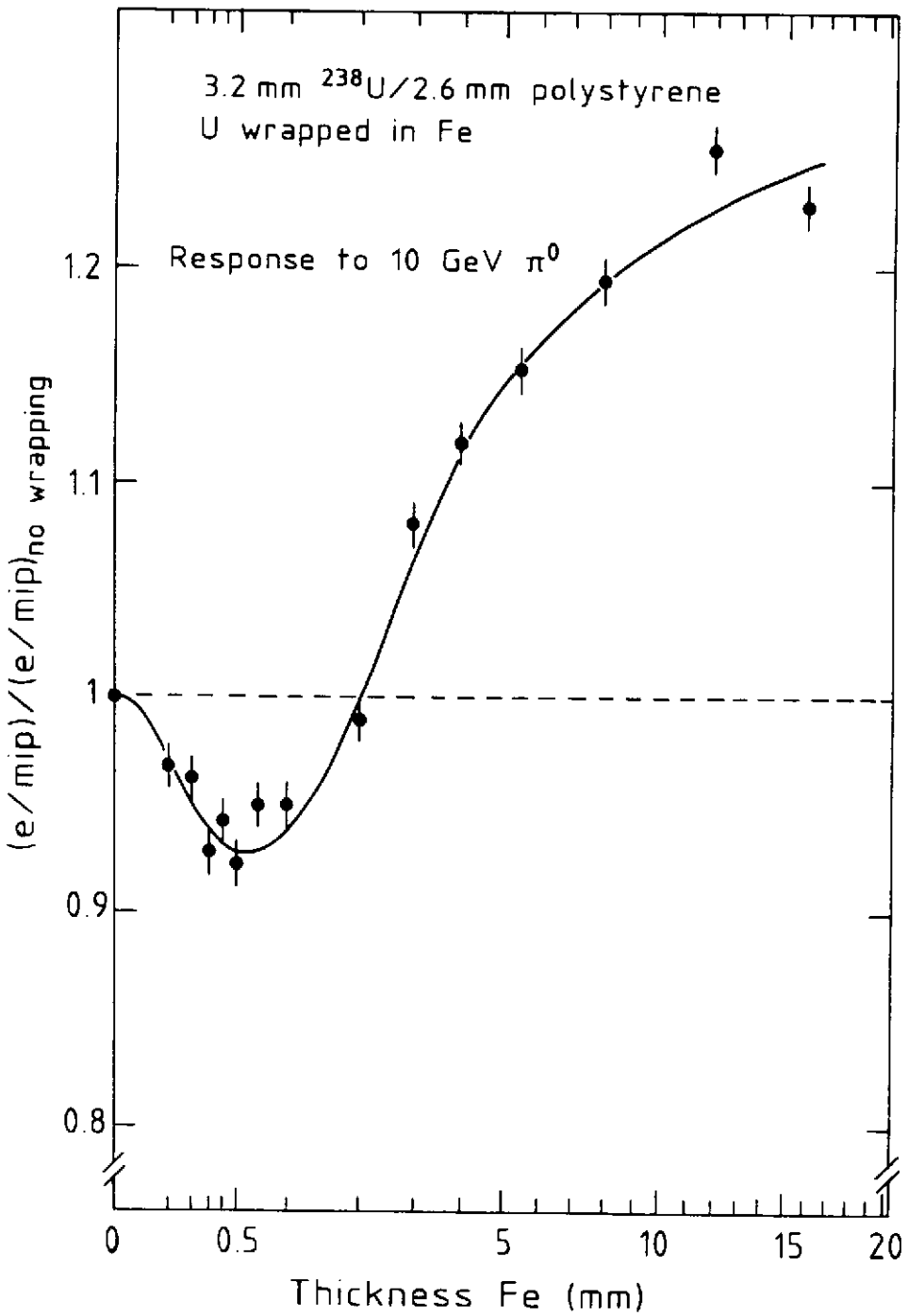

28. The effect of stainless steel wrapping of the absorber plates on the *e/mip* value of a uranium/plastic-scintillator calorimeter. The vertical scale is normalized to the case where no steel is applied. Results from EGS4 calculations.

b) One can tune the e/mip, and hence the e/h value to a certain extent, since the relative contribution of the soft component to the calorimeter signal depends on the thickness of the absorber layers and also on the thickness of the active layers (see fig. 27). This can be understood as follows. Only photo-electrons produced close to a boundary contribute to the signal. If they manage to reach the active layers they are usually so soft that they do not penetrate very far. If either the absorber or the readout thickness is decreased, the "effective" boundary region becomes a larger fraction of the calorimeter as a whole and, therefore, the calorimeter response is increased. These effects are mainly important for very fine sampling.

c) In a high-Z calorimeter one may further reduce e/mip by inserting a low-Z foil in between the active and passive layers. This prevents photo-electrons produced in the high-Z material from reaching the active layers. This is illustrated in fig. 28, where the results of EGS4 calculations on a uranium/plastic-scintillator calorimeter are shown. The uranium plates are wrapped in stainless steel, the thickness of which is varied. This wrapping decreases the "intrinsic" e/mip ratio by at maximum $\sim 8\%$ at 0.5 mm Fe. If the wrapping material is made thicker than that, interactions by the shower particles in iron will become more and more important, and tend to increase e/mip because $Z_{\mathrm{Fe}} \ll Z_{\mathrm{U}}$.

The detector inefficiency for the soft component of em showers in high-Z materials is an important ingredient for compensation, since it brings the em response closer to the non-em one. As we shall see later it is, however, not enough.

6.3 The response to nuclear gamma's (γ/mip)

In the non-em part of hadronic shower development large numbers of γ's are produced from nuclear deexcitation. Their energy spectrum depends on the characteristic nuclear level structure of the nuclides involved. In general, the vast majority of these γ's have an energy below 2 MeV.

In the previous subsection we saw that the transition effects observed for high-energy em showers are caused by the reduced detection efficiency for the soft γ shower component. The calorimeter signal suppression for nuclear γ's will, therefore, even be stronger than for these showers. This is confirmed by EGS4 calculations.

Since the mean photo-electron range is extremely energy-dependent, the detection efficiency decreases sharply below 1 MeV (fig. 29). At 0.511 MeV, the energy of the very abundant e^+ annihilation γ's, the signal is already reduced by a factor 7 compared

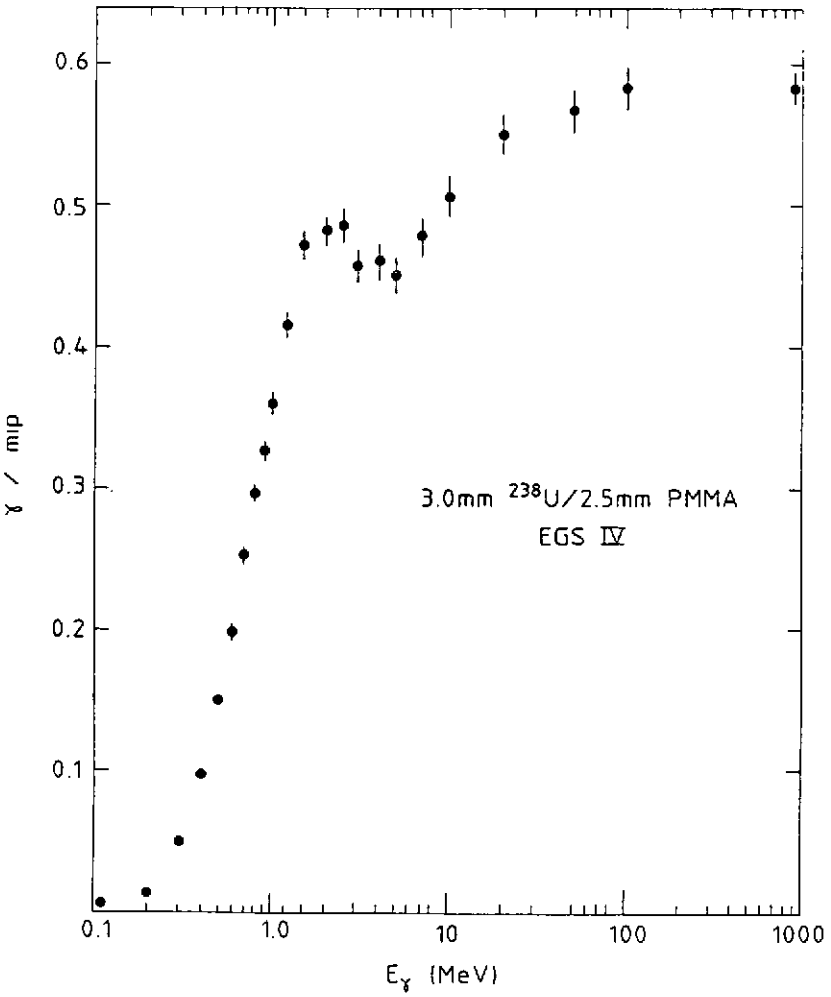

29. The γ/mip signal ratio as a function of E_γ, for a uranium/plastic-scintillator calorimeter. Results from EGS4 calculations.

Early example of the nuclear interaction of a π-meson of energy 3·8 BeV

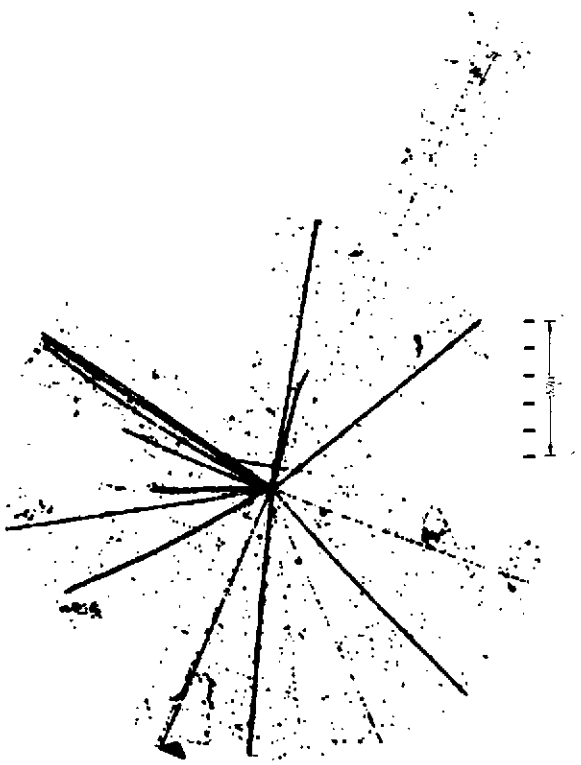

PLATE 11–9

Ilford G.5 emulsion Lock and Yekutieli (1952), unpublished

A π-meson of energy 3·8 BeV entered from a disintegration of type 7 — 10%, produces a secondary disintegration of type 18 — 1π. It is probable, but not established, that several of the lightly ionizing secondary particles are π-mesons

30. A nuclear reaction induced by a 3.8 GeV pion in an emulsion.

to mip's, for the calorimeter in this example (HELIOS). The γ/mip signal ratio needed for the computation of e/h is sensitively dependent on the γ energy spectrum. For the measured spectrum of ^{238}U fission γ's, that was used throughout the calculations, we found γ/mip to be $\sim$ 0.4 in uranium calorimeters, versus 0.6 for e/mip. The EGS4 calculations showed that also the other effects found for em showers (figs. 27,28) were enhanced for a nuclear γ-ray spectrum.

Nuclear fission is an important source of nuclear γ's in uranium calorimeters. We measured that in the non-em part of hadron showers on average $\sim$ 10 fissions per GeV are generated[12] . In each fission, on average 7.4 MeV is released in the form of prompt γ's[22] . Other processes like inelastic neutron scattering and thermal neutron capture further increase the fission-related nuclear γ component to a considerable fraction of the initial particle energy. The use of uranium absorber in hadron calorimeters was originally advocated because of this extra energy, which was assumed to make up for the inevitable losses in the non-em part of the shower (compensation)[23] . The reduced efficiency for detecting these γ's limits the effect of this, however, to the extent that the condition $e/h^{\rm intr} = 1$ can not be achieved in U/LAr calorimeters.

6.4 The non-em shower part ($f_{\rm ion}, f_{\rm n}, f_\gamma$)

The analysis of the calorimeter signal from em showers has taught us an important lesson, that is also relevant for understanding the details of the response to the non-em part. The lesson is, that the signal is decisively determined by the peculiarities of the processes occurring at the very last stages of the shower development. Although the energy is very low, the number of particles is so large that a considerable fraction of the total energy is deposited through these processes.

In the last stages of the development of the non-em shower part the production of pions, kaons, etc. is energetically impossible. It turns out that even at very high energies, the contribution of such particles to the calorimeter signal is small: Typically, only 10 – 15% of the non-em energy is deposited through ionization by charged pions. An easy way to see this is by realizing that charged pions lose on average only $\sim$ 0.2 GeV per nuclear interaction length through ionization of the medium that they traverse. A 100 GeV pion that produces in its first interaction 10 other charged pions will, therefore, have lost only $\sim$ 2% of its energy when the secondary pions undergo strong interactions. The average pion multiplicity in these secondary interactions is probably something like 2 - 3 (adding another 4 – 6% to the dE/dx loss). In further generations new pion production becomes rapidly negligible.

The remaining $85-90\%$ of the shower energy is spent on nuclear processes. It is used to release nucleons and nucleon aggregates from atomic nuclei (binding energy losses), and to give kinetic energy to the reaction products. Usually the nuclei also emit γ's in these processes (see section 6.3). Apart from these γ's, protons and neutrons may contribute to the calorimeter signal. The range of the nucleon aggregates and of the recoiling target nuclei is so small that their kinetic energy is virtually lost for detection.

Figure 30 shows a typical example of a reaction induced by a low-energy (3.8 GeV) pion, as measured in an emulsion. The struck nucleus virtually explodes, releasing at least 13 protons or (maybe some) nucleon aggregates (the densely ionising tracks). The many neutrons also produced in this event are not visible on the picture.

The way in which the protons and neutrons lose energy and contribute to the calorimeter signal is very different. The vast majority of the protons will lose their complete kinetic energy by ionization (see fig. 30). Only the fast component ($E_{\mathrm{kin}} > 100\,\mathrm{MeV}$) may cause new nuclear reactions to occur at a non-negligible level. The neutrons *exclusively* lose kinetic energy through strong interactions. In these reactions new neutrons, protons and γ's may be produced, and additional binding energy lost. In particular the fast neutrons produced in the initial phase of the shower may develop quite complicated showers themselves.

The numerical details of the nuclear reaction mechanisms which are important for our purpose (*e.g.* nuclear spallation) are extensively discussed in ref. 20. Here we only give the main conclusions. The neutron multiplicity in hadron showers developing in a material ($Z \gg 1$) is much larger than the proton multiplicity, particularly if Z is large. This has two reasons:

a) More neutrons than protons are available in the target nuclei.

b) At low energies the nuclear Coulomb barrier will prevent protons from escaping.

In the reactions that start the "nuclear" phase of the shower development, more kinetic energy will therefore be carried away by neutrons than by protons. Most of this kinetic neutron energy will, however, be lost as nuclear binding energy in a series of subsequent reactions, in which the neutron multiplicity increases considerably, and in which also some new protons may be produced. In each nuclear reaction on average $2-3\,\mathrm{MeV}$ is released in the form of nuclear γ's.

At some stage in the shower development the neutrons have degraded so much in energy, that they cannot release any more new protons from target nuclei. For high-Z absorbers this is the case below $E_n^{\mathrm{kin}} \approx 20\,\mathrm{MeV}$. What we need to know at this point in order to be able to compute e/h^{intr} (see sect. 6.1) are the fraction of the non-

em energy deposited through ionization by protons (the major component of $f_{\rm ion}$), the remaining kinetic neutron energy ($f_{\rm n}$), and the total number of nuclear reactions (needed for f_γ). Nuclear γ's have only eaten up $2-3\%$ of the energy at this stage. The other components depend obviously on the Z of the absorber material. Roughly one may say that $f_{\rm ion} \approx Z/A$, while $f_{\rm n}$ varies from 8% for Fe to 15% for ^{238}U. The rest of the energy is invisible (binding energy, target recoil, nucleon aggregates). The contribution of nuclear fission in uranium becomes mainly important beyond this point in the shower development, *i.e.* for $E_n < 20\,$MeV, because that is where the neutron multiplication and the energy gain from this process count most.

6.5 The response to ionizing hadrons (ion/mip)

As was shown in the previous subsection, this shower component is dominated by protons ($70-75\%$). The remaining contribution comes from pions, kaons, etc. These were considered mip's. The calorimeter signal ratio *p/mip* may deviate from 1 because of the following reasons:

i) The range of the spallation protons is limited (3 mm in U at 40 MeV, see also fig. 30). Sampling inefficiencies for the soft part of the spectrum *decrease* the *p/mip* value.

ii) The sampling fraction (see sect. 6.1) for non-relativistic particles may be very different from the mip value. The magnitude of this effect is very energy- and Z-dependent. Especially for high-Z absorbers *p/mip* may considerably *increase*.

iii) Saturation or recombination effects in the readout material *reduce* the response for densely ionizing particles, and hence the *p/mip* value.

iv) Multiple scattering of very soft protons *decreases p/mip* if $Z_{\rm abs} \gg Z_{\rm readout}$.

The combined effect of all these phenomena was investigated with a Monte-Carlo program. The *ion/mip* signal ratio turned out to depend on the material combination, on the proton energy spectrum, on the saturation properties of the readout material, and on the thickness of the active layers. The first three effects are obvious from *i* – *iv*, the last effect is presumably due to the fact that if the thickness of the active layers is increased, a larger fraction of the protons will stop inside them and hence produce a relatively small signal compared to the amount of energy deposited (saturation).

An example of the results is given in fig. 31. This figure illustrates the energy dependence and the saturation effects. For practical calorimeters with saturating readout materials (plastic scintillator, LAr), *ion/mip* signal ratios were found in the range $0.85-1.0$. For a non-saturating medium like Si the response would be $\sim 15\%$ larger.

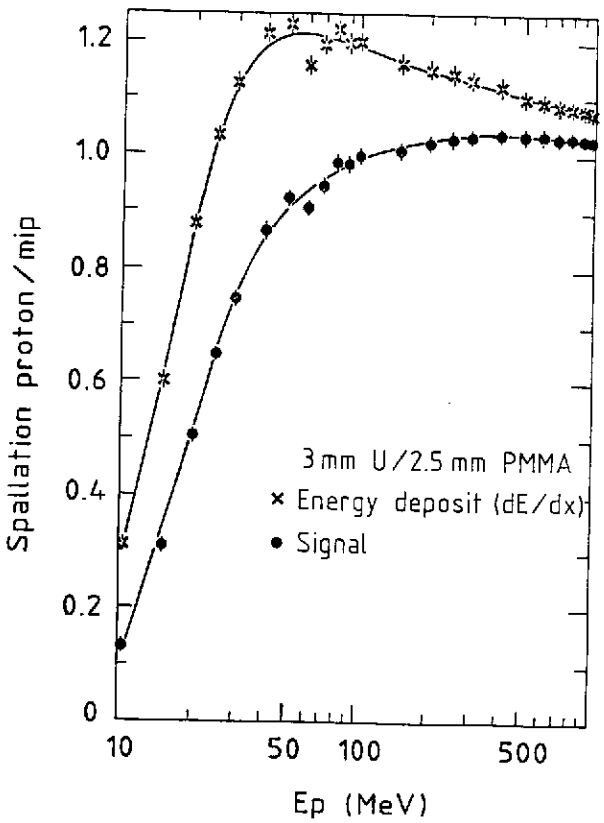

31. The energy deposit and the calorimeter signal for stopping protons relative to mip's, as a function of the proton energy, for a 3 mm U/ 2.5 mm plasic scintillator calorimeter.

6.6 The response to soft neutrons (n/mip)

Soft neutrons are the most interesting shower component, and the most crucial one for the calorimeter response. In the previous subsections we saw that the calorimeter response to the other shower components depends on rather global material properties, like $Z_{\rm abs}$. In order to be able to properly evaluate the neutron contribution, we have to go rather deeply into nuclear physics details. Nuclear level structures and cross sections for individual reactions are important for the result.

For example, the fact that the first excited state in the "double magic" nucleus ^{208}Pb lies as high as 2.6 MeV above the ground state level (which prevents inelastic neutron scattering below this energy), makes that the e/h ratio for a Pb/plastic-scintillator calorimeter would change considerably if the isotopes ^{204}Pb , ^{206}Pb , and ^{207}Pb , which can be excited by neutrons down to 0.6 MeV, would not be present. Small impurities with anomalously large cross sections for certain neutron-induced reactions, like Cd, may also have a large impact.

Fortunately, neutron scattering is one of the most systematically studied areas in physics. The wealth of existing experimental information allows to calculate rather precisely how the neutrons will lose their kinetic energy in a given calorimeter. Figure 32 shows cross sections, which are relevant for the calculations of neutron transport in a uranium/plastic-scintillator calorimeter. Proton production off uranium nuclei does no longer occur at these low neutron energies. However, the neutrons can still multiply themselves, through $(n,2n)$ or $(n,3n)$ reactions where additional binding energy is lost, or through nuclear fission. The latter process may occur down to $E_n^{\rm kin} \approx 1.5$ MeV. In inelastic scattering kinetic neutron energy is converted into γ's, but also the probability for this process sharply decreases below 2 MeV.

The last step in the neutron's lifetime as a free particle is capture. In this proces, the energy that was needed to liberate the neutron from the nuclear field, is gained back and emitted by the capturing nucleus in the form of γ's. The cross section for this process is only considerable when the neutron is practically thermalized. The dominating process to get rid of the last $1-2$ MeV is elastic scattering. The cross section for this process is very large, more than 4 b (mean free neutron path less than 5 cm). However, the energy loss per collision is very small, 1/239 on average. The reaction products, recoiling target nuclei, are undetectable.

The situation changes completely if the calorimeter also contains hydrogen, in the readout material. Hydrogen is well-known to be very efficient in thermalizing neutrons. In each elastic collision, on average half of the kinetic neutron energy is transferred. At 1 MeV the cross section for this process is 4 b, which corresponds to a mean free neutron

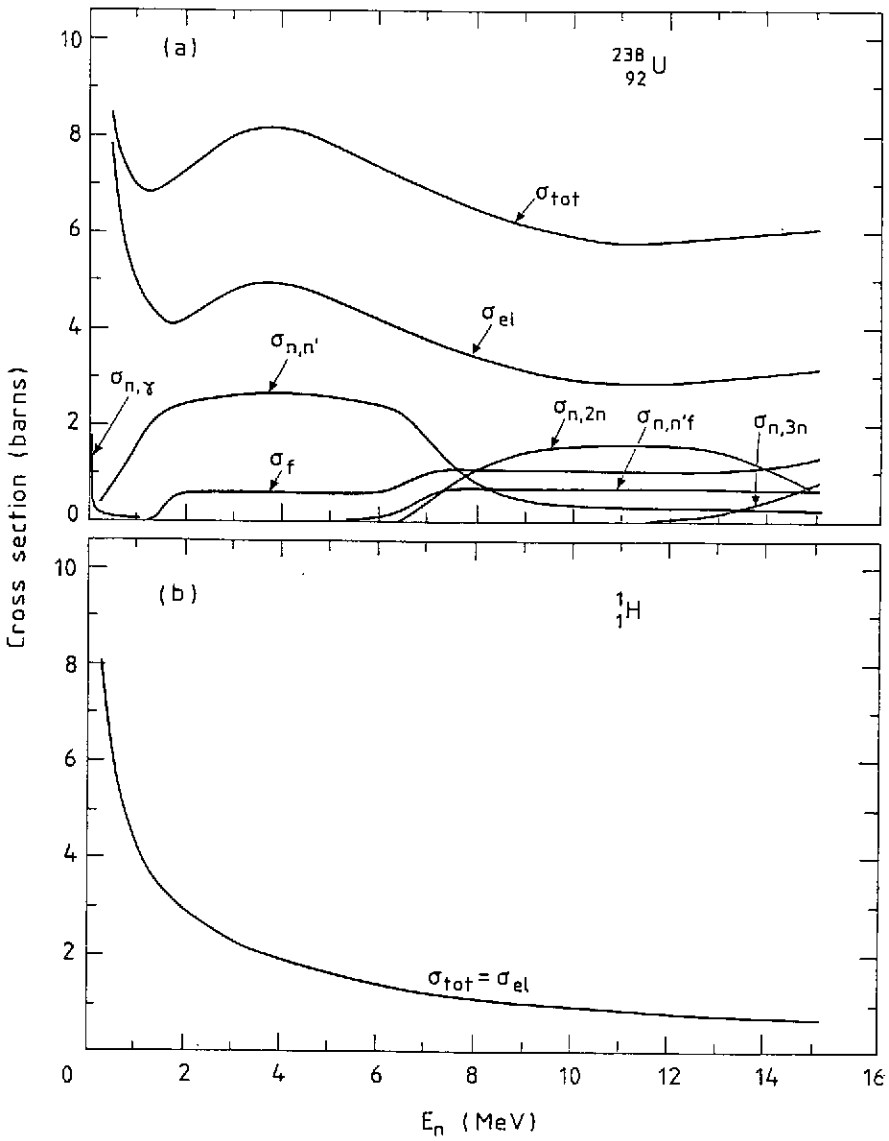

32. The cross sections for neutron-induced reactions on ^{238}U (a) and hydrogen (b) nuclei.

path of ~ 5 cm in polystyrene, and ~ 4 cm in TMP. The reaction products of this process are recoil protons. These are produced inside the active layers, and contribute *directly* to the calorimeter signal, *i.e.* they are not sampled like mip's. The range of 1 MeV protons in polystyrene is 22 μm and, therefore, in practice the kinetic energy of protons produced in this way will almost *completely* be deposited in the active calorimeter layers.

In calorimeters that contain hydrogen atoms, neutron-proton scattering is a very important source of energy loss, because at low energies there is almost no competition from other processes. This may be concluded from an experimental study on the distribution of radioactive nuclides produced by the neutrons from hadron showers[112]. Figure 33 shows the longitudinal distributions of ^{239}Np, produced from thermal neutron capture by ^{238}U, in different uranium calorimeter configurations. It turned out that the distribution in uranium/plastic-scintillator is very different from the ones in uranium calorimeters not containing hydrogen. The neutrons were much faster thermalized in the scintillator case and, therefore, must have lost a considerable fraction of their kinetic energy in elastic collisions with hydrogen nuclei. The reduced number of fissions measured in the scintillator calorimeter supports this conclusion as well.

We studied the transport of the soft neutron shower component in a given calorimeter structure with a Monte-Carlo program, that contained all the relevant information on the nuclear physics: The cross sections for all possible reactions in the absorber and readout materials, the energy transfer in these reactions, the physics on fission neutrons and γ's, etc. Since the recoil protons are very densely ionizing, the saturation characteristics of the readout materials are of crucial importance. We used Birk's law to convert from energy to signal (L):

$$L/E = [\int_0^{z_{max}} (1 + kB\frac{dE}{dx})dx]^{-1}$$

The values of the saturation constant kB are such that this meant a reduction of a factor $4 - 5$ for materials like LAr and plastic scintillator. Essential for the results was also the input neutron spectrum. We used a linear combination of two Maxwell distributions to account for the soft evaporation and fission neutrons on the one hand, and for the degraded spallation neutrons on the other hand. The validity of these assumptions was checked and found in excellent agreement with all the experimental data from the neutron-induced activation analysis mentioned before[112].

Figure 34 shows an example of the results, for a 3 mm U/3 mm plastic-scintillator calorimeter. Below 4 MeV, more than half of the kinetic neutron energy is converted into recoil protons, and below 1 MeV even more than 70%. The remaining part of the energy is converted into γ's (inelastic scattering, fission) and invisible forms (binding

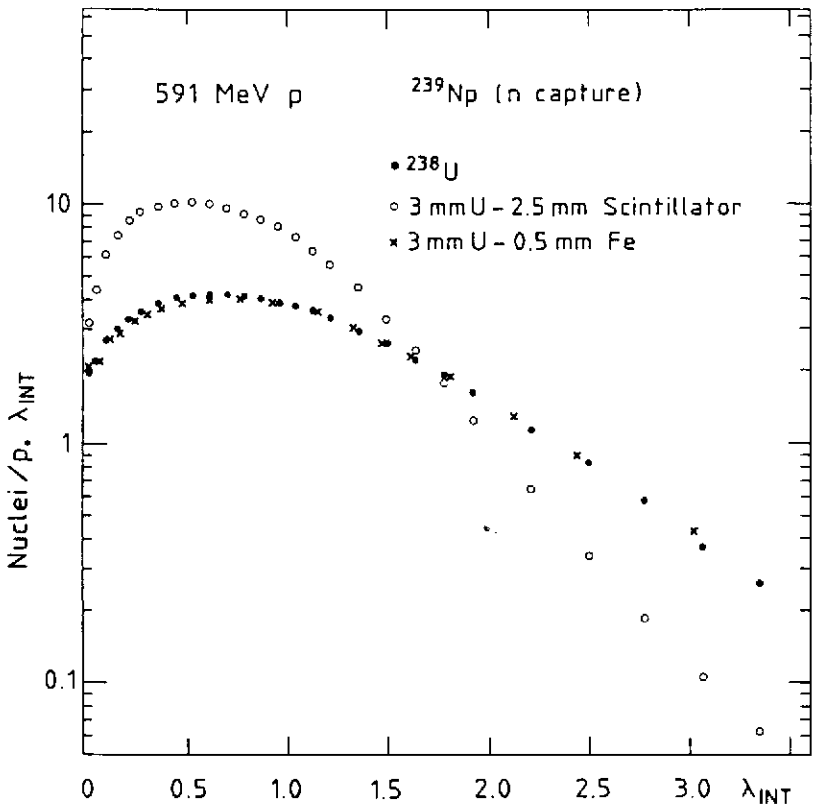

33. The longitudinal distributions of ^{239}Np nuclei (from neutron capture in ^{238}U), produced by hadron showers in various calorimeter configurations.

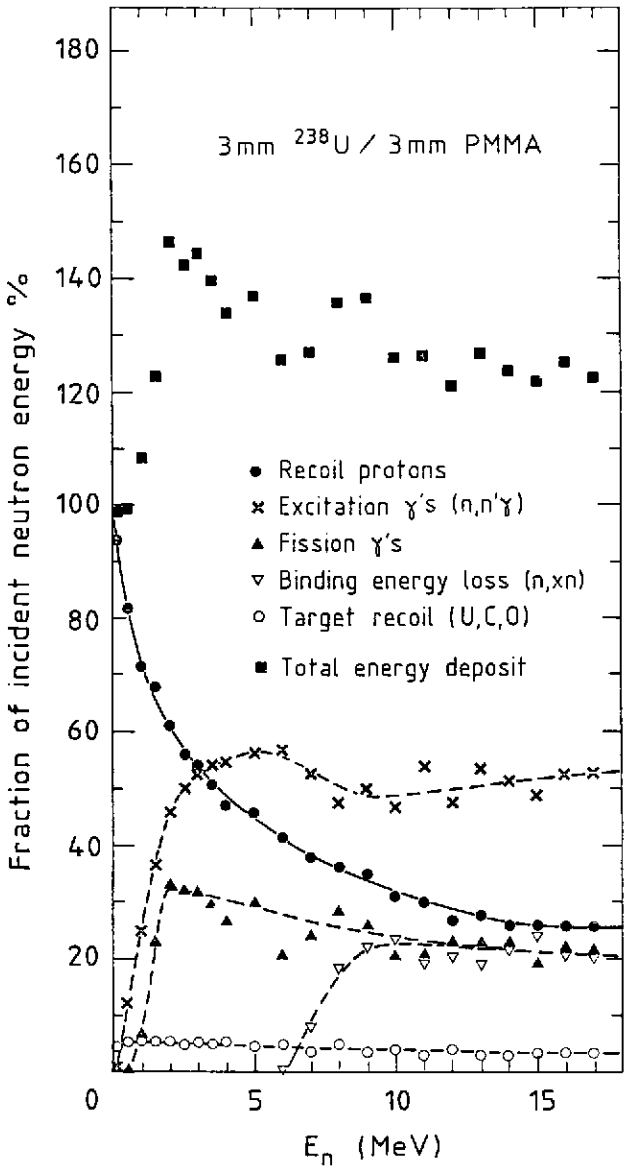

34. The various forms in which the kinetic neutron energy is deposited in a 3 mm U/3 mm plastic-scintillator calorimeter. Because of fission contributions, the total energy can be larger than 100%.

energy, target recoil). Note that the sampling fraction, *i.e.* the part of the energy that mip's deposit in the active layers, amounts to only $\sim 10\%$ for this calorimeter. The recoil protons will therefore substantially contribute to the calorimeter signal.

A nice example to illustrate this comes from the L3 Collaboration, who tested uranium calorimeters with proportional wire chamber readout[24] . When using isobutane (containing hydrogen) the hadronic response was found to be about twice as high as for Ar/CO_2 (no hydrogen), while the electron response was almost gas-independent (see fig. 35). The difference is due to $n-p$ scattering. Similar differences occur between plastic-scintillator (containing hydrogen) and LAr (no hydrogen) readout. These are smaller than for gaseous media because of saturation effects, but yet considerable.

The Monte-Carlo studies revealed another very interesting effect. It turned out that the n/mip signal ratio, or the relative contribution of recoil protons to the calorimeter signal, is sensitively dependent on the sampling fraction for mip's ($f_{\rm samp}$, see sect. 6.1). If $f_{\rm samp}$ gets smaller, n/mip increases; if $f_{\rm samp}$ gets larger, n/mip decreases. This can be understood as follows.

If the thickness of the absorber plates is increased, the signal from mip's will decrease proportionally. The energy transferred to recoil protons in the active layers by the neutrons is *not* sampled. We saw before that at low neutron energies, there is almost no alternative for this process and, therefore, the fraction of the neutron energy deposited in this form decreases much slower than the mip signal. In other words, if the sampling fraction is decreased, the n/mip signal ratio and hence the total non-em calorimeter response increases, and the e/h signal ratio decreases. The sampling fraction is, therefore, a crucial parameter for the performance of hadron calorimeters with hydrogenous readout.

Figure 36 shows some results of the calculations, for uranium/plastic-scintillator calorimeters. Instead of the sampling fraction, we used the more practical variable R_d, defined as the ratio of the thicknesses (in mm) of the passive and active calorimeter layers; R_d is approximately inversely proportional to $f_{\rm samp}$. In fig. 36a the n/mip signal ratio is given as a function of R_d. The neutron signal is split up in its various contributing components. The dominating recoil proton contribution strongly increases with R_d. The consequences of this for the calorimeter performance are of decisive importance, because of the relatively large contribution of the soft-neutron shower component to the calorimeter signal. In the case of the compensating HELIOS calorimeter[16,14] ($R_d = 1.2$), these neutrons contribute almost 40% to the total non-em part of the signal, and for the overcompensating WA78 detector[18] ($R_d = 2-3$) even 50%.

Figure 36a also shows that the neutrons do not only contribute to the calorimeter signal through recoil protons, but also through the γ's that they produce by fission,

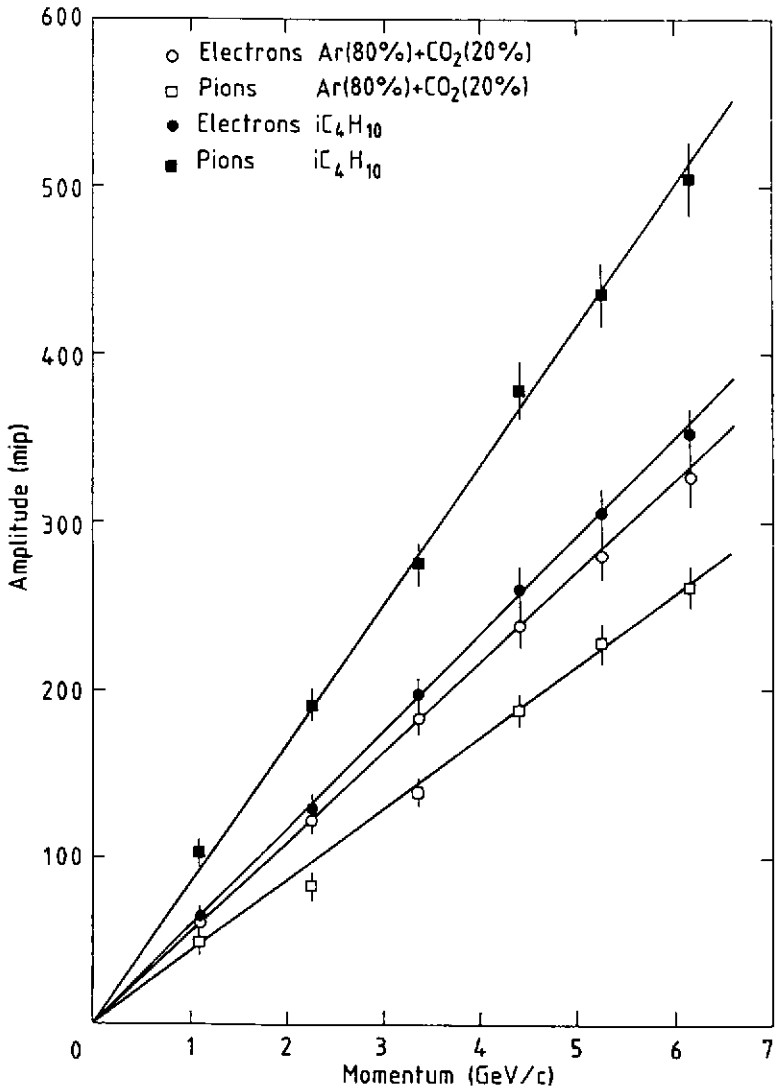

35. The response of a uranium gas-sampling calorimeter to pions and electrons, for different gases. Data from ref. 24.

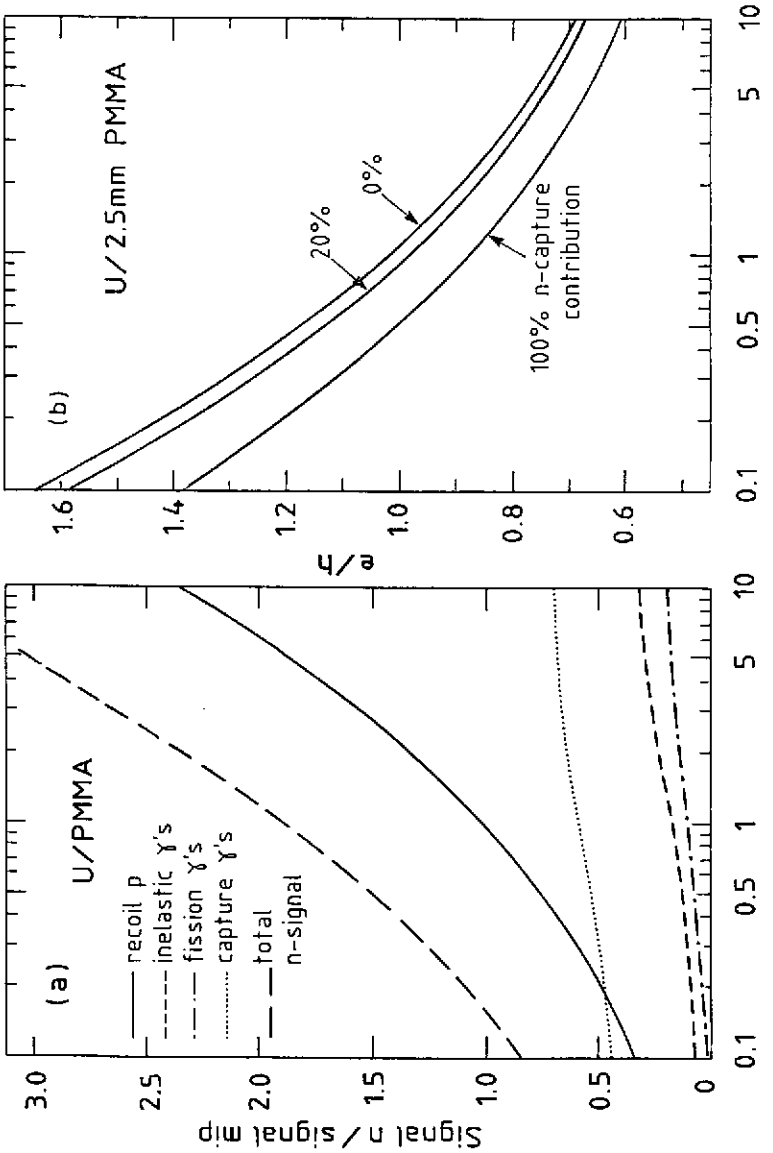

36. The signal ratio *n/mip* split up in its components, for U/plastic-scintillator calorimeters, as a function of the ratio of the thicknesses of passive and active layers R_d (a). The signal ratio e/h as a function of R_d, assuming that 0%, 20% or 100% of the γ's released in thermal neutron capture contribute to the calorimeter signal (b).

inelastic scattering and capture. This contribution is limited because of the small γ/mip signal ratio (sect. 6.3). Nevertheless, a considerable fraction of the energy is deposited in this form, in particular through the neutron capture process. We measured that in uranium $\sim$ 50 neutrons/GeV are produced in the non-em shower part[12] . If these are all captured, 240 MeV/GeV is released as capture γ's. Their contribution to the calorimeter signal depends on the capture cross section, on the calorimeter size and, since thermalization is a slow process, on the signal integration time (see fig. 37).

Figure 36b shows the sensitivity of the e/h signal ratio to the fraction of the neutrons that contribute to the signal through capture ($f_{\rm capt}$). Calculations by Brückmann[25] indicate that in 100 ns, a typical gate time for scintillator readout, $f_{\rm capt} \approx 20\%$. Measurements on the evolution of the e/h signal ratio as a function of the gate time clearly confirmed the predicted effect[14,10] . For LAr readout, the signal integration time is usually longer ($\sim 1\mu$s) and, therefore, $f_{\rm capt}$ may be up to $\sim$ 80% for sufficiently large detectors.

6.7 The e/h signal ratio

The e/h signal ratio was calculated in the way described in sect. 6.1. It was shown in sect. 6.2 - 6.6, that the results depend on a large number of factors, of which we recall:

a) The Z of the active and passive media (e.g for e/mip, γ/mip, $f_{\rm ion}$, $f_{\rm n}$).

b) The hydrogen content of the active medium (n/mip).

c) The saturation properties (kB value) of the active medium (ion/mip, n/mip).

d) The nuclear level structure of the absorber (n/mip).

e) The size of the detector ($f_{\rm capt} \rightarrow f_\gamma$).

f) The cross section for thermal neutron capture in the absorber (f_γ).

g) The signal integration time (f_γ).

h) The thickness of the passive layers (e/mip, γ/mip).

i) The thickness of the active layers (e/mip, γ/mip, ion/mip).

j) The sampling fraction (n/mip).

Because of the interesting consequences of the latter effect, e/h curves are presented as a function of the sampling fraction, or rather R_d, for a fixed choice of the readout thickness (figs. 36b, 38). These figures show that the e/h signal ratio for uranium calorimeters with hydrogenous readout decreases rather sharply with increasing R_d, *i.e.* with increasing absorber plate thickness. The e/h ratio can therefore be tuned through the sampling fraction, and for the hydrogenous materials shown (various plastic scintillators, TMP) an ideal sampling fraction ($e/h = 1$) exists.

The sensitivity of the e/h ratio to the sampling fraction depends on two factors:

i) The fraction of hydrogen atoms in the active medium. Since TMP contains more hydrogen atoms than plastic scintillator, the e/h signal ratio of TMP calorimeters is more sensitive to changes in the sampling fraction.

ii) Saturation of the active medium. Less saturation causes a larger sensitivity, and consequently leads to a larger optimal sampling fraction. This is illustrated in figure 38 , where the predictions for TMP readout are given for two different kB values. Contrary to plastic scintillator, the kB value has not been measured for soft protons in TMP, so far. The figure shows that this is a crucial parameter for the calorimeter performance.

For calorimeters with non-hydrogenous active layers (*e.g.* LAr, Si), the effect of the sampling fraction on the relative contribution of neutrons to the calorimeter signal (fig. 36a) is absent. The fact that e/h rises for small R_d values is caused by the effect of the absorber layer thickness on the electromagnetic response (fig. 27). It turned out that the e/h ratio depends quite sensitively on the contribution of captured neutrons to the hadronic calorimeter signal (sect. 6.6), which can be tuned through the signal integration time. Nevertheless, it looks as if the compensation condition cannot be reached for LAr. For Si readout it might just be possible. The difference between LAr and Si comes from the fact that Si does not saturate in detecting the spallation protons (sect. 6.5) and, therefore, gives a larger response to the non-em shower component.

The calculations were performed for infinitely large detectors. We investigated how sensitive the predictions are with respect to the various assumptions that went into the calculations. In fact fig. 36b is an example of this. Other uncertainties concern $f_{\rm ion}$, $f_{\rm n}$ and the spallation proton spectrum (sect. 6.4, 6.5). It turned out that these uncertainties concerning details of the hadronic shower development may considerably affect the absolute value of the vertical scale, but *not* the variation of e/h with the sampling fraction, nor the difference between the various active materials. Therefore, the absolute e/h signal ratio for a given absorber/readout combination cannot be predicted from scratch more accurately than to within $5 - 10\%$, but one reliable experimental measurement will make possible a reliable prediction of the optimal configuration.

The experimental results obtained with uranium calorimeters so far seem to support this conclusion. In particular, the predicted trend of a decreasing e/h ratio for increasing R_d in the case of scintillator readout is experimentally very well confirmed. The same is true for the differences between scintillator and LAr. Experimental results for TMP and Si readout are unfortunately still lacking.

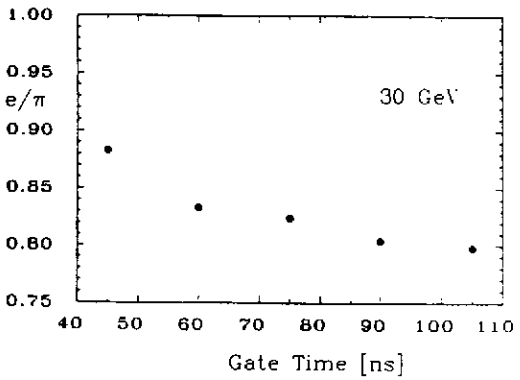

Figure 37

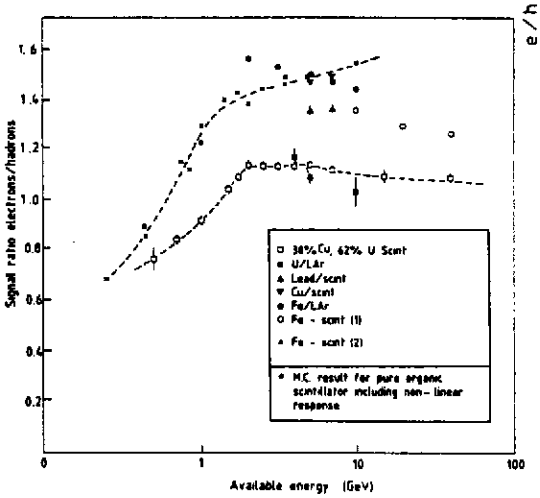

Figure 39

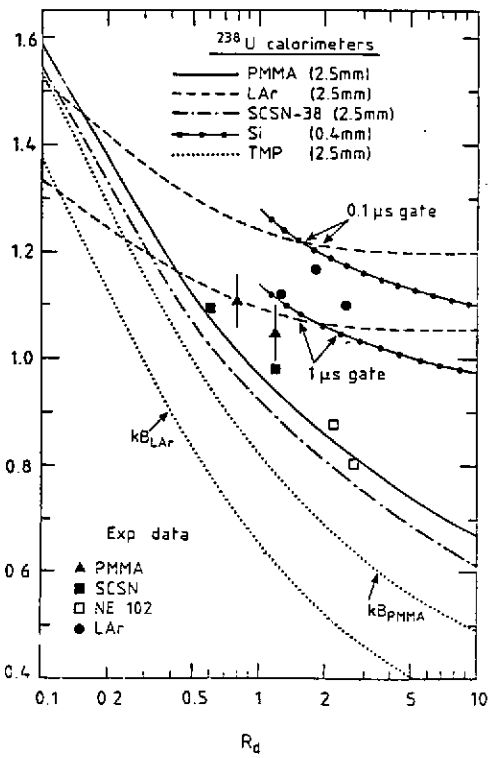

Figure 38

37. The e/h signal ratio as a function of the signal integration time. The decrease is due to an increase of the hadronic signal. Data from ref. 13.

38. The signal ratio e/h for uranium calorimeters employing different readout materials, as a function of the ratio of the thicknesses of absorber and readout layers. Results of experimental measurements are included.

39. The ratio of the em to hadronic response as a function of energy, for various calorimeter configurations.

We also did extensive calculations for calorimeters with Pb or Fe absorber. The lead results are most interesting. The differences with uranium mainly concern the amount of energy carried by the soft-neutron component, because of the absence of fission and because of the fact that the Pb nucleus is less neutron-rich than uranium. Figure 36a shows that this can be compensated for by choosing a smaller sampling fraction (larger R_d). This increases n/mip and hence brings the contribution of neutrons to the calorimeter signal at the appropriate level. Again, this trick works only for hydrogenous readout materials. For scintillator, e/h was predicted to become 1.0 for $R_d \approx 4$, *i.e.* if the lead plates are made 4 times as thick as the scintillator plates.

In sect. 6.6 we saw that γ's from thermal neutron capture represent a considerable fraction of the total hadronic energy, since it is by emitting these γ's that the nuclei render the binding energy lost when the neutrons were released. In plain lead calorimeters the contribution of this process to the signal will be negligible. The cross section for (n,γ) reactions is 0.17 b, against 2.7 b for uranium. This corresponds to a mean free path of $\sim$ 180 cm for a thermal neutron in lead (8 cm in U). Cadmium has a capture cross section of 2450 b. If one would add $\sim$ 1% Cd to the lead, thermal neutrons would be efficiently captured. This would in particular be interesting for LAr calorimeters with a long signal integration time. Also in U/LAr one might profit from adding a little Cd, since the energy released in neutron capture by Cd (9.0 MeV) is almost twice as large as in ^{238}U (4.8 MeV).

The calculations showed that even Fe calorimeters could be made compensating, at very small sampling fractions. Experimental data from the WA1 Collaboration seem to support this conclusion[17,20] .

A final word should be said about homogeneous hadron calorimeters. The mechanisms that are described in this section and that make compensating calorimeters possible, are based on the fact that we are dealing with *sampling* calorimeters: Only a (small) fraction of the shower energy is deposited in the active layers, and by carefully tuning variables one may equalize the em and non-em *response*. This does not work for homogeneous devices, like the fully sensitive liquid argon tank proposed by Ypsilantis[26] . In the non-em shower part inevitably losses will occur that cannot be compensated for, e.g. the binding energy required to release protons or nucleon aggregates from their nuclear environment. The $e/h^{\rm intr}$ signal ratio will, therefore, always have to be larger than 1.0 for such devices.

6.8 Alinearities at low energy

In sect. 5 we showed that deviations from $e/h = 1$ cause the calorimeter signal to be *not* proportional to the hadron energy. However, also for *compensated* calorimeters signal alinearities are unavoidable. They occur at low energies, typically for $E_{\rm hadr} < 2$ GeV.

In sect. 6.1 we saw that e/mip is considerably smaller than 1.0 for calorimeters with high-Z absorber material. If such a calorimeter is made compensating, the *hadronic* signal will thus be considerably reduced with respect to the signal from mip's too. At low energy, however, the probability that charged hadrons lose their energy *without* undergoing strong interactions, and the corresponding (binding energy) losses, increase rapidly. In that case, they deposit their energy by ionization alone, like mip's. The h/mip signal ratio will go up, and the e/h signal ratio down; the response to hadrons thus increases at low energy.

This is very clearly confirmed by experimental data. Figure 39 shows the e/h signal ratio as a function of energy, for various calorimeter configurations. A very clear decrease in this ratio, *i.e* an increase in the response to hadrons, is observed below ~ 2 GeV.

These effects can be calculated in a straightforward way, with the help of the tables from ref. 27. In fig. 40 a, the probability that *no* inelastic nuclear interactions occur is given for protons, as a function of the kinetic proton energy. This curve is only weakly material-dependent. Below $\sim$ 1 GeV, more than 10% of the protons will lose their energy exclusively by ionization. Figure 40 b shows the sampling fraction for low-energy protons, *i.e.* the fraction of the energy deposited in the active planes, assuming that they lose their total kinetic energy by ionization. This sampling fraction depends on the energy and on the calorimeter configuration, and is in any case larger than for mip's: The signal ratio h/mip is larger than 1 for protons stopped in this way.

In fig. 40 c the information from figs. 40 a and 40 b is combined, for a 3 mm U/2.5 mm plastic-scintillator calorimeter. For the fraction of the protons that *do* interact strongly, $e/h = 1$ is assumed; for the remaining fraction the results from fig. 40 b are taken, corrected for the saturation of the readout medium. The figure shows both the calorimeter response to protons, and the e/h signal ratio. The experimental results (fig. 39) are nicely reproduced. The hadronic response rises up to $\sim 60\%$ at $E_p^{\rm kin} = 0.1$ GeV. Below this energy, the effect of protons not reaching the first active plane comes in and no signal remains.

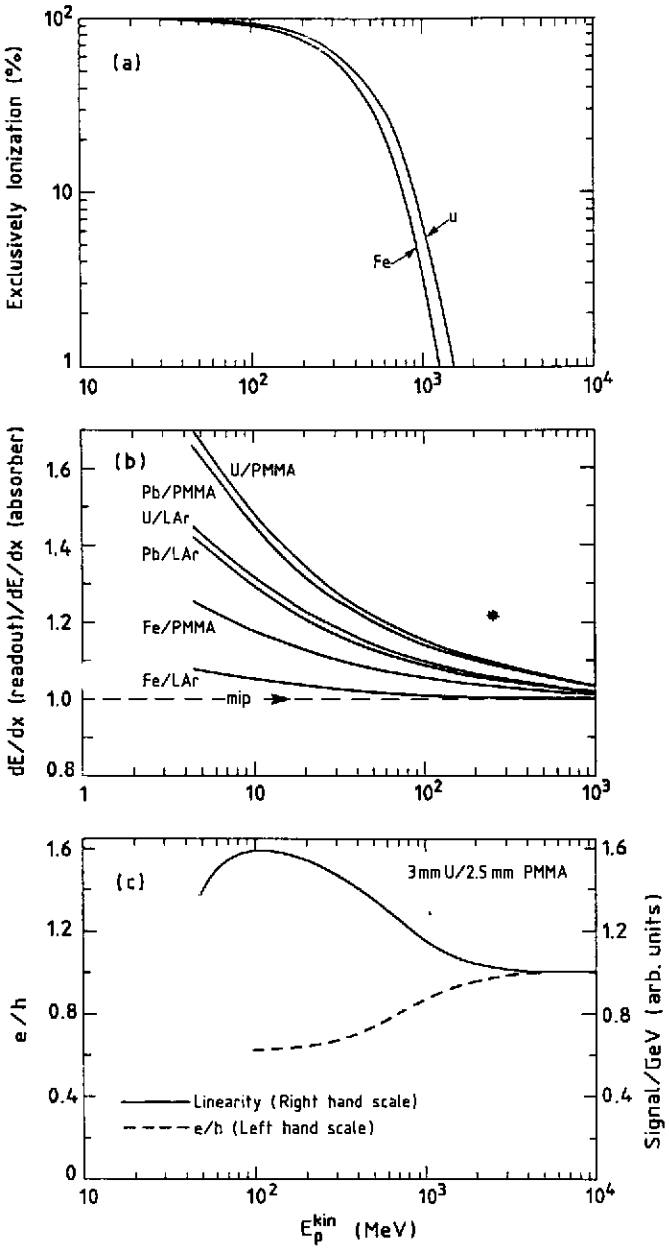

40. Signal alinearities at low energy for compensating calorimeters (calculated). The probability that protons do *not* inelastically interact before ranging out (a). The fraction of the ionization energy deposited in the active layers by non-interacting protons, in various calorimeter configurations (b). The e/h signal ratio (left hand scale) and the response to protons (right hand scale) in a uranium/plastic-scintillator calorimeter (c).

7. THE ENERGY RESOLUTION OF HADRON CALORIMETERS

After having discussed the e/h signal ratio and the factors that determine its value, we now return to the aim of this paper, *i.e.* trying to understand the energy resolution of hadron calorimeters, and the factors that limit their performance in this respect. The energy resolution of a hadron calorimeter with separate passive and active layers is determined by four factors:

1) Sampling fluctuations.

2) Detector imperfections.

3) Deviations from $e/h^{\rm intr} = 1$.

4) The intrinsic energy resolution.

The sampling fluctuations were already discussed in sect. 2.5. Fabjan *et al.*[23] have measured their contribution to the energy resolution of Fe/LAr and U/LAr hadron calorimeters. The results are usually quoted as[21]

$$\sigma_{\rm samp}/E = 0.09\sqrt{\frac{\Delta E({\rm MeV})}{E({\rm GeV})}}$$

where ΔE is the energy deposited by a mip in one sampling layer. The sampling fluctuations, *i.e.* the fluctuations in the number of particles contributing to the calorimeter signal, are larger than for em showers in the same calorimeter. The number of *different* particles contributing to the *hadronic* signal is smaller because of two effects:

a) Individual particles may traverse many planes before strongly interacting (pions, fast protons).

b) The average energy deposited by individual particles in the active planes is larger. At a given (low) energy, protons traversing an active plane will give a much larger signal than electrons (fig. 41).

In addition, the proton component in the shower will suffer from an equivalent of path length fluctuations (see sect. 2.5): Since these protons are very non-relativistic particles, the dE/dx loss, and hence the signal, is strongly energy dependent (fig. 41). The measurements cannot distiguish this effect from sampling fluctuations.

Detector imperfections will cause deviations from $1/\sqrt{E}$ scaling, and therefore limit the high-energy performance. It is believed that for well-designed calorimeters their contribution can be limited to $\sigma/E = 1\%$. Recently, HELIOS measured $\sigma/E = 1.9\%$ for the total energy distribution of reaction products from $^{16}{\rm O} + {\rm W}$ collisions at 3.2 TeV, at running conditions (fig. 42)[14]. This impressive result supports the previous statement. In our calculations we assumed the detectors to be perfect.

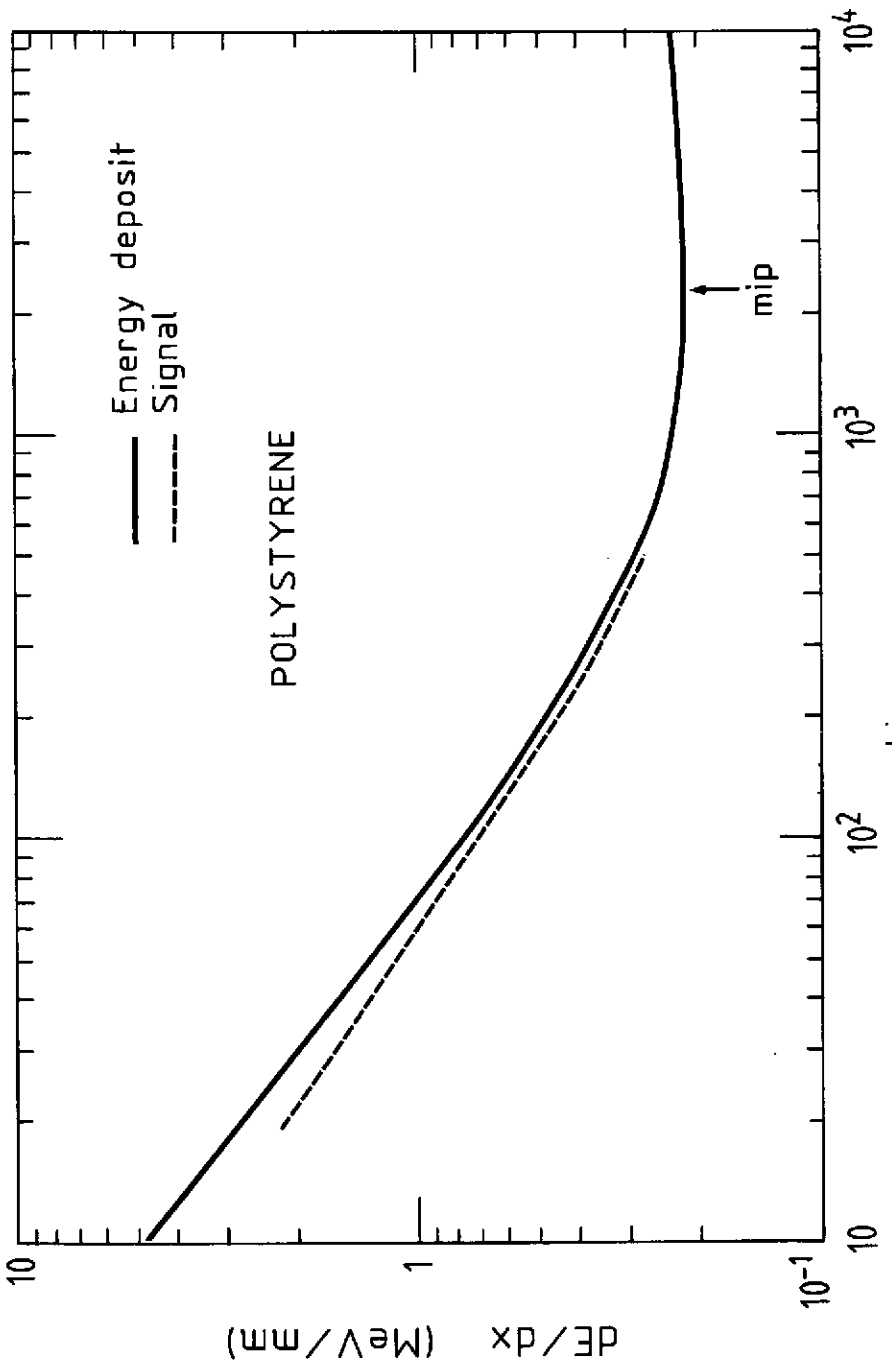

41. The ionization energy loss of protons traversing a thin polystyrene plate, and the saturation-corrected signal, as a function of the kinetic proton energy.

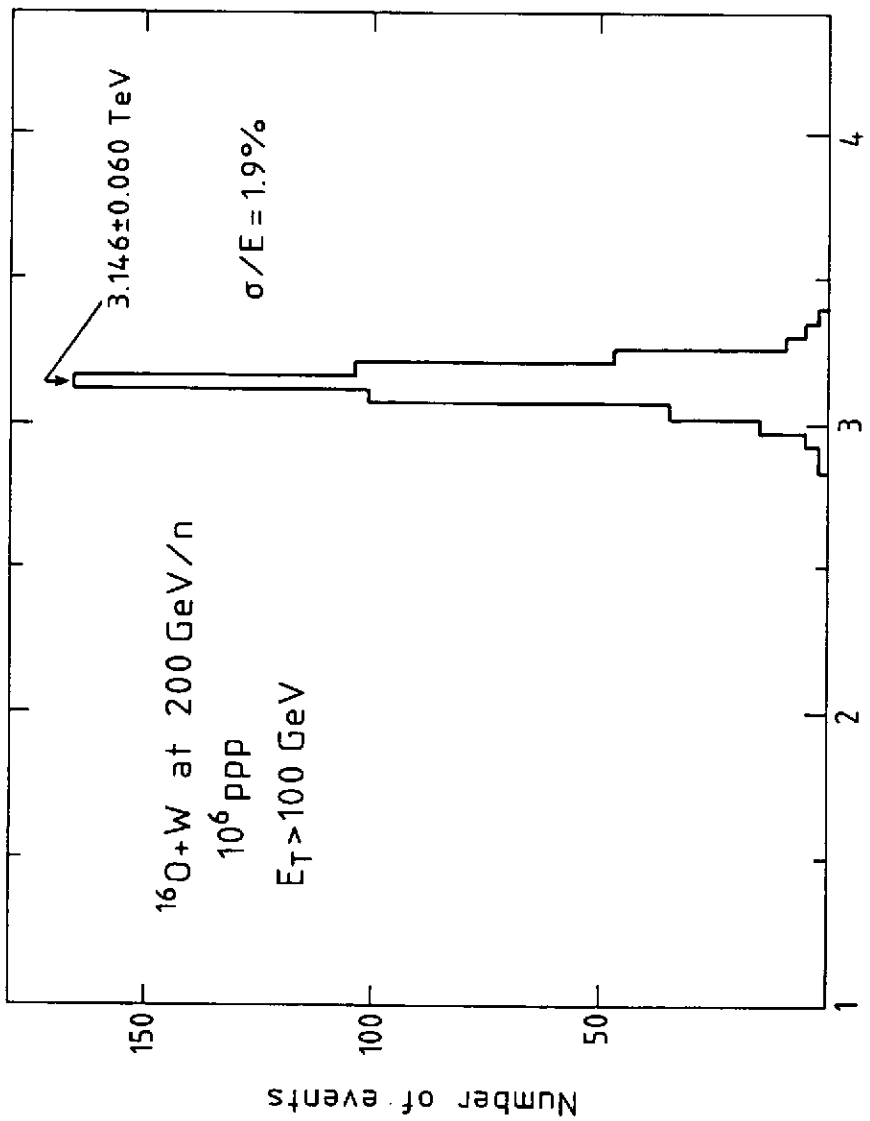

42. The total energy distribution for the reaction products from $^{16}O + W$ central collisions at 3.2 TeV, measured with the HELIOS uranium/plastic-scintillator calorimeter.

As was shown in sect. 5, deviations from $e/h^{\text{intr}} = 1$ contribute a constant term to the energy resolution σ/E. The value of this constant may be obtained from fig. 3a. In this section we will concentrate on the part that remains, *i.e.* on the intrinsic energy resolution for compensating calorimeters.

In hadron showers, a considerable fraction of the non-em energy is spent on nuclear binding energy losses, on average up to $\sim 40\%$ in high-Z materials. The fluctuations about this average are huge. This is illustrated in fig. 43a, where the binding energy lost in the various reactions that may occur when 1 GeV protons hit ^{238}U nuclei, is given. The total binding energy loss in a hadron shower (ΔB) is a convolution of many distributions of this type. We estimated that the contribution of event-to-event fluctuations in ΔB to the energy resolution amounts to $(30 - 35\%)/\sqrt{E}$, if the effects of neutron- and γ-detection are neglected. However, these effects are very important.

The total kinetic energy carried by neutrons (E_n^{tot}) is evidently correlated with ΔB (see fig. 43). A relatively large binding energy loss means that a relatively large fraction of the hadron energy is transferred to neutrons as well; detection of these particles corrects, at least partially, for the relatively small signal from ionizing particles in the event concerned, and vice versa. If the neutrons are detected with a good energy resolution themselves, *i.e.* if there is a strong correlation between E_n^{tot} and the neutron contribution to the calorimeter signal, the intrinsic resolution due to fluctuations in ΔB may be considerably reduced.

The energy resolution for neutron detection was studied with the same Monte Carlo package that was used to calculate the n/mip signal ratio (sect. 6.6). By transporting many neutrons through a given calorimeter structure, the signal distribution for a fixed E_n^{tot} was obtained. It turned out that the correlation between E_n^{tot} and the neutron contribution to the calorimeter signal may considerably improve, if elastic $n-p$ scattering in the active calorimeter layers occurs. The degree of correlation depends on the same factors that determined the n/mip signal ratio, *i.e.* on the hydrogen content, the kB value, and the sampling fraction. In addition, the thickness of the layers is important for the detection of the γ component.

With these results we calculated the total intrinsic energy resolution, assuming perfect correlation between ΔB and E_n^{tot}. The validity of this assumption breaks down at low E and/or low Z_{abs}. Results for uranium calorimeters are given in fig. 44. This figure shows that the intrinsic energy resolutions for practical detectors with hydrogenous readout material are considerably better than for LAr or Si, and may be as low as $20\%/\sqrt{E}$ for compensating calorimeters (note that the minima in the curves do not coincide with $e/h = 1$). The same conclusion holds for calorimeters with other absorbers.

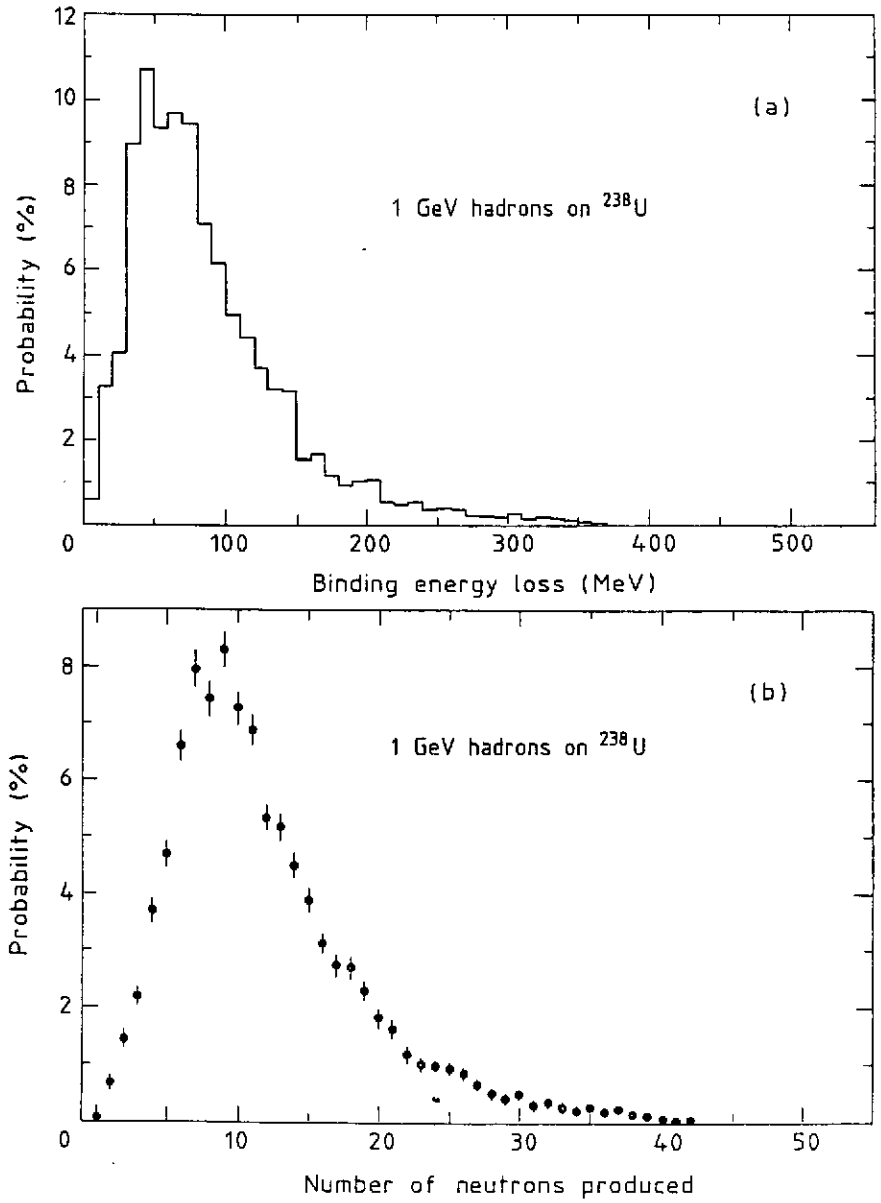

43. The binding energy lost in spallation reactions induced by 1 GeV hadrons on ^{238}U nuclei (a), and the number of neutrons produced in such reactions (b). Results of calculations described in ref. 20.

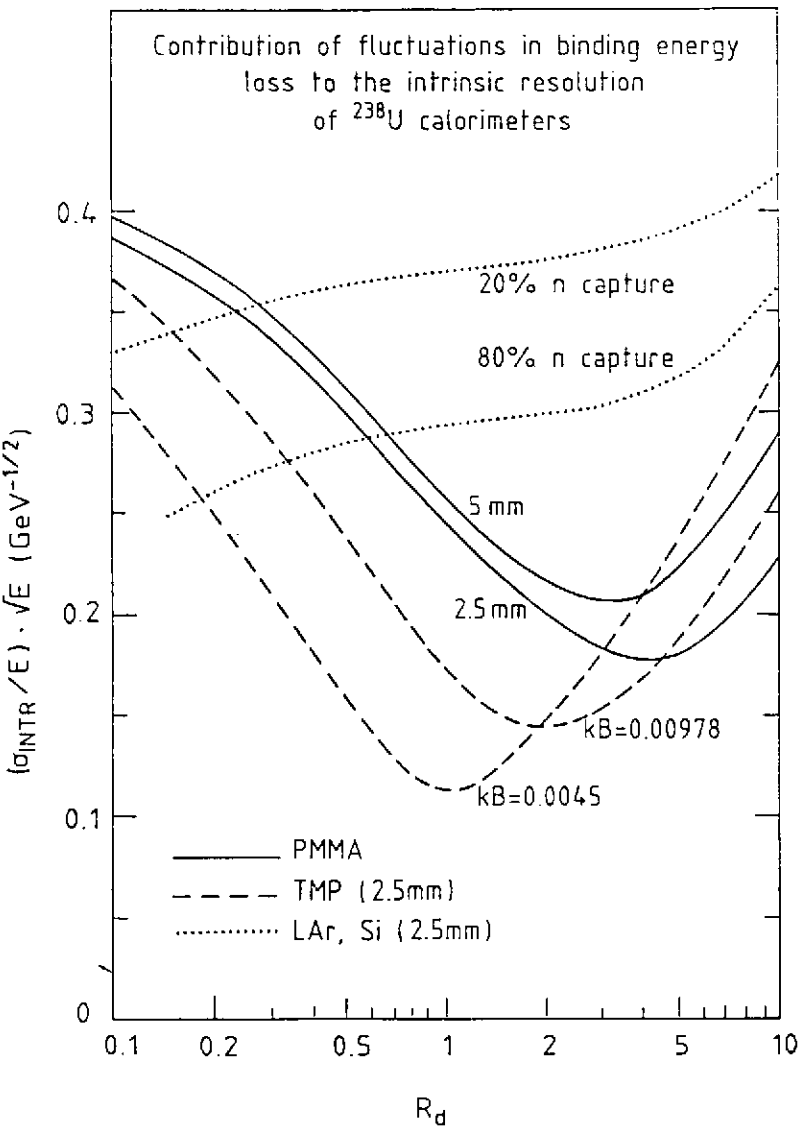

44. The contribution of fluctuations in nuclear binding energy loss to the intrinsic resolution of various types of uranium calorimeters, as a function of the ratio of the thicknesses of the passive and active layers.

This yields a new and independent argument in favour of hydrogenous readout material: The energy resolution of a U/Si calorimeter, even if this combination can be made compensating, will be inferior to plastic-scintillator or TMP calorimeters with $e/h = 1$.

The *total* hadronic energy resolution was computed as

$$\sigma/E = \sqrt{\frac{a_0^2 + a_1^2 \times t_{\rm abs}}{E}} + b$$

The intrinsic resolution (a_0) and the sampling fluctuations (a_1, see sect. 2.5), are added in quadrature. The constant term b vanishes for $e/h = 1$, and causes $\sigma/\sqrt{E}$ to be energy dependent in other cases. Figures 45-47 show some results of the calculations. Many more results are given in ref. 20. The figures show $\sigma/\sqrt{E}$ for 10 and 100 GeV, and the various contributions to it, for calorimeters with a given thickness of the active layers, as a function of the thickness of the absorber layers. The abcissa is plotted linear in the square root of the latter, which yields a straight line for the contribution of sampling fluctuations. Experimental results are included in the figures.

Figure 45 concerns uranium calorimeters with PMMA (polymethyl metacrylate, a plastic scintillator) readout. The total energy resolution reaches a minimum value for an absorber thickness close to the one for which $e/h = 1$. This is certainly true at high energies. At low energies, effects of sampling fluctuations and intrinsic contributions may slightly shift the optimal plate thickness. The curves for the total energy resolution at 10 and 100 GeV have a common point if $e/h = 1$: σ/E scales as $c/\sqrt{E}$, with $c = 0.32$ and 0.38 for 2.5 mm and 5 mm scintillator, respectively. These numbers are in good agreement with experimental values reported[16,14,28]. The results obtained by the WA78 Collaboration for non-optimal configurations[18] confirm the predicted violation of $c/\sqrt{E}$ scaling.

In fig. 46 results for U/LAr calorimeters are given. As for the e/h signal ratio, two cases were considered, $f_{\rm capt} = 0.20$ and 0.80, respectively (see sect. 6.7). The predictions are rather sensitive to this parameter. If $f_{\rm capt}$ is increased, the energy resolution improves and $\sigma/\sqrt{E}$ becomes less energy dependent. Since $e/h \neq 1$ for all configurations, $\sigma/\sqrt{E}$ will always increase with E. The experimental results are in better agreement with the low $f_{\rm capt}$ value. The small size of the test calorimeters with which they were obtained is likely to be (partly) responsible for this.

Figure 47 shows results for lead/plastic-scintillator calorimeters. As was discussed in sect. 6.7, this combination can be made compensating if the absorber layers are ~ 4 times as thick as the readout layers. Inspired by this prediction, Kötz *et. al.* from the ZEUS Collaboration tested a 10 mm Pb/2.5 mm plastic scintillator calorimeter[20] They

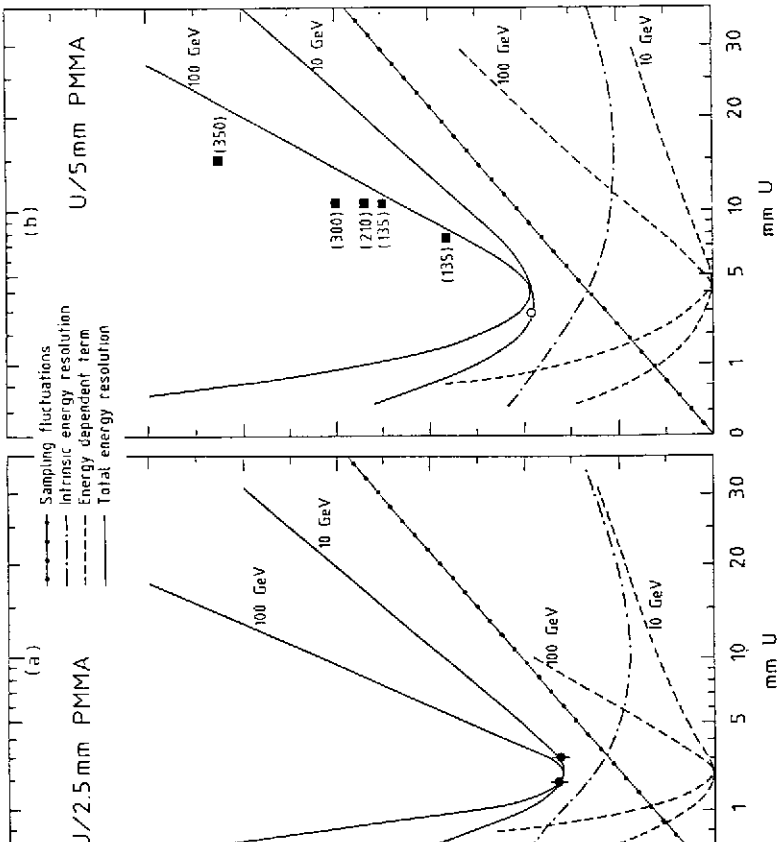

45. The total energy resolution and the various factors contributing to it, for detection of 10 and 100 GeV hadrons in U/PMMA calorimeters, as a function of the uranium plate thickness. The thickness of the scintillator plates amounts to 2.5 mm (a) or 5 mm (b). The numbers in brackets denote other energies at which experimental results were reported.

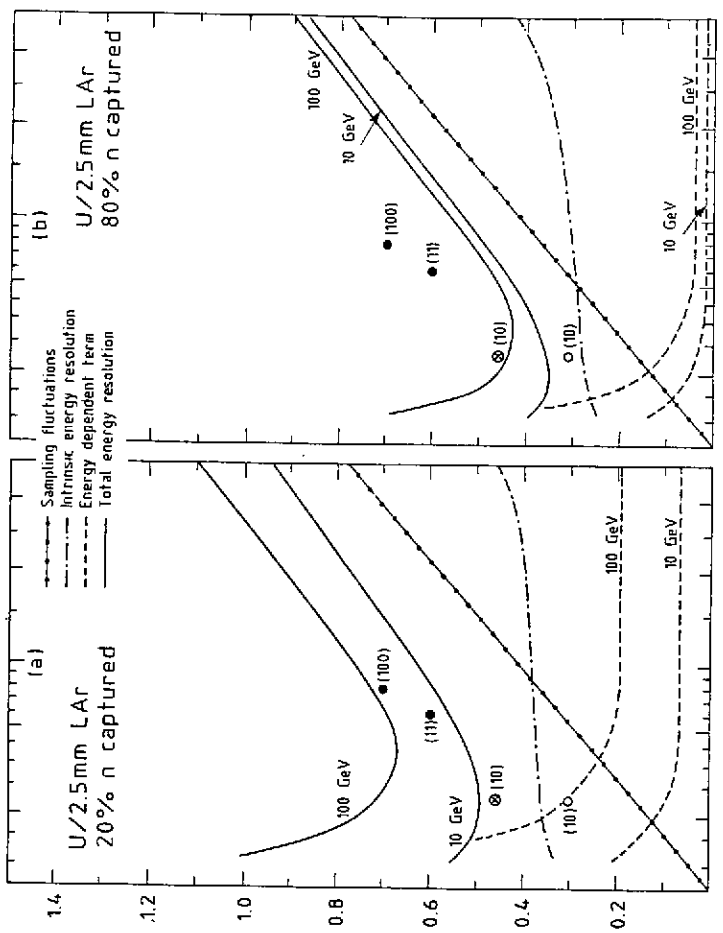

46. The total energy resolution and the various factors contributing to it, for detection of 10 and 100 GeV hadrons in U/Lar calorimeters, as a function of the uranium plate thickness. The liquid argon gap is 2.5 mm wide. The calculations assume that 20% (a) or 80% (b) of the thermalized neutrons are captured in the detector and contribute to the calorimeter signal.

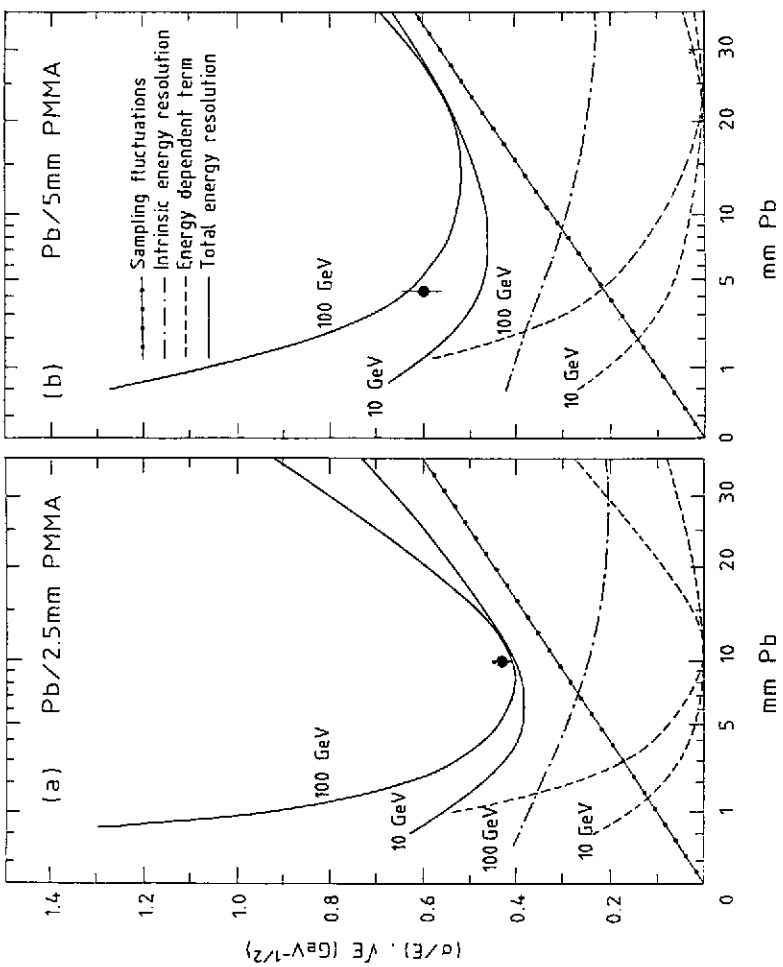

47. The total energy resolution and the various factors contributing to it, for detection of 10 and 100 GeV hadrons in Pb/PMMA calorimeters, as a function of the thickness of the lead plates. The thickness of the scintillator plates is 2.5 mm (a) or 5 mm (b).

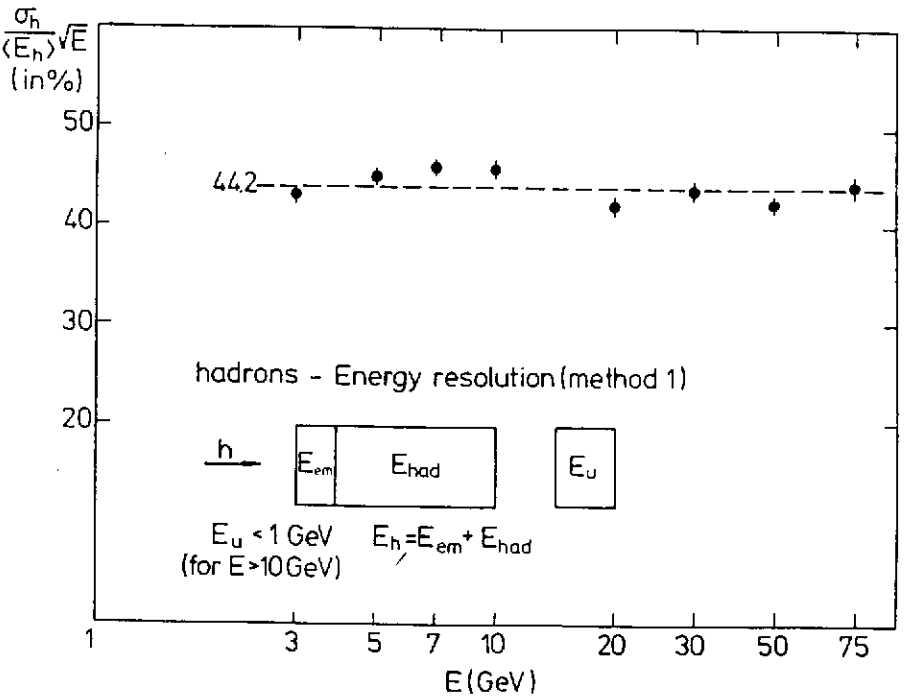

48. The hadronic energy resolution $\sigma/\sqrt{E}$ as a function of E, measured with a 10 mm Pb/2.5 mm plastic-scintillator calorimeter. Data from ref. 29.

measured an energy resolution σ/E of $44\%/\sqrt{E}$ for pion detection, scaling with $1/\sqrt{E}$ over the whole energy range they scanned ($3 - 75\,\mathrm{GeV}$), while $41\%/\sqrt{E}$ was predicted (see fig. 48). This is a remarkable result. Earlier, the same collaboration measured a considerably worse resolution ($60\%/\sqrt{E}$, fig. 47b) for a lead/plastic-scintillator calorimeter with a $4 - 5$ times larger sampling fraction[28] ($4 - 5\,\mathrm{mm}$ Pb/$5\,\mathrm{mm}$ scintillator). According to common wisdom, thicker absorber and thinner scintillator plates should have considerably deteriorated this result. Instead, an enormous improvement was observed, in agreement with our predictions.

8. OUTLOOK

The quality of experiments at a future supercollider will primarily be determined by the quality of the calorimetry. The calorimeters will have to deliver the information needed for reducing the event rates by ~ 7 orders of magnitude, while retaining those containing signatures of possible new physics. One will want to have the best possible calorimetry for that purpose. Energy resolution is an important issue in this respect, although by far not the only one. Three recent developments mark the considerable progress in this field:

i) The excellent energy resolutions measured by the HELIOS Collaboration at very high energies ($\sigma/E < 2\%$ at $3.2\,\mathrm{TeV}$).

ii) The experimental demonstration of a compensating lead calorimeter, with $\sigma/E = 43\%/\sqrt{E}$.

iii) The fact that ii) confirmed a theoretical prediction.

The first result implies that one may successfully aim for hadron calorimetry at the 1% precision level, for experiments at a multi-TeV machine. The second result shows that this goal can be achieved without uranium. The third result means that we understand *how* to achieve this goal.

In order to reach this level of precision, the calorimeter should have $e/h^{\mathrm{intr}} = 1$ to within $\sim 5\%$. This is definitely possible for four combinations: U/plastic-scintillator, Pb/plastic-scintillator, U/warm-liquid and Pb/warm-liquid. In all these cases energy resolutions $\sigma/E \approx 30\%/\sqrt{E}$ seem possible for practical detectors. Compensation can probably also be reached for U/LAr if a substantial fraction (more than 10%) of methane can be added, and for U/Si if the silicon is sandwiched between thin foils of hydrogenous material, e.g. polyethylene[14] . The energy resolution is expected to be considerably

worse for these combinations, $\sim 50\%/\sqrt{E}$. In the first case this is due to the small sampling fraction (thick U-plates) needed, in the second case the absence of the effects that compensate for fluctuations in the nuclear binding energy loss limit the energy resolution[30].

An essential condition for achieving good energy resolutions is also that the calorimeter structure be the same throughout the complete sensitive volume. The energy resolution of the U/TMP calorimeter being built by the UA1 Collaboration[31] will, expectedly, not nearly be as good as the HELIOS and ZEUS ones, if only because of the fact that it is longitudinally subdivided into sections with very different sampling fractions (*i.e.* $e/h^{\rm intr}$ values).

Another important criterion for choosing a particular calorimeter will be compactness. In this respect it is interesting to remark, that the effective nuclear interaction length (λ_{int}^{eff}) of *compensating* uranium and lead calorimeters using the same readout are practically the same, because of the quite different sampling fractions needed for compensation. In spite of its much larger density, uranium does not give any advantage in this respect. If only because of the well-known disadvantages of uranium, the lead alternatives deserve to be thoroughly explored[10]. For plastic scintillator, λ_{int}^{eff} amounts to $\sim$ 20 cm. For TMP, λ_{int}^{eff} depends sensitively on the kB saturation constant, but is likely to be considerably larger than 20 cm. Silicon readout yields the most compact devices ($\lambda_{int}^{eff} \approx 15$ cm for U/Si).

Other important selection criteria concern the hermiticity, granularity, charge collection time, radiation resistance and calibration of the candidate calorimeter. The latter may well turn out to be the major limiting factor in the era of high resolution calorimetry.

Hadron calorimetry has become a mature scientific activity. The R&D activities needed for designing future detectors will get a solid basis.

REFERENCES

1) C.W. Fabjan, Calorimetry in High Energy Physics, CERN-EP/85-54.

2) Y.S. Tsai, Rev. Mod. Phys. **46** (1974) 815.

3) E. Storm and H.I. Israel, Nucl. Data Tables **7** (1970) 565.

4) L. Pages *et al.*, Atomic Data **4** (1972) 1.

5) W.R. Nelson, H. Hirayama and D.W.O. Rogers, The EGS4 Code System, SLAC Report 165 (1985).

6) M. Aguilar-Benitez *et al.*, Particle Properties Data Booklet (1986) 78.

7) T. Yuda, Nucl. Instr. and Meth. **73** (1969) 301.

8) U. Amaldi, Phys. Scripta **23** (1981) 409.

9) G. Fisher, Nucl. Instr. and Meth. **156** (1978) 81.

10) P. Jenni *et al.*, The High Resolution Spaghetti Hadron Calorimeter, NIKHEF-H/87-07 (1987).

11) T. Akesson *et al.*, Detection of Jets with Calorimeters at Future Accelerators, Proc. of the Workshop on Physics at Future Accelerators, La Thuile and CERN (1987); CERN-EP/87-88.

12) C. Leroy, Y. Sirois and R. Wigmans, Nucl. Instr. and Meth. **A252** (1986) 4.

13) M.G. Catanesi *et al.*, Hadron-, Electron-, and Muon Response of a Uranium-Scintillator Calorimeter, preprint DESY 87-027 (1987).

14) T. Akesson *et al.*, Performance of the Uranium/Plastic Scintilator Calorimeter for the HELIOS Experiment at CERN, CERN-EP/87-111.

15) C.W. Fabjan and W.J. Willis, in Proceedings of the Calorimeter Workshop, Batavia Illinois (1975), p. 1, M. Atac, ed.

16) T. Akesson *et al.* Nucl. Instr. and Meth. **A241** (1985) 17.

17) See for example H. Abramowicz *et al.*, Nucl. Instr. and Meth. **180** (1981) 429.

18) M. de Vincenzi *et al.*, Nucl. Instr. and Meth. **A243** (1986) 348.

19) H. Brückmann and H. Kowalski, The Dependence of Calorimeter Responses on the Gate Width, DESY, Hamburg, ZEUS - Internal Note 86 / 026 (1986).

20) R. Wigmans, On the Energy Resolution of Uranium and Other Hadron Calorimeters, CERN-EP/86-141 (1986), accepted for publication in Nucl. Instr. and Meth.

21) C.W. Fabjan and T. Ludlam, Ann. Rev. Nucl. Part. Sci. **32** (1982) 335.

22) V.M. Gorbachev, Y.S. Zamyathin and A.A. Lbov, Nuclear Reactions in Heavy Elements, a Data Handbook (Pergamon Press, London, 1980).

23) C.W. Fabjan *et. al.*, Nucl. Instr. and Meth. **141** (1977) 61.

24) Y. Galaktionov *et. al.*, Nucl. Instr. and Meth. **A251** (1986) 258.

25) H. Brückmann, Hadron Sampling Calorimetry, preprint DESY/86-155 (1986).

26) T. Ypsilantis, Proc. of the Int. Conf. on Advances in Experimental Methods for Colliding Beam Physics, SLAC (1987).

27) J.F. Janni, Atomic Data and Nuclear Data Tables **27** (1982) 147-529.

28) J. Engelen and H. Tiecke, Performance of a Hadron Test Calorimeter for the ZEUS Experiment, preprint NIKHEF-H/86-18 (1986).

29) E. Bernardi *et al.*, Performance of a Compensating Lead-Scintillator Calorimeter, preprint DESY 87-041 (1987).

30) R. Wigmans, Signal Equalization and Energy Resolution for Uranium/Silicon Hadron Calorimeters, to be published.

31) see M. Albrow *et al.*, Performance of a Uranium/Tetramethylpentane Electromagnetic Calorimeter, CERN-EP/87-55 (1987).